

Process development of a solvent-free, chemoenzymatic reaction sequence for the enantioselective synthesis of β -amino acid esters

Vom Promotionsausschuss der
Technischen Universität Hamburg-Harburg
zur Erlangung des akademischen Grades
Doktor der Naturwissenschaften (Dr. rer. nat.)
genehmigte Dissertation.

von
Simon Strompen
aus
Münster

2012

Vorsitzender des Prüfungsausschusses:

1. Gutachter:

2. Gutachter:

Tag der mündlichen Prüfung:

Prof. Dr.-Ing. F. Keil

Prof. Dr. rer. nat. A. Liese

Prof. Dr. rer. nat. H. Gröger

07.06.2012

Publications

S. Strompen, M. Weiß, T. Ingram, I. Smirnova, H. Gröger, L. Hilterhaus, A. Liese. Kinetic investigation of a solvent-free, chemoenzymatic reaction sequence towards enantioselective synthesis of a β -amino acid ester. *Biotechnology and Bioengineering*, 2011, 109, 1479-1489.

R. Yuryev, S. Strompen, A. Liese. Coupled (chemo)enzymatic reactions in continuous flow. *Beilstein Journal of Organic Chemistry*, 2011, 7, 1449-1467.

Oral presentations

S. Strompen, M. Weiß, L. Hilterhaus, H. Gröger, A. Liese. Reaction engineering of a solvent-free, chemoenzymatic reaction sequence for the continuous production of chiral β -amino acid esters *ProcessNet*, 44. Jahrestreffen Deutscher Katalytiker mit Jahrestreffen Reaktionstechnik, March 16-18th, 2011, Weimar, Germany

S. Strompen, D. Kaufhold, C. Korupp, J. J. Müller, A. Liese, L. Hilterhaus. Engineering Aspects of Polyol Biotransformations 3rd Workshop on Fats and Oils as Renewable Feedstock for the Chemical Industry Mar. 14-16th, 2010 Emden, Germany

A. Liese, N. Kurlmann, J. Müller, S. Strompen, R. Yuryev, L. Hilterhaus. Enabling Efficient Chemo- and Biocatalyzed Syntheses via Reaction Engineering XIth Netherlands Catalysis and Chemistry Conference (NCCC), Mar. 1-3th, 2010, Nordwijkerhout, the Netherlands

Poster presentations

S. Strompen, M. Weiß, L. Hilterhaus, H. Gröger, A. Liese. Solvent-free aza-Michael addition and enantioselective biocatalytic aminolysis as a route to chiral β -amino acid esters 5th International Congress on Biocatalysis (Biocat 2010), Aug. 29th - Sep. 2nd., 2010 Hamburg University of Technology, Hamburg, Germany (Awarded a poster prize)

S. Strompen, M. Weiß, L. Hilterhaus, H. Gröger, A. Liese. Solvent-free production of chiral short-chain aliphatic β -amino acid esters via aza-Michael addition and subsequent enantioselective biocatalytic aminolysis Gordon Research Conference (GRC) - Biocatalysis, Jul. 11-16th, 2010 Bryant University, Smithfield, RI, USA

S. Strompen, M. Weiß, L. Hilterhaus, H. Gröger, A. Liese. Chemoenzymatic reaction sequence for the continuous production of chiral short-chain aliphatic β -amino acid esters XIth Netherlands Catalysis and Chemistry Conference (NCCC), Mar. 1-3th, 2010, Nordwijkerhout, the Netherlands

I would like to acknowledge the following people for their contributions to this thesis:

First, I would like to thank my supervisor Prof. Dr. Andreas Liese for his excellent guidance throughout my studies, his "infectious" enthusiasm towards scientific projects and his willingness to offer support at all times.

Prof. Dr. Harald Gröger from the University of Erlangen-Nuremberg (now University of Bielefeld) not only for reviewing my thesis as second examiner, but also for offering the opportunity to work on this common project. In this context, thank you also to Markus Weiß for introducing me to his work on β -amino acids, that represented the basis for my studies, and the valuable discussions.

Prof. Dr. Bernd Niemeyer, Dr. Stephanie Peper and Daniela Herbst from the Helmut Schmidt University of Hamburg for the collaboration on biotransformations under high pressure.

Prof. Dr. Irina Smirnova and Thomas Ingram from the Institute of Thermal Separation Processes, TUHH for the kind support on COSMO-RS based calculations of activity coefficients.

Prof. Dr. Jon Stewart for giving me the opportunity to study the potential of Old Yellow Enzyme for the synthesis of β -amino acids in his lab at the University of Florida.

Dr. Lutz Hilterhaus for countless fruitful discussions, comments and suggestions, but most of all his motivating and optimistic attitude.

Dr. Ruslan Yuryev and Dennis Kaufhold for their support with MATLAB programming, but also numerous high-class darts competitions during coffee breaks.

All technical assistants, bachelor- and project work students for their practical contributions: Charlotte Arnold, Azucena Chaides Zuñiga, Claire Ellebrandt, Ganesh Kumar Padmanabhan, Heike Mushardt, Wolfgang Pietrowski, Inga Rexrodt and Sandra Wirth.

Jan Brummund, Dr. Lutz Hilterhaus, Bastian Kannengiesser, Dr. Selin Kara, Martin Kisch and Dr. Daniel Sellin for their critical review of this thesis.

Jakob Müller und Patrick Prühs, my flat mates and colleagues, for those great times in Hamburg at and after work. The "Susi-WG" will remain unforgotten.

All former and current members of the ITB-team for their practical and theoretical help and their contribution to a very pleasant work atmosphere during these years.

Finally, I want to thank my parents for their unlimited support and encouragement to pursue any goal that I aim for.

Abstract

The development of new, scalable routes towards β -amino acids has gained increasing importance in recent years as β -amino acids are attractive building blocks for the synthesis of pharmaceuticals. While a large number of routes towards aryl-substituted β -amino acids using both chemo- and biocatalysts have been described, few efficient and scalable methods for the preparation of short-chained aliphatic β -amino acids can be found in literature. A solvent-free chemoenzymatic reaction sequence for the enantioselective formation of (*S*)-ethyl-3-amino butanoate with $> 99\%$ *ee* was developed by Weiß and Gröger [140]. In a first step, benzylamine and *trans*-ethyl crotonate form the racemic β -amino acid ester *rac*-ethyl 3-(benzylamino)butanoate in a thermal aza-Michael addition. Without isolation, the (*R*)-ester can directly be converted into the corresponding amide *rac*-N-benzyl-(3-benzylamino)butanamide with benzylamine as an amine donor in a subsequent resolution via lipase (Novozym 435)-catalyzed aminolysis. In this study, the reaction sequence was characterized in detail with respect to kinetic and thermodynamic properties of the system, and the continuous operation of the solvent-free reaction sequence was realized in a coupled reactor setup.

The target product *rac*-ethyl 3-(benzylamino)butanoate was obtained via irreversible aza-Michael addition as the main product. A slow, successive side reaction led to the formation of the amide side product via non-catalyzed aminolysis of the ester in low amounts. Kinetic constants for both reactions were determined for various temperatures in the range from 40 °C to 70 °C by numerical integration of the second order rate equations combined with non-linear regression of the experimental data. Activation energies of $E_{A,1} = 40.4 \text{ kJ mol}^{-1}$ and $E_{A,2} = 54.3 \text{ kJ mol}^{-1}$ were calculated according to Arrhenius' Law for the aza-Michael addition and successive side reaction, respectively. Based on the kinetic parameters, conversion-time plots could be predicted with very good accuracy as proven experimentally. The determined activation energies could be used to predict the course of reactions at temperatures for which no experimental data was available.

Kinetic investigations of solvent-free biocatalytic reactions are hampered by an alternating reaction medium both depending on conversion and applied substrate ratios. Therefore, an alternative strategy was conceived starting in an organic solvent in order to reduce the complexity of the system and subsequently transferring the kinetic data to the solvent free system. Thermodynamic activities of all compounds were calculated using COSMO-RS and used to account for solvation in the respective solvent- or solvent-free system. The stability of the biocatalyst was determined under reaction conditions and found to strongly depend on the applied molar fractions of the substrates. The devised approach proved to be expedient for modelling of the reaction over a broad substrate range ($\chi_{rac-ester} = 0.33-0.8$) and therefore meets the target with respect to simplicity and

applicability for process development purposes.

The selectivity of enzymatic reactions can be influenced by alteration of physicochemical parameters. Particularly, the enantioselectivity of an enzyme can be modified by reaction media, temperature and pressure. All three parameters were therefore investigated in this study for the Novozym 435-catalyzed kinetic resolution of *rac*-3-ethyl-3-(benzylamino)butanoate with benzylamine. A decreasing apparent enantioselectivity E' from 34 in tetrahydrofuran to 12 in *n*-hexane with increasing polarity was observed. In the solvent-free system, an apparent enantioselectivity of $E'=32$ was observed at 60 °C largely independent of the applied substrate ratio. A linear decrease of the selectivity from $E'=40$ to $E'=18$ was found with increasing temperature from 40 °C to 80 °C. No change in enantioselectivity was observed in tetrahydrofuran at 200 MPa in a high pressure reactor compared to reactions carried out at ambient pressure. In diisopropylether as a more hydrophobic solvent on the other hand, a significant loss of enantioselectivity was detected at high pressure. The application of high pressure is therefore not of practical relevance for the reaction system under investigation, but shows the general possibility to modify the enantioselectivity in *Candida antarctica* lipase B-catalyzed reactions.

Based on the kinetic data obtained for both aza-Michael addition and Novozym 435-catalyzed aminolysis, a continuous reactor setup for the two-step chemoenzymatic process was developed. A tube reactor for the thermal aza-Michael addition and a packed-bed reactor for the biocatalytic aminolysis were found to be suited best for the efficient production of (*S*)-ethyl 3-(benzylamino)butanoate. The coupled reactors were operated continuously for a time period of 4 days without significant loss of enzyme activity. The target β -amino acid ester was obtained at 92 % conversion in the tube reactor and 59 % conversion in the packed bed reactor with high enantiomeric excess of > 98 %. A space-time yield of 0.4 kg L⁻¹ d⁻¹ was calculated for the total reactor volume and 1.8 kg L⁻¹ d⁻¹ based solely on the volume of the packed bed reactor. A total turnover number of 158000 was calculated for the biocatalyst under process conditions. Based on the current market price for Novozym 435, biocatalyst costs were estimated to result in about 5.80 € mol⁻¹. Costs for the chiral β -amino acid (*S*)-3-aminobutanoic acid as the final product after downstream processing were estimated at about 782 € kg⁻¹, which is well below the current market price for comparable products. The solvent-free process thus represents an efficient method for the enantioselective production of value added (*S*)- β -amino acid esters starting from cheap substrates.

Abstract

β -Aminosäuren stellen attraktive Bausteine zur Herstellung pharmazeutischer Wirkstoffe dar. Allerdings wurden bisher nur wenige effiziente und skalierbare Methoden für die Synthese kurzkettiger, aliphatischer β -Aminosäuren publiziert. Eine lösungsmittelfreie, chemoenzymatische Methode zur enantioselektiven Synthese von (*S*)-Ethyl-3-aminobutanoat mit hohem Enantiomerenüberschuss von $> 99\%$ wurde von Weiß und Gröger entwickelt [140]. Im ersten Schritt der Reaktionssequenz reagieren Benzylamin und *trans*-Ethylcrotonat in einer aza-Michael-Addition zum racemischen β -Aminosäureester *rac*-Ethyl-3-(benzylamino)butanoat. Die Reaktion verläuft thermisch und ohne Katalysator. Ohne vorherige Aufreinigung des entstandenen Produkts wird das (*R*)-Enantiomer des Esters selektiv mittels Novozym 435-katalysierter Aminolyse zum entsprechenden Amid (*R*)-*N*-Benzyl-(3-benzylamino)butanamid umgesetzt. In dieser Arbeit wurde die Reaktionssequenz eingehend hinsichtlich der Kinetik und Thermodynamik untersucht und der kontinuierliche Betrieb im lösungsmittelfreien System mit zwei gekoppelten Reaktoren ermöglicht.

Das Zielprodukt *rac*-Ethyl-3-(benzylamino)butanoat wird durch die irreversible aza-Michael-Addition als Hauptprodukt erhalten. In einer langsamen Folgereaktion wurden jedoch geringe Mengen des Amids (*R*)-*N*-Benzyl-(3-benzylamino)butanamid via Aminolyse gebildet. Kinetische Konstanten für die thermische aza-Michael-Addition sowie die Aminolyse-Folgereaktion wurden im Bereich von $40\text{ }^{\circ}\text{C}$ bis $70\text{ }^{\circ}\text{C}$ durch numerische Integration der Geschwindigkeitsgleichungen 2. Ordnung und nicht-linearer Regression der experimentellen Daten ermittelt. Aktivierungsenergien von $E_{A,1} = 40.4\text{ kJ mol}^{-1}$ und $E_{A,2} = 54.3\text{ kJ mol}^{-1}$ wurden durch Anwendung der Arrhenius-Gleichung für die aza-Michael-Addition und die Folgereaktion durch Aminolyse berechnet. Anhand der kinetischen Parameter konnten Umsatz-Zeit-Verläufe mit sehr guter Genauigkeit simuliert, und mithilfe der Aktivierungsenergien auch Verläufe bei nicht experimentell untersuchten Temperaturen vorhergesagt werden. Die Selektivität enzymatischer Reaktionen kann durch Veränderung der physikochemischen Bedingungen beeinflusst werden. Dazu zählen insbesondere die Abhängigkeit der Enantioselektivität vom Reaktionsmedium, sowie von Temperatur und hohen Drücken. Diese Parameter wurden in der vorliegenden Arbeit anhand der Novozym 435-katalysierten kinetischen Racematspaltung von *rac*-Ethyl-3-(benzylamino)butanoat mit Benzylamin untersucht. In fünf organischen Lösungsmitteln wurde eine Abnahme der apparenten Enantioselektivität E' mit steigender Polarität von 34 in Tetrahydrofuran auf 12 in *n*-Hexan beobachtet. Im lösungsmittelfreien System wurde bei $60\text{ }^{\circ}\text{C}$ eine apparente Enantioselektivität von $E' = 32$ weitestgehend unabhängig vom Substratverhältnis ermittelt. Eine lineare Abnahme der Selektivität von $E' = 40$ auf $E' = 18$ wurde bei Erhöhung der Temperatur von $40\text{ }^{\circ}\text{C}$ auf $80\text{ }^{\circ}\text{C}$ beobachtet. Im Hochdruckreaktor bei 200 MPa wurde bei Verwendung von Tetrahydrofuran als

polarem Lösungsmittel keine Veränderung der Enantioselektivität festgestellt. In Diisopropylether als hydrophobem Lösungsmittel dagegen wurde ein deutlicher Verlust der Enantioselektivität ermittelt. Die Anwendung hoher Drücke ist somit nicht von praktischer Bedeutung für die synthetische Anwendung im getesteten Reaktionssystem, zeigt aber die generelle Möglichkeit zur Beeinflussung der Enantioselektivität *Candida antarctica* Lipase B katalysierter Reaktionen durch Hochdruck auf.

Die kinetische Beschreibung biokatalytischer Reaktionen im lösungsmittelfreien System wird durch die sich in Abhängigkeit des Umsatzes und des eingesetzten Verhältnisses der beiden Substrate ändernden Bedingungen erschwert. Daher erfolgte die Bestimmung kinetischer Parameter der Novozym 435-katalysierten Aminolyse von *rac*-Ethyl-3-(benzylamino)butanoat mit Benzylamin zunächst im organischen Lösungsmittel, um die Komplexität des Systems zu verringern. Die experimentellen Daten konnten mit einem vereinfachten Modell basierend auf der Michaelis-Menten Zweisubstrat-Kinetik inklusive Substratüberschussinhibierung durch Benzylamin und Produktinhibierung durch (*R*)-*N*-Benzyl-(3-benzylamino)butanamid gut beschrieben werden. Um das Modell auf das prozesstechnisch relevante lösungsmittelfreie System übertragen zu können, müssen die unterschiedliche Solvatisierung sowie weitere Lösungsmittelleffekte im kinetischen Modell berücksichtigt werden. Daher wurden thermodynamische Aktivitäten aller Reaktanden mittels COSMO-RS-Software berechnet und anstelle von Konzentrationen in das Modell integriert. Die Stabilität des Biokatalysators wurde unter Reaktionsbedingungen im Satzreaktor untersucht. Es wurde eine starke Abhängigkeit vom eingesetzten Verhältnis der Substrate sowie der Temperatur ermittelt. Die Reaktionen im lösungsmittelfreien System konnten mithilfe des entwickelten Modells über einen weiten Bereich unterschiedlicher Substratverhältnisse ($\chi_{rac-Ester}=0,33-0,8$) mit guter Genauigkeit simuliert werden, so dass das Modell für die Prozessentwicklung eingesetzt werden kann.

Auf Basis der kinetischen Daten beider Reaktionen wurde ein kontinuierlicher Reaktor für den zweistufigen, chemoenzymatischen Prozess entwickelt. Für die thermische aza-Michael-Addition wurde dazu ein Strömungsrohr in Form eines Schlauchreaktors verwendet. Für die biokatalytische Aminolyse wurde ein Festbettreaktor als der geeignetste Reaktortyp für die effiziente Produktion von (*S*)-Ethyl-3-(benzylamino)butanoat ermittelt. Die gekoppelten Reaktoren wurden kontinuierlich unter optimierten Reaktionsbedingungen über einen Zeitraum von 4 Tagen ohne signifikanten Verlust von Enzymaktivität betrieben. Der zu produzierende β -Aminosäureester wurde bei 92 % Umsatz im Schlauchreaktor und 59 % Umsatz im Festbettreaktor mit hohem Enantiomerenüberschuss von > 98 % erhalten. Eine Raum-Zeit-Ausbeute von $0,4 \text{ kg d}^{-1} \text{ L}^{-1}$ bezogen auf das Gesamtvolumen des Reaktors sowie $1,8 \text{ kg d}^{-1} \text{ L}^{-1}$ bezogen ausschließlich auf das Volumen des Festbettreaktors wurde erreicht. Eine maximale Zykluszahl des Biokatalysators von 158000 unter Prozessbedingungen wurde ermittelt. Die Kosten für den Biokatalysator belaufen sich demnach auf ca. $5,80 \text{ € mol}^{-1}$. Die Kosten für die chirale β -Aminosäure (*S*)-3-Aminobutanoat als Endprodukt nach Aufarbeitung belaufen sich auf ca. 782 € kg^{-1} und sind somit deutlich niedriger als der gegenwärtige Marktpreis für vergleichbare Produkte. Der lösungsmittelfreie Prozess stellt somit eine effiziente Methode zur enantioselektiven Produktion von β -Aminosäureestern ausgehend von kostengünstigen Substraten dar.

Contents

1	Introduction	1
1.1	Kinetic resolution	2
1.2	Industrial biocatalysis	4
1.2.1	(Bio)process development	4
1.2.2	Highly concentrated and solvent-free reactions	6
1.3	Synthesis of β -amino acids	7
1.4	(Chemo-)enzymatic reaction sequences	10
2	Aim of thesis	13
3	Aza-Michael addition	15
3.1	Thermodynamic aspects	17
3.2	Kinetic aspects	18
3.3	Reaction engineering aspects	19
3.4	Summary	24
4	Biocatalytic aminolysis	25
4.1	Selectivity of Novozym 435	26
4.1.1	Temperature effect on selectivity	27
4.1.2	Selectivity in solvent system	29
4.1.3	Selectivity in solvent-free system	30
4.2	Stability of Novozym 435	31
4.3	Diffusion limitation	33
4.4	Enzyme kinetics	34
4.4.1	Solvent polarity	35
4.4.2	Water activity control	37
4.4.3	Thermodynamic activity calculation	39
4.4.4	Kinetics in organic solvent	40
4.4.5	Kinetics in solvent-free medium	42
4.5	Prediction of progress curve	44
4.6	Batch vs. fed batch operation	46
4.7	Summary	49
5	Inline analytics via FTIR	51
5.1	Inline monitoring in batch processes	54
5.1.1	aza-Michael addition	55
5.1.2	Biocatalytic aminolysis	56

5.2	Inline monitoring in continuous processes	58
5.2.1	aza-Michael addition	58
5.2.2	Biocatalytic aminolysis	60
5.3	Summary	62
6	Continuous chemo-enzymatic process	65
6.1	Continuous aza-Michael addition in tube reactor	68
6.1.1	Flow characteristics	68
6.1.2	Temperature dependence in tube reactor	70
6.2	Biocatalytic aminolysis in packed bed reactor	71
6.3	Coupled reactor setup for continuous production	73
6.4	Summary	78
7	High pressure reaction	79
7.1	Selectivity at high pressure	81
7.2	Reaction rate at high pressure	83
7.3	Protein stability at high pressure	85
7.4	Summary	86
8	Discussion and outlook	87
8.1	Evaluation of process economics	88
8.2	Perspectives for optimization	89
8.3	Conclusion	91
9	Summary	93
A	Materials and methods	95
A.1	Applied equipment	95
A.2	Applied chemicals	97
A.3	Methods	98
A.3.1	Analytical methods	98
A.3.2	Analyses in batch mode	100
A.3.3	Analyses in continuous flow	102
A.3.4	Computational methods	103
B	Supplemental information	109

List of used abbreviations and symbols

Abbreviations

cat.	catalyst
(<i>R</i>), (<i>S</i>)	absolute stereoconfigurations
(<i>rac</i>)	racemic
ACN	acetonitrile
ATR	attenuated total reflectance
CALA/B	<i>Candida antarctica</i> lipase A/B
CSTR	continuously stirred tank reactor
DEA	diethylamine
DIPE	diisopropylether
DKR	dynamic kinetic resolution
DNA	deoxyribonucleic acid
EC	enzyme commission
FTIR	Fourier transformation infrared
HPLC	high-pressure liquid chromatography
IR	infrared
MCT	mercury, cadmium, telluride
MIR	mid-infrared
MTBE	methyl <i>tert</i> -butyl ether
N435	Novozym 435
<i>n</i> Hex	<i>n</i> -hexane
NIR	near-infrared
NMR	nuclear magnetic resonance
PCA	principle component analysis
PFR	plug flow reactor
PLS	partial least square
PTFE	polytetrafluorethen
RMSEC	root mean square error of calibration
RMSEP	root mean square error of prediction
RNA	ribonucleic acid
THF	tetrahydrofurane
UV/VIS	ultraviolet/visible

Symbols:

[A]	M^{-1}	molar concentration of compound A
[Enz.]	$g\ g^{-1}$	concentration of immobilized enzyme
d_i	mm	inner tube diameter
E_A	$kJ\ mol^{-1}$	activation energy
E		enantioselectivity
E	$kg_{waste}\ kg_{product}^{-1}$	E-factor
ee		enantiomeric excess
$E_T(30)$		solvent polarity scale
$F(\theta)$		normalized response to upstream step input
J	Hz	spin-spin coupling constant
k_{cat}	h^{-1}	turnover number
k_{deact}	h^{-1}	enzyme deactivation constant
k_j	$mmol\ g^{-1}\ h^{-1}$	rate constant, $j=1,2$
K_i	$mmol\ g^{-1}$	inhibition constant
K_m	$mmol\ g^{-1}$	Michaelis-Menten constant
L	m	length of reactor
MW_n	$g\ mol^{-1}$	average molecular weight
p	MPa	pressure
Q	$kg\ kg^{-1}\ h^{-1}$	catalyst productivity
R	cm	channel radius of curvature
STY	$kg\ L^{-1}\ d^{-1}$	space-time yield
t	h	time
\bar{t}	h	mean residence time
Δt	h	time interval
T_b	[°C]	boiling point
ttn	mole mole ⁻¹	total turnover number
\dot{v}	$ml\ h^{-1}$	flow rate
V	ml	volume
ΔV^\ddagger		activation volume
ν	$mmol\ h^{-1}\ g_{N435}^{-1}$	reaction rate
$\nu_{max(R/S)}$	$mmol\ h^{-1}\ g_{N435}^{-1}$	maximal initial reaction rate in conversion of (<i>R</i>) or (<i>S</i>)-enantiomer
$\nu'_{max(R/S)}$	$mmol\ (mmol\ g^{-1})^{-1}\ h^{-1}\ g_{N435}^{-1}$	kinetic parameter consisting of ν_m and K_m
$\nu'^*_{max(R/S)}$	$mmol\ (mmol\ g^{-1})^{-1}\ h^{-1}\ g_{N435}^{-1}$	ν'_m adapted for solvent effects
X_s	%	conversion
α, β		position to functional group
γ_i		activity coefficient of compound <i>i</i>
δ_{cs}	ppm	chemical shift

δ	g mol^{-1}	density
η	Pa s	dynamic viscosity
η_p		yield
π^*		solvent polarity scale
σ_p		selectivity
θ		reduced time, number of residence times
τ	h	residence time
χ		mole fraction

1 Introduction

Biotechnology as the technical application of biological systems or parts thereof has gained invaluable importance in meeting everyday demands of human life. Biotechnological processes are established in virtually all areas from health care, food or feed production, fine and bulk chemistry to waste treatment and diagnostics. Enzymes that nature has provided us with represent an important tool in all of these fields. The first biotechnological application of enzymes not being part of living cells dates back to 1833, when Payen and Persoz were able to hydrolyze starch to dextrin and sugar using extracts of germinating barley [119]. Since then, scientific progress in the understanding of enzyme action has led to a vast number of biotechnological and in particular enzyme-catalyzed processes being established in industry today. Many enzymes isolated from nature, however, do not directly meet the requirements of an industrial process. By application of random protein engineering tools such as gene shuffling and directed evolution, rational design or combinations thereof, however, significant improvements can often be achieved [9]. Engineering efforts usually target the enhancement of enzyme stability, activity, solvent tolerance or selectivity (for selected examples and reviews see the following references: [3, 75, 83, 109, 113]). Sequential, mechanistic and/or structural information is a prerequisite for either strategy of enzyme engineering. High-throughput sequencing tools for DNA, RNA and amino acids sequencing are available today. Via comparative sequence analyses, putatively interesting biocatalysts showing similarities to known enzymes whose sequential data has been published in one of the large protein databases can be identified *in silico*.¹ It may be assumed that a better understanding of the evolution of enzyme function in nature will also yield improved strategies for artificial evolution *in vitro* [95]. Of less industrial importance up to date, but certainly of great value in the long run are very recent successes in the *de novo* design of enzymes [37]. Such enzymes designed from scratch, however, usually suffer from very low activities [107]. Protein dynamics as an additional, rather recent discipline has helped to link enzyme motion to function [47]. How structural motions of enzymes are related to catalysis is still poorly understood [99], but should, in the future, provide valuable information that may help to better and faster engineer enzymes for industrial application.

Depending on the process, biocatalysts may be applied as whole cell catalysts without purification from their production organism, in free form as a cell free extract or purified from contaminating proteins, or immobilized on diverse carrier materials. Immobilized enzymes offer several advantages such as ease of separation from reactants for multiple usage in repetitive reactions or application in continuous processes such as fixed-

¹e.g. BRENDA, UniPROT, NCBI, RCSB PDB, PRECISE

bed, fluidized-bed and stirred tank reactors equipped with filters for catalyst retention. Additionally, enzyme immobilization often yields significantly more stable catalysts as compared to their free counterparts. *Candida antarctica* lipase B for example denatures at temperatures between 50 and 60 °C in free form in aqueous media and thus suffers from significant activity loss upon further temperature increase [2]. The same enzyme immobilized by adsorption on a porous methacrylate resin which was also used in this work, however, is highly thermostable and has been used at elevated temperatures up to 160 °C in supercritical CO₂ as a reaction medium [98].

1.1 Kinetic resolution

The significance of chirality in living systems is well-recognized today [115]. In virtually all cellular processes chiral recognition processes are involved. Therefore, it is not surprising that the biological activity of many drugs on living organisms is related to its chiral structure. Several strategies are available to the chemist in order to produce enantiomerically pure compounds. In chiral pool synthesis, enantiomerically pure compounds already available in nature are used as starting material for subsequent modifications throughout which the chiral information is retained. A second source for pure enantiomers are racemates, which can be resolved e.g. by preferential crystallization, diastereomeric crystallization or kinetic resolution.

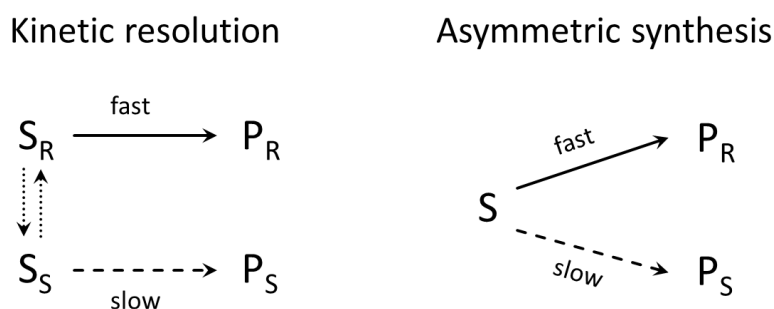


Figure 1.1: Kinetic resolution of racemates vs. asymmetric synthesis. Grey arrows indicate a possible dynamic kinetic resolution (DKR).

The resolution of racemates has the inherent disadvantage of leading to maximum yields of 50 %, unless the unreacted enantiomer is racemized. Such processes in which chemical or enzymatic means are used for the racemization of the unwanted enantiomer (indicated by grey arrows in Figure 1.1) are called dynamic kinetic resolutions. Asymmetric synthesis theoretically allows the achievement of 100 % yield and therefore seems to imply a clear advantage over kinetic resolutions. In practice, however, cheaper raw materials and more efficient syntheses often compensate for this disadvantage [115]. Additionally, the enantiomeric excess (*ee*) in asymmetric synthesis entirely depends on the catalyst selectivity and is often not sufficient for application. In case the non-reacting enantiomer is the desired compound, high *ee* values of >99 % *ee* can be obtained regard-

less of the selectivity of the catalyst at the cost of higher degrees of conversion (Figure 1.2). The enantioselectivity of an enzyme is commonly expressed by the enantioselectivity E introduced by Chen et al. [21]. E can be calculated according to Equations 1.1-1.2 from pairs of X/ee_p , X/ee_s or ee_s/ee_p -values.

$$E = \frac{\ln[1 - X(1 - ee_s)]}{\ln[(1 - X(1 + ee_s))]} = \frac{\ln[1 - X(1 + ee_p)]}{\ln[(1 - X(1 - ee_p))]} \quad (1.1)$$

$$E = \frac{\ln\left(\frac{1 - ee_s}{1 + \frac{ee_s}{ee_p}}\right)}{\ln\left(\frac{1 + ee_s}{1 + \frac{ee_s}{ee_p}}\right)} \quad (1.2)$$

The methods introduced here are sensitive for substrate contamination or background reactions, but independent of product inhibition or reversibility of the reaction [120]. Further methods exist for the determination of E . These are often more accurate than those presented above, but depend on computational fitting methods and thus require a larger amount of data or on information on kinetic parameters. A detailed discussion of scopes and limitations of each method can be found in [120]. An E -value of 10 is commonly considered the lower limit for industrial application [77]. However, process costs and the availability of alternative synthetic pathways may vary largely and make an individual assessment necessary.

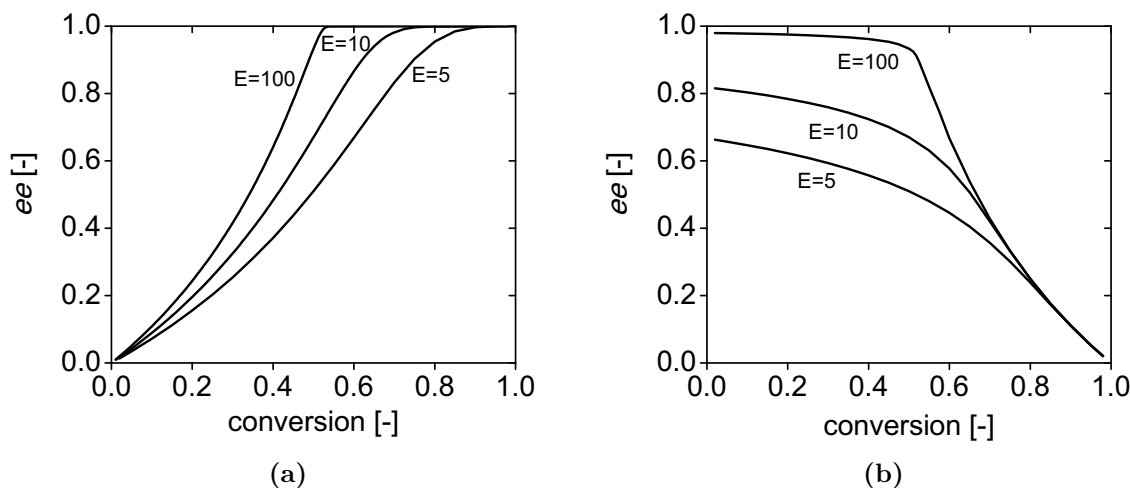


Figure 1.2: Enantiomeric excess of the substrate (a) or product (b) as a function of conversion in dependence of enzyme enantioselectivity E .

1.2 Industrial biocatalysis

Numerous processes utilizing biocatalysts for the production of fine and bulk chemicals, pharmaceuticals or agrochemicals are established in industry today [72]. An ever increasing availability of novel biocatalysts, improvements in bioengineering tools for the optimization and modification of enzymes as well as safety, health and environmental issues still boost the number of industrial application of enzymes [143, 148]. Examples of implemented biocatalytic processes include the use of a racemase/D-hydantoinase/D-carbamoylase enzyme system for the production of enantiomerically pure α -amino acids at Evonik shown in Figure 1.3 [84], the use of pig liver esterase for the production of various pharmaceutical intermediates at manufacturing scale at DSM [39] or the bulk production of acrylamide from acrylonitrile using nitrile hydratases in whole cells of *Rhodococcus sp.* at Nitto Chemical Ltd. [72].

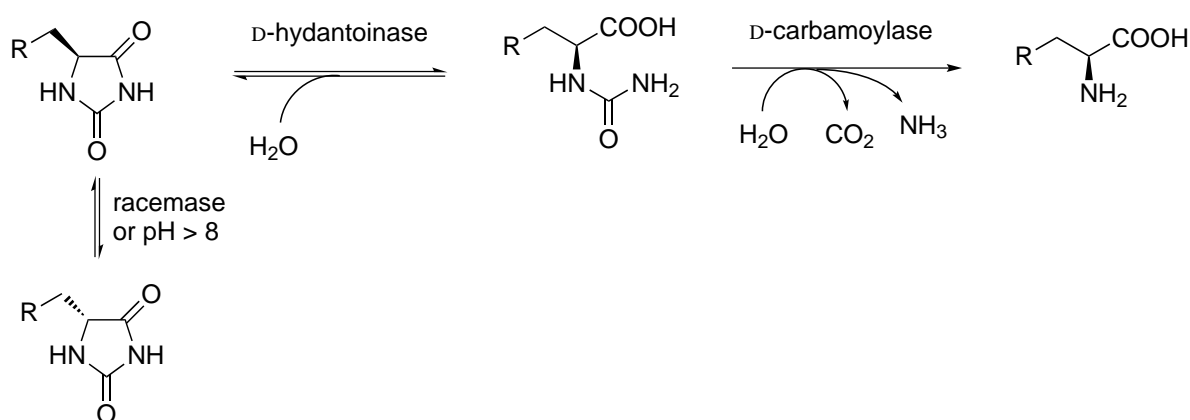


Figure 1.3: Reaction scheme of the racemase/D-hydantoinase/D-carbamoylase system for the enantioselective production of α -amino acids [84].

1.2.1 (Bio)process development

The development and optimization of bioprocesses needs to consider the properties of the biocatalyst and the chemical reaction it catalyzes on the one hand, and principles of chemical engineering on the other hand [43]. Biocatalyst and reaction characteristics are traditionally mainly addressed by the natural scientist as they require comprehensive (bio)-chemical know-how, whereas reactor design, optimization and scale-up are classically performed by the process engineer. As depicted in Figure 1.4, all disciplines are highly interconnected and require interdisciplinary thinking from an early stage of development on. Some general aspects are discussed in the following. An extensive discussion of strategic approaches in bioprocess development can be found in literature [22, 43, 66].

With regard to the biocatalyst, two major questions need to be answered: (1) is there a need for optimization of the enzyme itself via protein engineering? (2) Should whole cell catalysts, immobilized enzymes or free, isolated enzymes be used? Nature provides

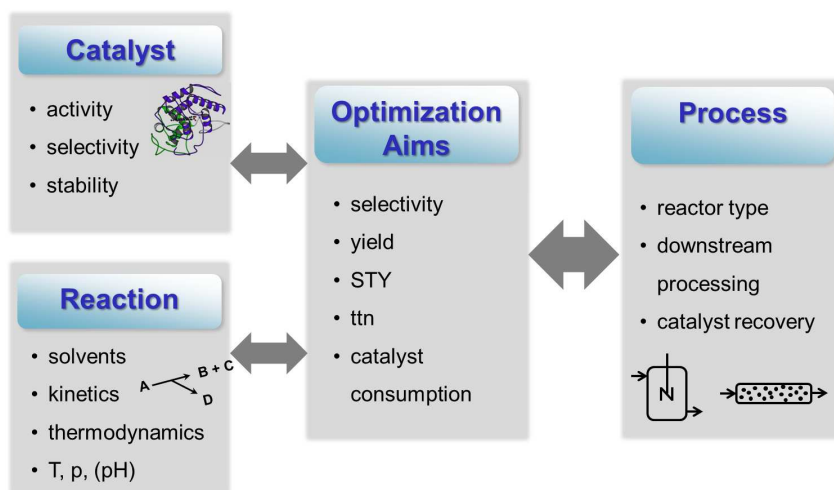


Figure 1.4: (Bio)process development: aspects for optimization.

a good toolbox of diverse catalysts, but often these require tailoring in order to adapt the catalyst to non-natural substrates and industrial process conditions [92]. The use of whole-cell biocatalysts has many advantages such as low cost enzyme supply and good stability and are therefore often preferred industrially. However, side reactions and limitations with regard to mass transfer may occur and limit the applicability of whole-cell preparations. One or more additional steps are necessary to obtain isolated enzymes, which usually goes in hand with loss of activity yield. On the other hand, side reactions may be completely suppressed and stability issues improved by immobilization. The type of enzyme preparation has immediate consequences on the choice of a suited reactor type. Since enzyme costs usually add significantly to the overall cost of the process, enzyme retention and reuse is of major concern. For reactions carried out in batch mode, enzyme recovery can be achieved by (ultra)filtration, centrifugation and other physical methods such as magnetic forces when magnetic carriers are used. In continuous processes, membranes of a suited pore size can be used for the retention of whole-cells and isolated enzymes. Packed bed reactors are often used in the case of immobilized enzymes.

Once a suitable biocatalyst has been chosen, a detailed investigation of suited physico-chemical reaction conditions (T, pH, solvent etc.) and their influence on enzyme stability as well as kinetic and thermodynamic properties of the reaction is usually carried out. Based on the obtained results a suited reactor type may be chosen. A number of optimization targets may be defined. These include aspects such as facility of downstream-processing and reducing general process costs (energy consumption, hardware), as well as specific process parameters such as the achievement of a high space-time yield (STY), conversion X , (enantio)selectivity, a low E-factor² and maximal total turnover number (ttn) of catalyst and cofactor.³

²The E-factor introduced by Sheldon [114] measures the "greenness" of a reaction and is defined as the weight of waste produced per weight of product.

³Important definitions frequently used in this study are summarized in Appendix B on page 109.

1.2.2 Highly concentrated and solvent-free reactions

In industrial application it is generally highly desired to use high substrate concentrations in biocatalytic processes. The use of solvent-free reactions as the extreme is therefore especially interesting. Higher yields and reaction rates can usually be achieved. Additionally, energy costs are reduced and a largely improved E-factor can be obtained. The necessity for smaller reactor sizes leads to decreased capital investments [135]. While a number of solvent-free chemical and biocatalytic reactions including e.g. polymerizations and esterifications have been described in literature up to date, only relatively few solvent-free enantioselective biocatalytic processes can be found of which some are summarized here. Von Langemann et al. used an (*S*)-selective hydroxynitrile lyase from *Manihot esculenta* for the conversion of acetophenone and derivatives to the corresponding cyanohydrins according to Figure 1.5 [134]. Excellent *ee*'s of > 99 % were obtained at a very good yield of up to 78 %.

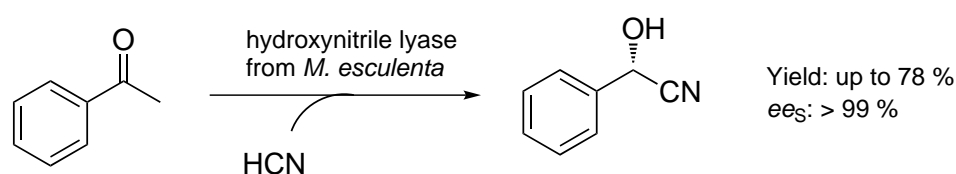


Figure 1.5: Hydroxynitrile lyase-catalyzed conversion of acetophenone to corresponding cyanohydrin [134].

Li et al. observed an interesting unnatural ability of nuclease p1 to catalyze the solvent-free aldol addition of aromatic aldehydes and cyclic ketones according to Figure 1.6 in a solvent-free system [71]. However, the obtained yields of 17-55 % at *ee* 49-99 % were low to satisfactory.

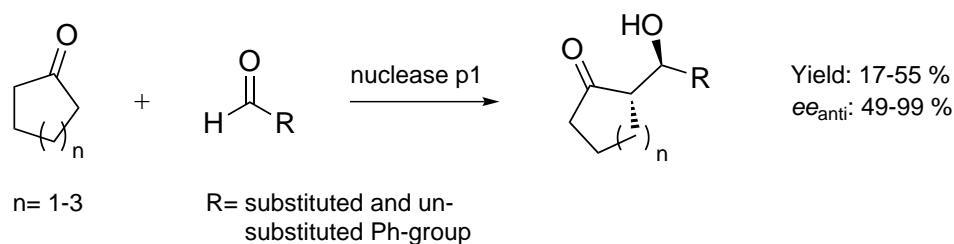


Figure 1.6: Nuclease p1-catalyzed aldol addition in solvent-free system [71].

The *Candida antarctica* lipase A (CALA)-catalyzed enantioselective transesterification of methyl 2-chloromandelate via transesterification with vinylpropionate in a solvent-free system was described bei Uhm et al. [131]. The resulting chiral (*S*)-chloromandelic acid ester is a precursor for pharmaceutical products such as the antiplatelet agent (*S*)-clopidogrel. A high *ee* of >99 % was reached at a yield of 41 %.

Xiong and coworkers described the enantioselective lipase-catalyzed transesterification of mandelonitrile and vinyl acetate [145]. Depending on the lipase used, > 99 % *ee* were

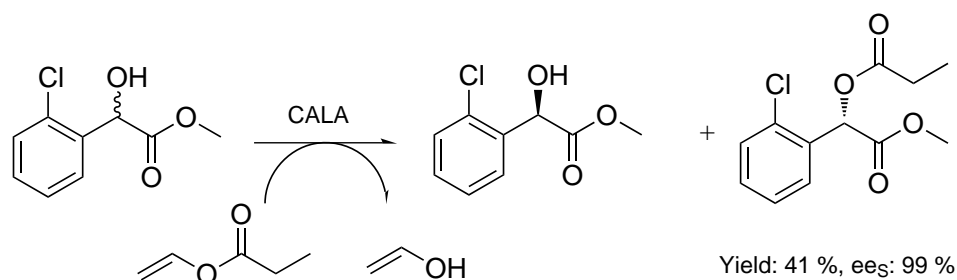


Figure 1.7: *Candida antarctica* lipase A (CALA)-catalyzed kinetic resolution of methyl 2-chloromandelate via transesterification with vinylpropionate [131].

achieved in the best case at 47.9 % conversion. Vinyl acetate was used in large excess and served as a substrate and solvent at the same time. The enzymatic hydrolysis to resolve racemic ketoprofen described by Jin et al. was carried out in a two-phase system due to the immiscibility of water and the organic substrate [52]. Such reaction systems in which one of the substrates also acts as a solvent may be considered quasi-solvent-free. Two-phase aqueous-organic systems where the organic phase is solely composed of substrates represent a valuable alternative in case biocatalysts require an aqueous phase and do not tolerate the use of fully organic, solvent-free systems due to stability loss.

Some interesting examples of enantioselective solvent-free reactions catalyzed enzymatically have been presented above. The diversity of enzymes used and the reactions catalyzed imply the large potential of such reaction systems. Nonetheless, only few examples in solvent-free asymmetric catalysis exist using both chemo- and biocatalysts [135]. In addition to an increased awareness of solvent-free reaction systems in the scientific community, a combination of protein engineering for the generation of stable catalysts and (bio)process development for the careful control of solvent-free reactions (which for example may rapidly generate heat) will certainly bring about a large number of processes in the years to come.

1.3 Synthesis of β -amino acids

The stereoselective synthesis of β -amino acids has attracted an increasing interest within recent years [54, 73]. Due to their "unnatural" β -functionality the deactivation of drugs containing β -amino acids as a structural element is much slower within organisms compared to drugs based on naturally occurring α -amino acids. Additionally, as small bifunctional compounds they can easily be modified into more complex structures. These inherent features make β -amino acids especially interesting for the pharmaceutical industry as building blocks for peptide mimetics. In nature, β -amino acids can be found in free form or as structural elements of biologically active peptides, even though not as frequently as α -amino acids. A large number of routes towards aryl-substituted β -amino acids using both chemo- and biocatalysts can be found in literature that have been reviewed extensively [54, 73]. Some recent examples of synthetic routes employing enzymes from different enzyme classes are presented in the following paragraphs.

1 Introduction

A phenylalanine aminomutase (PAM, EC 5) from *Taxus chinensis* was used for the enantioselective conversion of (*E*)-cinnamic acid to (*S*)- α -phenylalanine and (*R*)- β -phenylalanine (Figure 1.8) [126, 144]. Both products are obtained with excellent *ee*'s of >99 % at a ratio of 51:49 α/β . The enzyme also acted on a number of cinnamic acid derivatives, whereas the substituent had a large effect on the α/β -ratio but not on enantioselectivity. Additional examples for ammonia lyase and aminomutase-catalyzed syntheses of β -amino acids have been reviewed by Turner, 2011 [130].

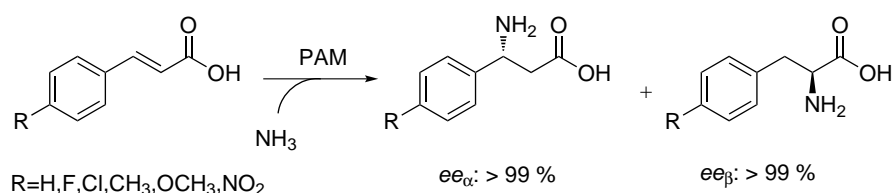


Figure 1.8: Phenylalanine aminomutase (PAM)-catalyzed synthesis of (*S*)- α -phenylalanine and (*R*)- β -phenylalanine [144].

Kim et al. isolated and characterized a β -transaminase (EC 2) from *Mesorhizobium sp.* [62]. A sequential route towards the enantioselective synthesis of (*S*)- β -phenylalanine was described in which *Candida rugosa* lipase was used to convert ethylbenzoylacetate *in situ* into the corresponding unstable benzoylacetic acid. In a subsequent β -transaminase-catalyzed step, an amino group is transferred enantioselectively from 3-aminobutyric acid to the β -keto acid to form (*S*)- β -phenylalanine. Similarly, Brucher and coworkers synthesized aromatic β^3 -amino acids via kinetic resolution starting from the racemic β^3 -amino acids [12]. The approach, however, is limited to 50 % conversion.

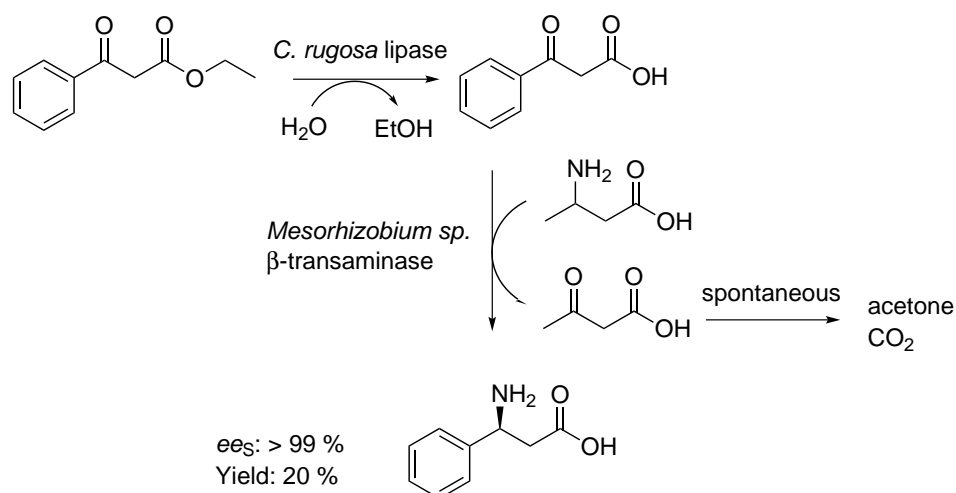


Figure 1.9: Asymmetric synthesis of (*S*)- β -phenylalanine via sequential action of *Candida rugosa* lipase and *Mesorhizobium sp.* β -transaminase [62].

The asymmetric reduction of β -nitro acrylates for the synthesis of β -amino acids was achieved using *Saccharomyces carlsbergensis* old yellow enzyme (EC 1) with 87-96 %

ee [125]. The β -nitro acrylates was synthesized chemically via Henry reaction from an α -keto ester and a nitroalkane using solid-phase base catalysis. The approach, however, is limited to β^2 -amino acids. Additionally, olefin isomerization in the aqueous reaction system and low substrate solubility hamper the preparative application.

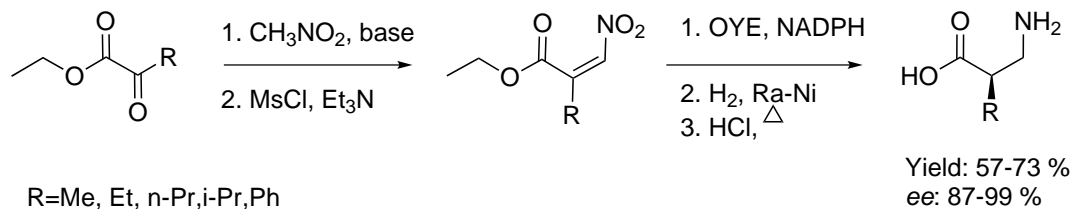


Figure 1.10: Asymmetric route towards β^2 -amino acids applying old yellow enzyme (OYE) [125].

A wide range of hydrolases (EC 3) has been applied for the enantioselective synthesis of β -amino acids including lipases, amidases, proteases, esterases, β -lactamases and nitrilases. Many of these are reviewed elsewhere [73]. Exemplarily, the nitrile hydratase/amidase system used by Ma and coworkers is presented here [76]. Whole cells of *Rhodococcus erythropolis* AJ270 were used as a catalyst for the enantioselective conversion of β -amino alkanenitriles to the corresponding amides and acids (Figure 1.11). Poor results had initially been achieved using unprotected β -amino alkanenitriles. Introduction of a benzyl group for amine protection, however, allowed the formation of highly enantioenriched products. The good overall enantioselectivity was attributed to the action of the amidase, whereas the nitrile hydratases (EC 4) exhibited only low enantioselectivity.

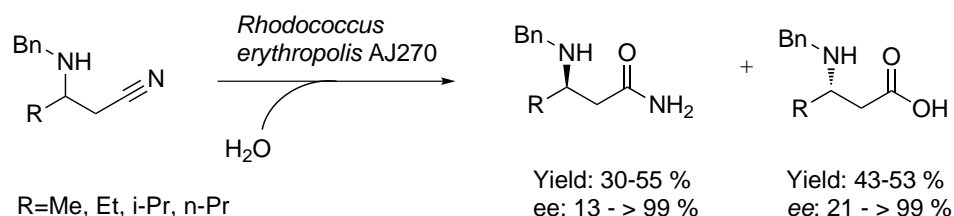


Figure 1.11: Enantioselective conversion of benzyl-protected β -amino alkanenitriles to the corresponding β -amino amides and acids, respectively, applying *Rhodococcus erythropolis* AJ270 as a whole cell catalyst [76].

A number of synthetic routes towards aromatic β^3 -amino acids has been described here and many more have been published. However, only few efficient and scalable methods for the preparation of short-chained aliphatic β -amino acids can be found [140]. The solvent-free chemoenzymatic reaction sequence investigated in this study therefore represents an attractive method that allows the enantioselective formation of short chain β -amino acids with up to 99 % *ee* [138–140].

1.4 (Chemo-)enzymatic reaction sequences

For a long time, heavy metal catalysis has dominated the field of asymmetric synthesis. The development of excellent chiral auxiliaries such as Whitesell's or Evans' auxiliary boosted the field of organocatalysis and is nowadays accepted as a competitive method in stereoselective synthesis [35]. Additionally, biocatalysis has emerged as a third key player in enantioselective catalysis. Many synthetic routes towards often complex bioactive drugs require several modifications. Optimal catalysts for specific reactions involved in a reaction sequence may be found in either of the three disciplines. In order to fully exploit the potential of all disciplines, the coupling of sequential steps without tedious and costly work-up procedures is highly desired.

Table 1.1: Advantages and disadvantages of the three approaches to continuous coupled-reaction (chemo)enzymatic processes according to Yuryev et al. [147].^a

Criterion	<i>in vitro</i> single reactor	<i>in vitro</i> cascade reactor	<i>in vivo</i> whole cell
Separation of incompatible steps	-	+	-
Incorporation of chemical steps	0	+	-
Optimization by reaction engineering	0	+	-
Modularization/incorporation of downstream processing units	-	+	-
Enzyme preparation/costs	-	-	+
Cofactor regeneration	0	-	+
Atomic efficiency	0	0	-

^a (+) advantage; (-) disadvantage; (0) no general comment possible, dependent on respective reaction system.

In an attempt to classify (continuous) catalytic reactions in the field of applied biocatalysis, the consideration of the type of biological principles of cell metabolism has been suggested as a concept [147]. Hereafter, simple "single-reaction/single-enzyme" systems are termed first-generation enzymatic processes. Single-reaction processes in continuous flow are termed second-generation enzymatic processes. They resemble cell metabolism in which a constant flux of nutrients is required for the cell to stay alive. Third-generation processes are those that involve the coupling of two or more reactions in a single batch. The compatibility of all (chemo)enzymatic steps involved is the major challenge in the development of new cascade processes.

Coupled reaction processes in continuous flow as described in chapter 6 on page 65 combine the biological principles of second- and third-generation processes and therefore most closely mimic the principles of cell metabolism. These systems can be classified as fourth generation processes. Relatively few examples of such fourth generation processes can be found in literature due to their inherent complexity. In principle, coupled

reaction processes in continuous flow can be carried out in a single reactor containing multiple catalysts or in a cascade of physically separated reactors. Whole cell biotransformations may formally be considered fourth generation processes as well although they proceed *in vivo* instead of *in vitro*. Challenges in fourth generation processes often result from chemical compatibility problems of the single steps, different (bio)catalyst lifetime or cross-inhibition phenomena. Advantages and disadvantages of each of the three approaches to continuous coupled-reaction (chemo)enzymatic processes are summarized in Table 1.1 on the facing page.

2 Aim of thesis

A solvent-free chemoenzymatic reaction sequence towards β -amino acid esters as precursors of the corresponding β -amino acids has been developed by Dr. Markus Weiß and Prof. Dr. Harald Gröger¹ at the Department of Chemistry and Pharmacy, University of Nuremberg-Erlangen.² A range of benzylamine derivatives as donor substrates and α , β -unsaturated ester acceptors were found to be suitable starting materials. The aim of this thesis is to characterize the chemoenzymatic reaction sequence starting from benzylamine and *trans*-ethyl crotonate as a model reaction system with regard to kinetics and thermodynamics. The determination of kinetic parameters of biocatalytic reactions in solvent-free systems is particularly challenging. It has been reported frequently in literature, that the reaction medium is decisive for enzyme activity. In the case of solvent-free reactions, the reaction medium is subject to frequent changes with conversion and varying initial substrate fractions. Therefore, a kinetic model as simple as possible that allows the accurate prediction of progress curves is aimed for. The development and optimization of a reactor concept based on the obtained thermodynamic and kinetic data is envisioned. Online-analytics via FTIR should be established in order to allow online-monitoring of the concentration-time course of all reactants in a continuous reactor setup.

In particular, the following tasks are planned:

- Kinetic and thermodynamic evaluation of the solvent-free aza-Michael addition.
- Kinetic and thermodynamic evaluation of the Novozym 435-catalyzed aminolysis in a solvent-free system.
- Development of a reactor concept allowing an efficient, continuous operation with the overall aim of maximizing the space-time yield.
- Establishment of FTIR-analytics as a tool for the online-monitoring of both aza-Michael addition and biocatalytic aminolysis.
- Evaluation of high-pressure effects on enantioselectivity in the lipase-catalyzed aminolysis.

Each task will be addressed in an individual chapter in this work.

¹Current address: Bielefeld University, Faculty of Chemistry, Universitätsstr. 25, 33615 Bielefeld, Germany.

²Weiß and Gröger, 2009; Weiß et al., 2011 [138, 140]

2 *Aim of thesis*

3 Aza-Michael addition¹

Named after the American scientist Arthur Michael, the Michael addition reaction has become an invaluable method in synthetic chemistry. It can be used to couple nucleophilic Michael donors to α , β -unsaturated Michael acceptor molecules. Importantly, C-C bond formations can be achieved when carbanions are used as nucleophiles, but amines or thiols are commonly used as Michael donors as well (Figure 3.1). Acceptor molecules are electron-deficient alkenes activated usually by a carbonyl group (aldehyde, ketone, ester) or a nitro group. Michael additions to less strongly activated nitriles or amides have also been described using both chemo- and biocatalysts [91, 100].

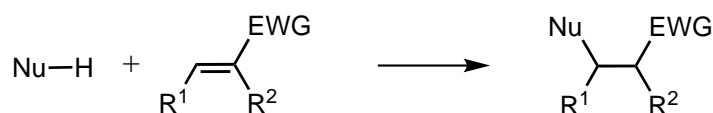


Figure 3.1: General scheme of Michael addition. $R_1, R_2 = H$, alkyl. EWG = electron withdrawing group. Nu = amine-, thiol- or carbanionic nucleophile.

Aza-Michael additions can be carried out thermally without the addition of catalysts in a solvent-free system using various amine-nucleophiles and carbonyl or nitrile acceptors [103, 140]. The reaction rate of such reactions can be dramatically lowered using e.g. sulfated zirconia catalysts [105]. Of major importance in organic chemistry, however, is the asymmetric Michael addition and in order to obtain β -amino acids particularly asymmetric aza-Michael additions. Strategies to obtain chiral β -amino acids or precursors thereof include (I) the diastereoselective addition of chiral amines to prochiral α , β -unsaturated ester acceptors, (II) the diastereoselective addition of an amine nucleophile to a Michael acceptor incorporating a chiral auxiliary as a chiral inductor or (III) the enantioselective addition of an achiral amine to a prochiral acceptor using chemo- or biocatalysts. Examples of methods I and II have been reviewed in [53] and [54]. Method III has been studied extensively for the synthesis of short-chain β -amino acids also under investigation in this study by Weiß using chemocatalysts [138]. Particularly, bicyclic amidine and phase transfer catalysts were applied. The success with regard to enhancement of reaction rates and particularly enantioselectivity was unfortunately limited yielding in the best case a maximum of 22 % *ee* at 30 % catalyst loading. Various hydrolytic enzymes including esterases and lipases [15, 17, 63, 122, 124, 128], proteases [15, 16] and acylases [100] have been described to catalyze C-C, C-N and C-S-bond forming reactions via Michael-type addition. A hypothetical model for the catalytic mechanism has been proposed [124]. Stabilization of the activated acceptor

¹This chapter has in part been published in [123].

3 Aza-Michael addition

seems to occur by the oxyanion hole while the Michael donor is activated by conserved histidine and aspartate residues of the catalytic triad of hydrolases (Figure 3.2). Thus far, however, enantioselectivity in biocatalytic Michael type additions has only been reported by Kitazume in 1986 [63].²

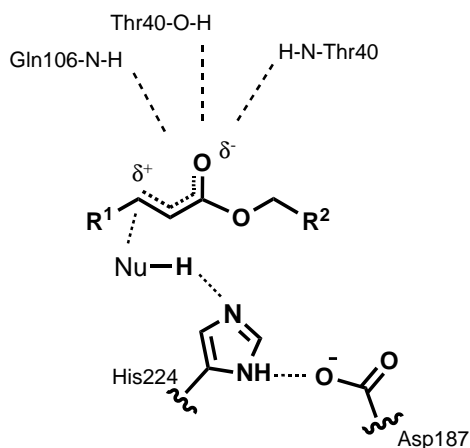


Figure 3.2: General scheme of *Candida antarctica* lipase B catalyzed Michael addition of thiol, amine- or carbon nucleophile to α, β -unsaturated carbonyl.

The direct and efficient asymmetric synthesis of short-chain aliphatic β -amino acids via aza-Michael addition remains difficult to achieve by chemo- or biocatalytic means despite advances in the field within the last decade [146]. An efficient method to the same class of compounds comprising a non-catalyzed aza-Michael addition and a subsequent biocatalytic kinetic resolution was developed by Weiß et al. [138, 140]. The chemoenzymatic reaction sequence as depicted in Figure 3.3 can be carried out under solvent-free conditions.

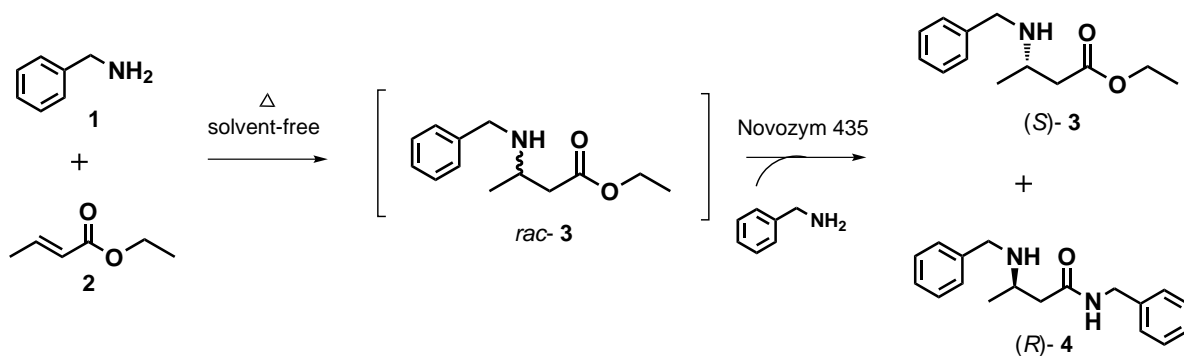


Figure 3.3: Chemoenzymatic reaction sequence for the synthesis of β -amino acid ester (*S*)-**3**.

²The results from [63] could unfortunately not be reproduced in this study.

3.1 Thermodynamic aspects

The aza-Michael addition of benzylamine (**1**) and *trans*-ethyl crotonate (**2**) as the first step is carried out thermally without addition of chemo- or biocatalysts. However, while the target ester *rac*-**3** is formed as the main product, HPLC analysis revealed the slow formation of the amide **4** as a side product. Additionally, the formation of the unsaturated crotonamide *trans*-*N*-benzyl-but-2-enamide (**5**) was detected in trace amounts. Thus, two pathways for the formation of *rac*-**4** may be considered as depicted in Figure 3.4: the formation of *rac*-**3** with subsequent aminolysis of the ester (route A) or the (slow) aminolysis of **2** leading to **5** followed by a rapid aza-Michael addition to form *rac*-**4** (route B). In order to elucidate the possibility of a pathway via the unsaturated crotonamide **5**, the compound was synthesised and purified via chromatography and crystallization. However, no formation of *rac*-**4** was detected when starting from **1** and **5** as substrates. On the other hand, the synthesis of amide **4** could be detected when starting from **1** and *rac*-**3**. Neither a reverse aza-Michael addition nor an ethanolysis of *rac*-**4** could be observed in detectable quantities. Therefore, the irreversible aza-Michael addition reaction of **1** with **2** followed by the successive aminolysis of *rac*-**3** with **1** according to route A in 3.4 was devised as a model for the kinetic characterization.

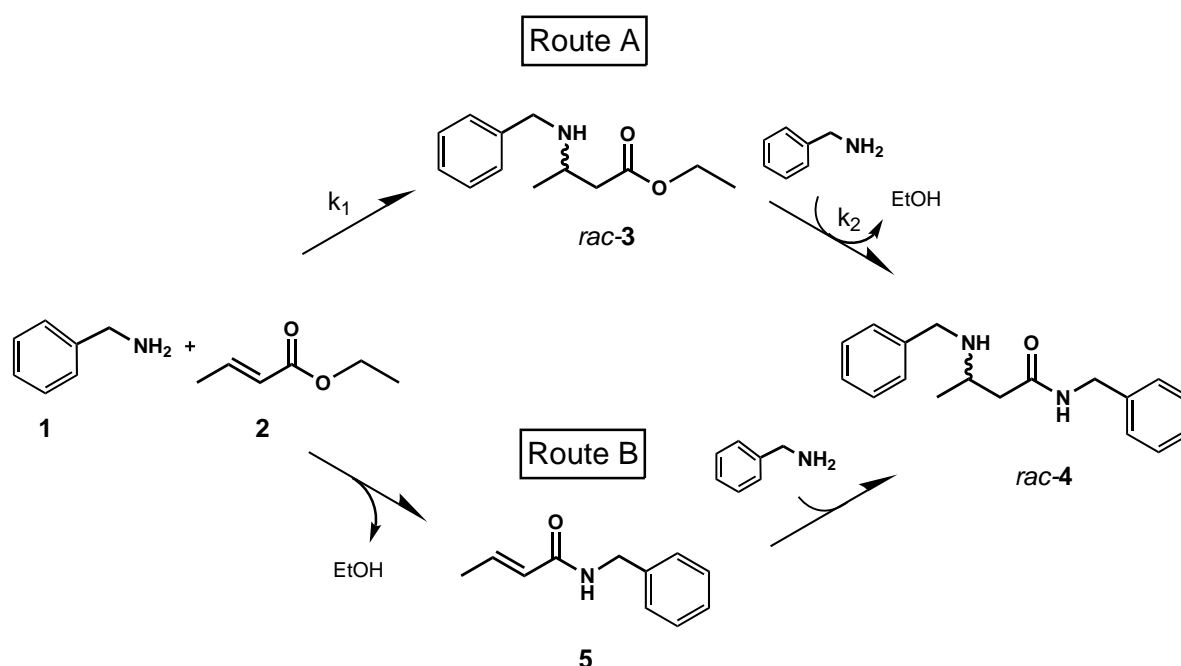


Figure 3.4: Potential routes towards the amide side product *rac*-**4**.

3.2 Kinetic aspects

Most bimolecular reactions follow second-order kinetics. In this case, the consumption of substrate A in a reaction with substrate B can be described by the following equation 3.1 with the reaction order being $\alpha + \beta = 2$.

$$-\frac{[A]}{dt} = k \cdot [A]^\alpha \cdot [B]^\beta \quad (3.1)$$

Two "classical" strategies are commonly applied for the determination of kinetic constants in chemical reactions that do not involve complex catalytic mechanisms. One approach involves the use of a large excess of one substrate over the other. The concentration of the excess substrate can then be considered constant and Equation 3.1 is converted into a pseudo-first order reaction rate dependent only on the concentration of one substrate. The resulting rate equation can easily be integrated to $\ln([A]/[A]_0) = k \cdot t$ where k can be derived from plotting $\ln([A]/[A]_0)$ vs. t . In a second approach, equal concentrations of A and B are applied leading to an integrated rate equation $1/[A] - 1/[A]_0 = k \cdot t$ that can likewise be used to obtain k by linear regression from a plot of $1/[A] - 1/[A]_0$ vs. t . The latter approach has been used here for a reaction carried out at 60 °C and yielded the kinetic rate constant $k_{BA} = 5.7 \times 10^{-2} \text{ g mmol}^{-1} \text{ h}^{-1}$ for the diminishment of benzylamine (**1**) and $k_{tEC} = 4.9 \times 10^{-2} \text{ g mmol}^{-1} \text{ h}^{-1}$ for *trans*-ethyl crotonate (**2**). The difference in the observed rate constants can be related to the subsequent side reaction forming *rac*-**4** from **1** and *rac*-**3**. Thus, k_1 in Figure 3.4 is represented as $k_1 = k_{tEC} = 4.9 \times 10^{-2} \text{ g mmol}^{-1} \text{ h}^{-1}$ and k_2 can be estimated to be $k_2 = k_{BA} - k_{tEC} = 7.8 \times 10^{-3} \text{ g mmol}^{-1} \text{ h}^{-1}$. The described approach being facile and quick is, however, more prone to errors since parameter estimation is solely based on a single substrate ratio.³

Numerical integration of the rate equations in combination with non-linear fitting of the experimental data represents an alternative, powerful strategy for parameter determination and verification. No restrictions with regard to the applied substrate ratio emerge using this technique. Assuming route A in Figure 3.4 as the reaction course and simple second-order kinetics, the respective rate equations for each compound can be outlined as follows (Equation 3.2-3.5):

$$\frac{d[\mathbf{1}]}{dt} = -k_1 \cdot [\mathbf{1}] \cdot [\mathbf{2}] - k_2 \cdot [\mathbf{1}] \cdot [\textit{rac} - \mathbf{3}] \quad (3.2)$$

$$\frac{d[\mathbf{2}]}{dt} = -k_1 \cdot [\mathbf{1}] \cdot [\mathbf{2}] \quad (3.3)$$

$$\frac{d[\textit{rac} - \mathbf{3}]}{dt} = k_1 \cdot [\mathbf{1}] \cdot [\mathbf{2}] - k_2 \cdot [\mathbf{1}] \cdot [\textit{rac} - \mathbf{3}] \quad (3.4)$$

³The goodness of fit was $R^2=0.995$ for k_{BA} and $R^2=0.972$ for k_{tEC} , respectively. Standard deviations cannot be given using this method here, since only single reactions were analyzed.

$$\frac{d[rac - \mathbf{4}]}{dt} = k_2 \cdot [\mathbf{1}] \cdot [rac - \mathbf{3}] \quad (3.5)$$

Batch experiments were then carried out on ~ 0.5 g scale with different molar ratios of the two substrates **1** and **2** and at different temperatures in the range from 40 °C to 70 °C. Applying the procedure of numerical integration of the rate equations and non-linear fitting, the kinetic constants k_1 and k_2 summarized in Table 3.1 for different temperatures were obtained.

Table 3.1: Kinetic parameters for aza-Michael addition.

T [°C]	k_1 [g · mol ⁻¹ · h ⁻¹] · 10 ⁻²	k_2 [g · mol ⁻¹ · h ⁻¹] · 10 ⁻³
40	2.52 ± 0.06	0.19 ± 0.11
50	3.70 ± 0.10	0.40 ± 0.11
60	6.10 ± 0.13	0.72 ± 0.13
70	9.68 ± 0.41	1.17 ± 0.20

Figure 3.5 accordingly shows the concentration-time profile of experimental and simulated data for the substrates **1** and **2** and the products *rac-3* and *rac-4*, respectively, for a reaction carried out at 60 °C. Parameters obtained for k_1 and k_2 using the integration and linear regression technique as described above or using the non-linear regression methodology were of the same order of magnitude.

Validation of the determined kinetic parameters was demonstrated by application for the prediction of the progress curve of a reaction with a starting mole fraction not considered for parameter estimation. As shown in Figure 3.6, the reaction course of all compounds can be described accurately with the given parameters.

Activation energies of $E_{A,1} = 40.4$ kJ mol⁻¹ (R²=0.995) and $E_{A,2} = 54.3$ kJ mol⁻¹ (R²=0.995) were calculated for the aza-Michael addition and successive side reaction according to Arrhenius Law and can be used to calculate the kinetic constants at temperatures for which no experimental data is available.

3.3 Reaction engineering aspects

Based on the kinetic model (Equation 3.2 - 3.5) including the kinetic constants as summarized in table 3.1, the fundamental process engineering parameters conversion, selectivity and yield can be simulated for various temperatures (Figure 3.7a). As expected, increasing temperature accelerates the reaction. Within ~ 18 h full conversion of the limiting substrate **2** is reached at 70 °C in a reaction with a 2:1 molar excess of **1** over

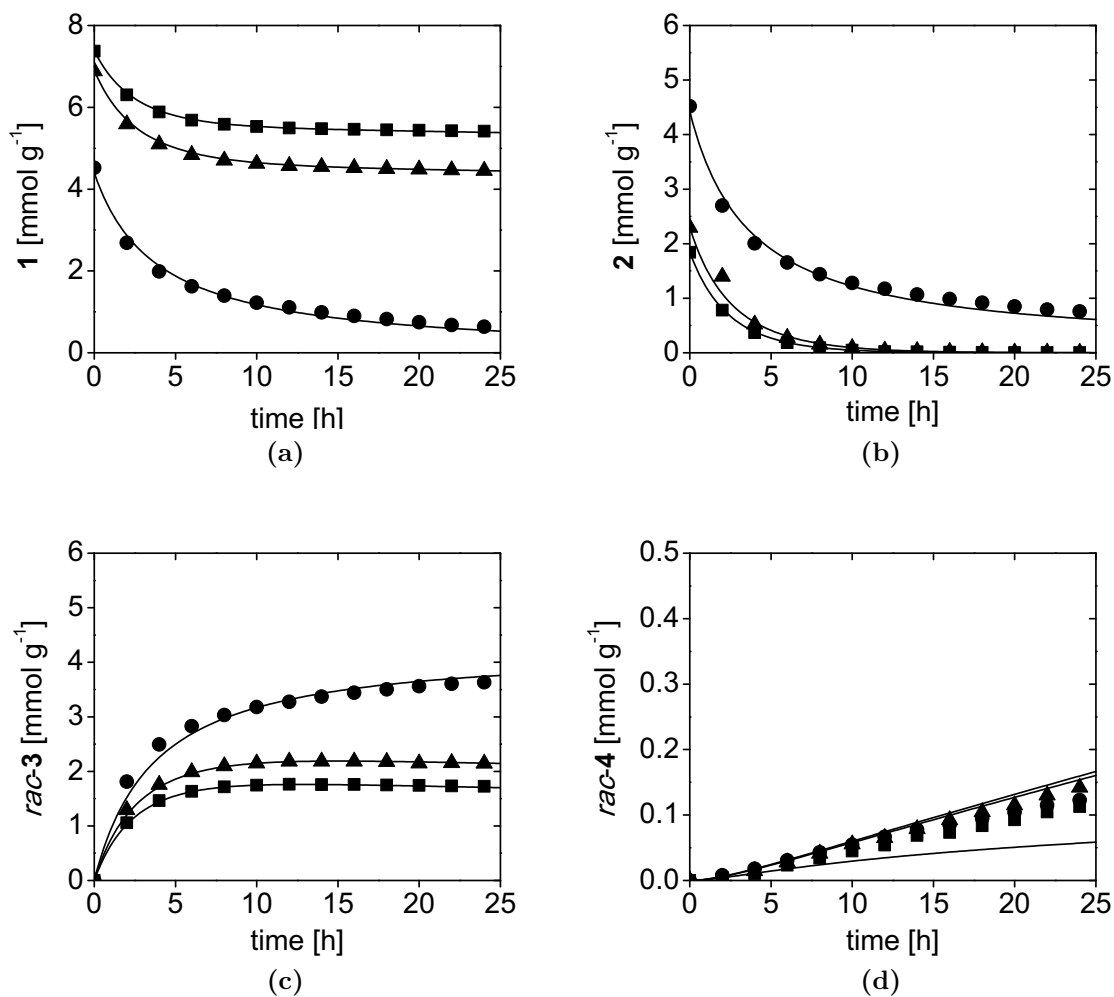


Figure 3.5: Progress curve of the solvent-free aza-Michael addition of benzylamine (**1**) and *trans*-ethyl crotonate (**2**) at 60 °C. Starting molar ratios of **1** and **2** were 1:1 (●), 3:1 (▲) and 4:1 (■) mole eq. (a) Depletion of **1**. (b) Depletion of **2**. (c) Formation of target product *rac*-**3**. (d) Formation of successive side product *rac*-**4**. Non-linear regression was performed according to Equation 3.2-3.5.

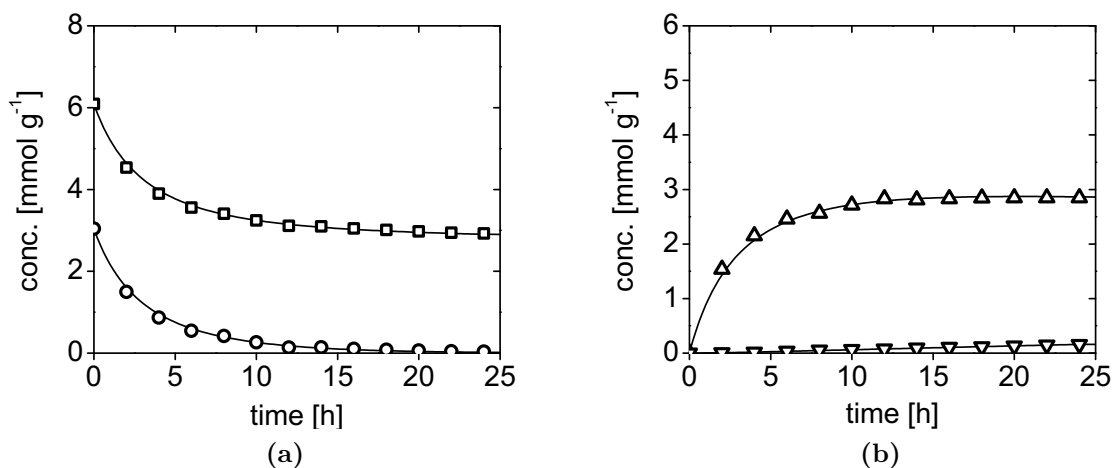


Figure 3.6: Simulation of progress curve of solvent-free aza-Michael addition with starting molar ratio of substrates **1** and **2** of 2:1 mole equivalents at 60 °C. Parameters used were those summarized in Table 3.1. (a) Depletion of substrates **1** (□) and **2** (○). (b) Formation of main product *rac-3* (△) and side product *rac-4* (▽).

2 while already ~25 h are needed at 60 °C. A maximum obtainable yield of 0.947 is reached after 13 h at 70 °C (Figure 3.7c). Further conversion leads to an increased formation of the successive side product **4** as indicated by the decreasing selectivity (Figure 3.7b), thus reducing yield.

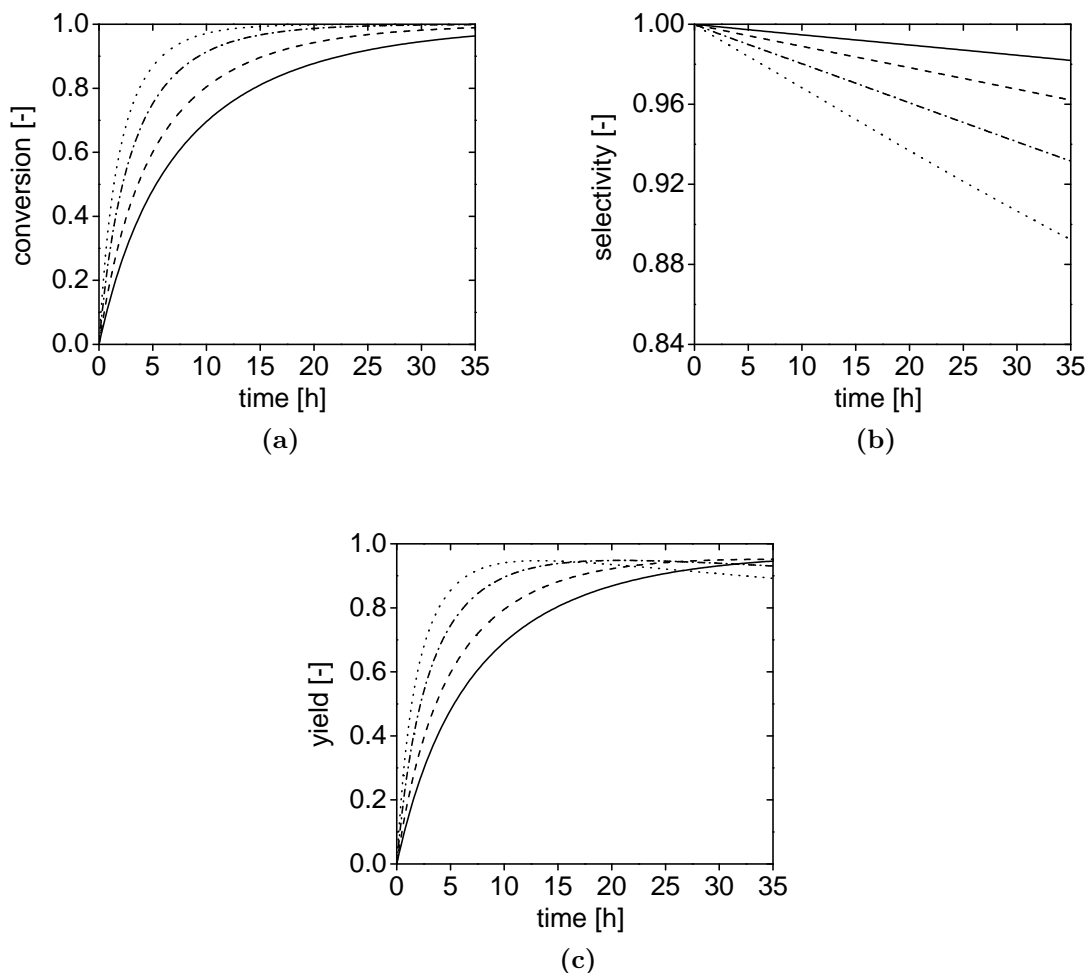


Figure 3.7: Fundamental reaction engineering parameters as a function of time in thermal aza-Michael addition at 2:1 molar ratio of substrates **1** and **2**. (a) conversion, (b) selectivity and (c) yield. (–) 40 °C, (– –) 50 °C, (– · –) 60 °C, (···) 70 °C.

Plotting yield and selectivity as a function of conversion, the differences in the maximum obtainable yields depending on temperature become obvious (Figure 3.8). At 40 °C a maximum yield of 0.964 can be achieved. On the other hand, the necessary reaction time is > 50 h, thus dramatically lowering the space-time yield compared to a reaction carried out at 70 °C.

The space-time yield (STY) can be calculated from the yield, the reaction time and the necessary volume. The yield depends on temperature, conversion and on the substrate ratio. A density of approximately 0.99 g ml⁻¹ at 20 °C and volume increase of 3.6 % upon heating from 20 °C to 70 °C were determined experimentally for a 2:1 mole eq. mixture of **1** and **2**. Increasing conversion led to a decreased volume. For calculation of the STY, the initial volume was considered. The subsequent enzymatic step, atom efficiency aspects and reduced downstream processing efforts demand the achievement of maximum reaction yields. Therefore, the time necessary to obtain such high yields is

considered for STY calculation despite the fact that reduced reaction rates with increasing conversion lead to a lower STY. The highest STY of $1.06 \text{ kg L}^{-1} \text{ d}^{-1}$ was obtained at $70 \text{ }^\circ\text{C}$, which corresponds to the highest temperature tested.

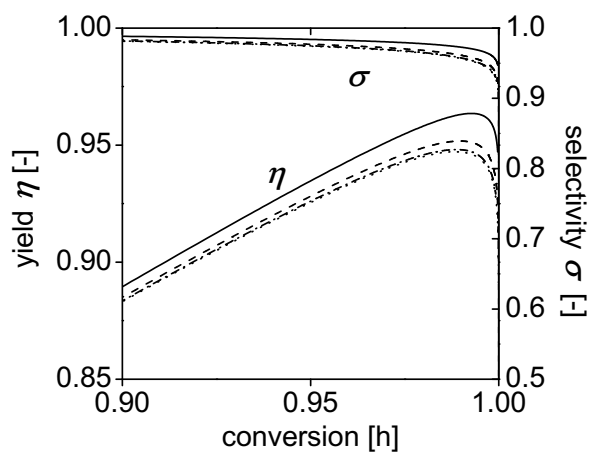


Figure 3.8: Yield η and selectivity σ as a function of conversion in thermal aza-Michael addition at 2:1 molar ratio of substrates **1** and **2**. (—) $40 \text{ }^\circ\text{C}$, (---) $50 \text{ }^\circ\text{C}$, (-·-) $60 \text{ }^\circ\text{C}$, (···) $70 \text{ }^\circ\text{C}$.

3.4 Summary

This chapter covered the characterization of the solvent-free aza-Michael addition of benzylamine (**1**) and *trans*-ethyl crotonate (**2**) towards *rac*-**3** as the first step in the chemo-enzymatic synthesis of ethyl-(*S*)- β -amino butyrate. The following observations have been made:

- The reaction pathway was proven to proceed solely via aza-Michael addition in a first step and an aminolytic side reaction as a second, subsequent step.
- The reactions can be considered irreversible within limits of detection.
- The aza-Michael addition follows simple second-order kinetics. Kinetic parameters for both aza-Michael addition and aminolysis were determined in the temperature range from 40-70 °C.
- Activation energies of $E_{A,1} = 40.4 \text{ kJ mol}^{-1}$ and $E_{A,2} = 54.3 \text{ kJ mol}^{-1}$ were determined for both steps and allow the simulation of reactions carried out at temperatures not investigated experimentally.
- At a starting molar ratio of 2:1 of substrates **1** and **2**, a maximum space-time yield of $1.06 \text{ kg L}^{-1} \text{ d}^{-1}$ was achieved at the highest temperature tested in batch mode of 70 °C. Lower temperatures only slightly improve selectivity while the necessary reaction time to obtain maximum yields is considerably elongated.

4 Biocatalytic aminolysis¹

Candida antarctica lipase B (CALB) immobilized on acrylic resin, which is commercially available as Novozym 435 from Novozymes, Denmark, catalyzes the kinetic resolution of *rac*-**3** with benzylamine (**1**) according to Figure 4.1. The reaction can be carried out under solvent-free conditions at elevated temperatures.

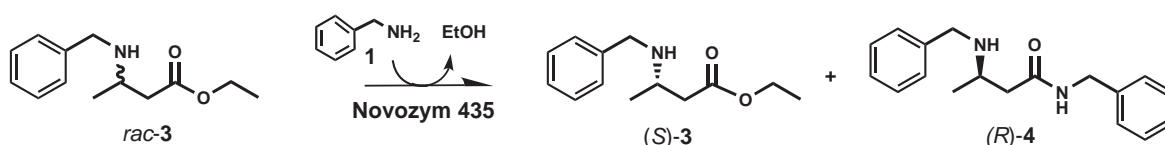


Figure 4.1: Novozym 435-catalyzed aminolysis for the kinetic resolution of *rac*-**3**.

The enantioselectivity of an enzyme-catalyzed reaction is mainly determined by the structure of the active site and the interactions of particular active site amino acids with the substrate. Improvement of the enantioselectivity of a biocatalyst can effectively be achieved using random mutagenesis strategies, rational design as well as combinations thereof [9]. In addition, several physicochemical parameters commonly influence the enantioselectivity of enzyme-catalyzed kinetic resolutions, in particular solvent, temperature and pressure [18]. These parameters are addressed in this chapter and in chapter 7. In literature, a large number of enzyme-catalyzed kinetic resolutions are described with a majority being related to the hydrolase-catalyzed resolution of prochiral alcohols [33]. The separation of racemic carboxylic acids or esters can also be readily achieved via esterification or transesterification using the same class of enzymes. Kinetic resolutions of prochiral amines or esters with amines as nucleophiles have been realized, even though less frequently. The mechanism generally proceeds via the well-known catalytic triad mechanism of lipases, which is depicted in Figure 4.2 on the next page.²

The nucleophile attacking the acyl-intermediate in step I can be either an amine or an alcohol. Aminolysis reactions usually proceed more slowly compared to transesterifications with alcohols, while at the same time enantioselectivities are generally improved. The lower reaction rates are probably due to the higher pK_a value of amines causing a decreased hydrogen transfer rate from the neutral amine to the histidine residue in step I of Figure 4.2. The better selectivity can be explained by an increased stability of the produced amide [26].

¹Parts of this chapter have been published in [123]

²Abbreviated form, the acyl-intermediate of step I is itself formed via an activated intermediate.

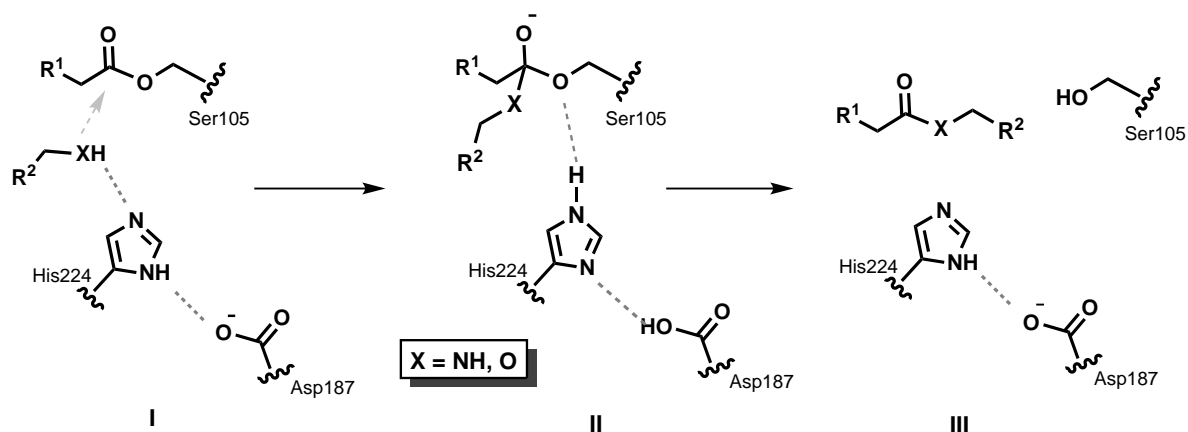


Figure 4.2: Mechanism of ester cleavage via acyl-enzyme intermediate. The nucleophile can either be an amine or an alcohol. Figure according to [26].

With regard to the economic feasibility of a process, factors such as the selectivity of the biocatalytic reaction and enzyme kinetics play a crucial role. Both these criteria and enzyme stability largely depend on the reaction system applied. In solvent-free reactions as investigated here, high space-time yields can generally be achieved and thus carry an inherent advantage compared to solvent-systems. This chapter is devoted to the characterization of such a solvent-free system for the production of an industrially interesting β -amino acid precursor via kinetic resolution of a racemic β -amino acid ester.

4.1 Selectivity of Novozym 435

The Novozym 435-catalyzed, solvent-free kinetic resolution of *rac*-**3** with benzylamine as depicted in Figure 4.1 has been reported to proceed enantioselectively with an *E*-value of 27 at 60 °C by Weiß and Gröger [138, 140]. The *E*-value was calculated according to Equations 1.1 and 1.2 on page 3 from X/ee_p and ee_s/ee_p -values at a single conversion point, respectively.

The enantioselectivity of the same Novozym 435-catalyzed reaction is shown in Figure 4.3 as a conversion vs. *ee*-plot. The reaction was carried out with an initial molar fraction of $\chi_{rac-3} = 0.5$ at 60 °C. Approximately 60 % conversion are needed to obtain an attractive $ee_{(S)-3}$ of > 99% in the solvent-free reaction. Thus, (*S*)-**3** is also slowly converted to the corresponding amide (*S*)-**4**. Equation 4.1 can be used to determine the value of *E* by nonlinear regression according to the procedure suggested by Rakels et al. [102].

$$ee_p = \frac{ee_s}{\left[\frac{(1+ee_s)^E}{(1-ee_s)} \right]^{1/(E-1)} - 1} \quad (4.1)$$

An *E*-value of 32 was determined using this method. Among other phenomena, diffusional limitations and side reactions can interfere in the accurate determination of *E*

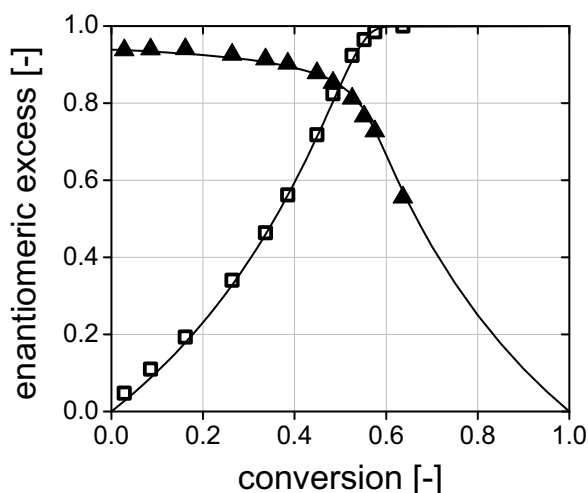


Figure 4.3: Selectivity of the Novozym 435-catalyzed solvent-free kinetic resolution of *rac*-**3** via aminolysis at 60 °C ($\chi_{0, rac-3} = 0.5$, $\chi_{0,1} = 0.5$, $0.152 \text{ g}_{N435} \text{ g}^{-1}$). (□): ee of substrate **3**; (▲): ee of product **4**.

[120]. A possible diffusion limitation using an immobilized enzyme on a porous carrier was excluded by observing equal reaction rates using pestled lipase Novozym 435 instead of the intact carrier (see section 4.3 on page 33). The intrinsic enantioselectivity E of the enzyme may also be altered by spontaneous side reactions. Such a side reaction is to be expected here, since a thermal aminolysis reaction was observed in the Michael addition in section 3.1 on page 17, even though it proceeded very slowly. Therefore, an intrinsic enantioselectivity E of the enzyme and an apparent enantioselectivity E' is defined. The E -value as an intrinsic parameter depends on the values of k_{cat}/K_m for each enantiomer and is constant by definition. In the case of a solvent-free reaction, the composition of the medium changes with conversion and, thus, can have an impact on the enantioselectivity. However, the effect is considered negligible here, since fitting of the experimental data using the equations introduced previously for the calculation of E is possible.

4.1.1 Temperature effect on selectivity

The effect of temperature on enantioselectivity was investigated in the range from 40-80 °C in Figure 4.4. The respective apparent enantioselectivity E' was again determined by nonlinear regression using Equation 4.1 as described above for each temperature. The determined E -values could be used to fit ee_S and ee_P as a function of conversion.

Both E and E' are depicted as a function of temperature in Figure 4.5. E' was calculated from the rate constant of the overall reaction obtained from initial rate measurements, the rate constant for the spontaneous aminolysis (see Appendix, Table B.1 on page 111) and the apparent E' -value using the software Selectivity-KRESH.³ A dramatic linear decrease of both E and E' with increasing temperature is observed in the analyzed temperature range. Thus, mainly the loss of intrinsic enzyme selectivity accounts for the observed effect while the thermal side reaction does not contribute significantly to

³1995 by K. Faber, M. Mischitz, and A. Klewein. <http://www-orgc.tu-graz.ac.at/>.

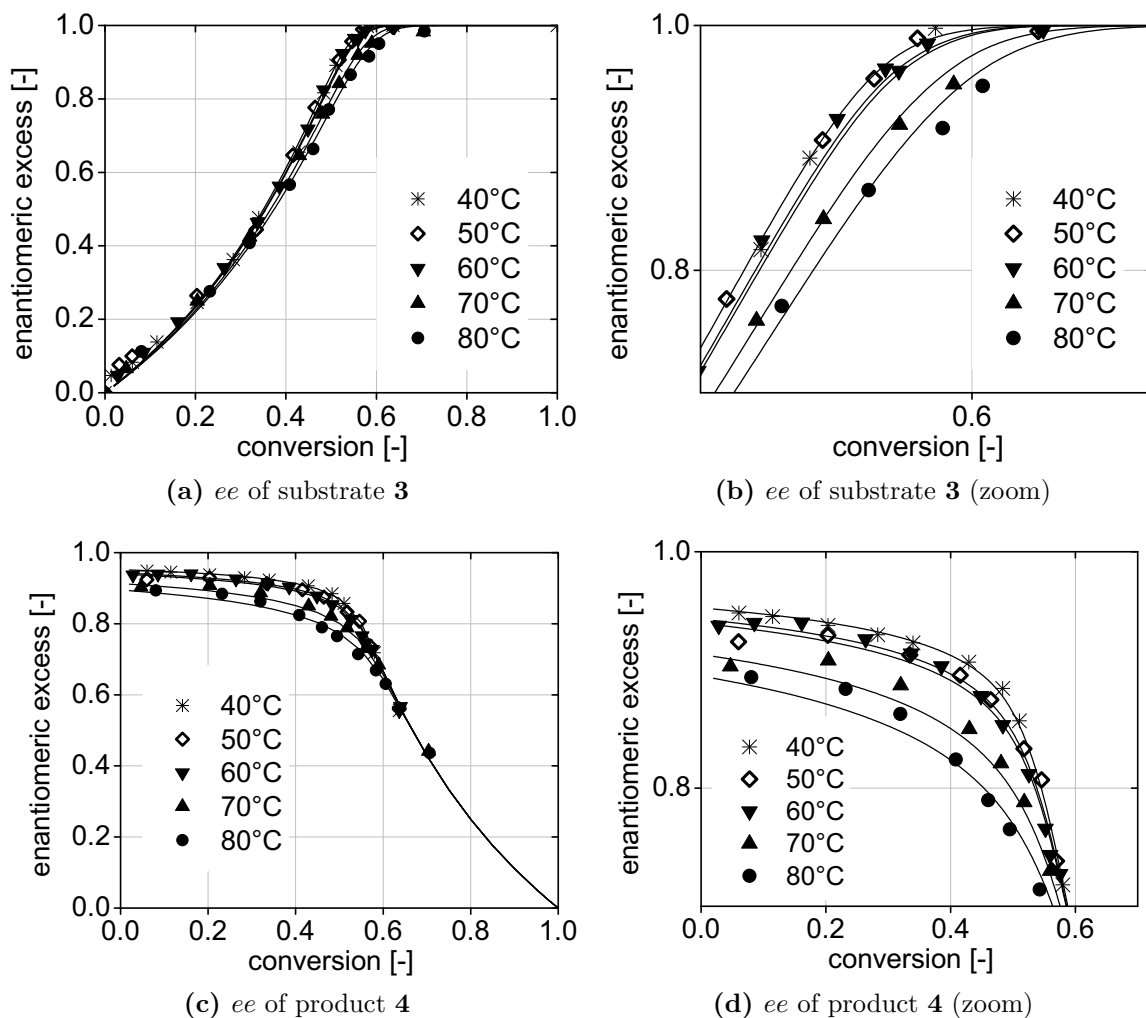


Figure 4.4: Temperature dependence of enantioselectivity of Novozym 435 in solvent-free kinetic resolution of *rac*-**3** via aminolysis. $\chi_{0,rac-3} = 0.5$, $\chi_{0,1} = 0.5$, $0.152 \text{ g}_{N435} \text{ g}^{-1}$.

the overall decrease of selectivity in the analyzed temperature range. Ottosson et al. analyzed temperature effects on enantioselectivity in a lipase catalyzed transesterification of secondary alcohols and found that both enthalpic and entropic changes contribute to the temperature dependence of E [96, 97]. Therefore, depending on the order of magnitude of each term, negative, neutral or positive effects of E with temperature may occur. Indeed, several examples of an at first glance somewhat unexpected increasing E value with temperature have been described in literature [8, 94]. Generally though, E decreases with increasing temperature which corresponds to the observation made here.

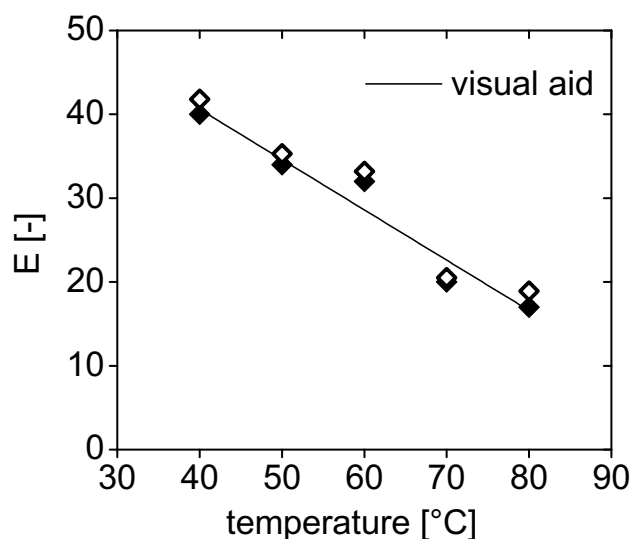


Figure 4.5: Enantioselectivity as a function of temperature in the Novozym 435-catalyzed solvent-free kinetic resolution of *rac*-**3** via aminolysis. (◆): E' ; (◇): E . $\chi_{0, rac-3} = 0.5$, $\chi_{0,1} = 0.5$, $0.152 \text{ g}_{N435} \text{ g}^{-1}$.

4.1.2 Selectivity in solvent system

The influence of different solvents was investigated by carrying out reactions in five different solvents of different polarity. The enantioselectivity E was calculated from the average of ee_S and ee_P -pairs. The respective conversion vs. ee -plots can be found in the appendix (B.1 on page 111). Figure 4.6 shows the obtained E -values as a function of solvent polarity expressed as $\log P$. Significant differences were observed depending on the solvent used with E -values ranging from 12 in *n*-hexane to 34 in tetrahydrofuran. A trend of decreasing enantioselectivity with increasing solvent hydrophobicity is seemingly observed. A correlation of solvent hydrophobicity and enantioselectivity has been reported previously, amongst others by Sakurai et al. and Terradas et al. [110, 127]. Hirose et al. even observed a complete change of enantiopreference in a lipase catalyzed kinetic resolution from 99 % (*R*)-preference in diisopropylether to 91 % (*S*)-preference in cyclohexane [44]. However, solvent hydrophobicity alone is not a generally valid indicator [30]. A correlation of the molecular size of the solvent with enantioselectivity was observed by Ottosson et al. [96]. Similar trends but with significant scattering of the data were found here when plotting E -value vs. other polarity scales (π^* , $E_T(30)$; data not shown).⁴ Therefore, a larger number of data from further solvents is required

⁴See section 4.4.1 on page 35 for details on polarity scales

in order to show if the observed correlation with $\log P$ can be verified or if it is merely coincidental.

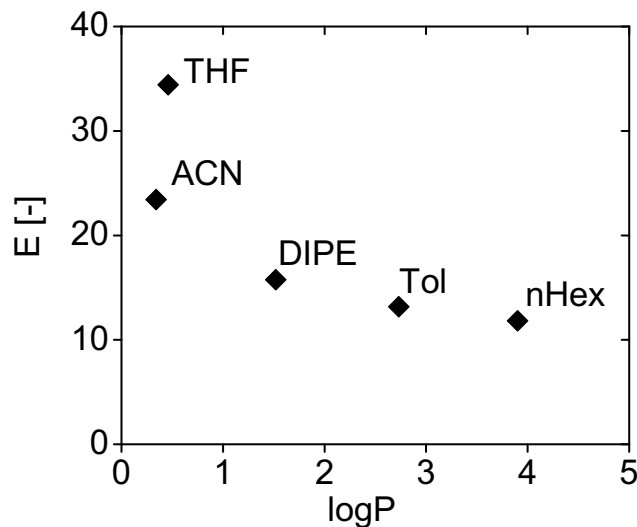


Figure 4.6: Dependence of enantioselectivity on solvent polarity expressed as $\log P$. ACN: acetonitrile; THF: tetrahydrofuran; Tol: toluene; DIPE: diisopropylether; nHex: *n*-hexane. 0.2 M of **1** and *rac*-**3**, 45 mg_{N435} ml⁻¹, 60 °C.

4.1.3 Selectivity in solvent-free system

In a solvent-free reaction system polarity of the medium depends on the initial mole fraction χ of the two substrates *rac*-**3** and **1** and was found to decrease with χ_{rac-3} (see section 4.4.1 on page 35). However, only minor differences were observed in enantioselectivity using different substrate mole fractions in the range from $\chi_{rac-3} = 0.5 - 0.8$. At $\chi_{rac-3} = 0.33$ a significantly lower E' -value is noted (Table 4.1).

Table 4.1: Apparent enantioselectivity E' at different initial substrate mole fractions.

χ_{rac-3}	0.33	0.5	0.6	0.67	0.8
E'	17	31	32	31	30

Simulations using the kinetic model introduced in section 4.4.5 on page 42 revealed, however, that the apparent loss of selectivity is caused entirely by the chemical side reaction. Figure 4.7 shows the experimental and simulated conversion vs. *ee*-plot of a reaction with an initial molar fraction of $\chi_{rac-3} = 0.33$. The term for the uncatalyzed side reaction was erased from the model and a new conversion vs. *ee*-plot simulated. The analogous procedure was applied for the reaction with an initial mole fraction of $\chi_{rac-3} = 0.67$. Simulated data of the latter reaction did not reveal noticeable differences with and without consideration of the side reaction due to the high reaction rate of

the enzymatic reaction. In the case of the reaction with an initial mole fraction of $\chi_{rac-3} = 0.33$ the enzymatic reaction is significantly slower leading to a larger impact of the blind reaction and a significant shift of the conversion vs. ee plot. Additionally, a significant enzyme deactivation at high benzylamine concentrations leads to a further reduction of the enzyme catalyzed reaction rate (see section 4.2 on page 31). Thus, only the side reaction impacts E' , whereas polarity changes in the solvent-free reaction investigated here have no or negligible influence on the enantioselectivity of Novozym 435.

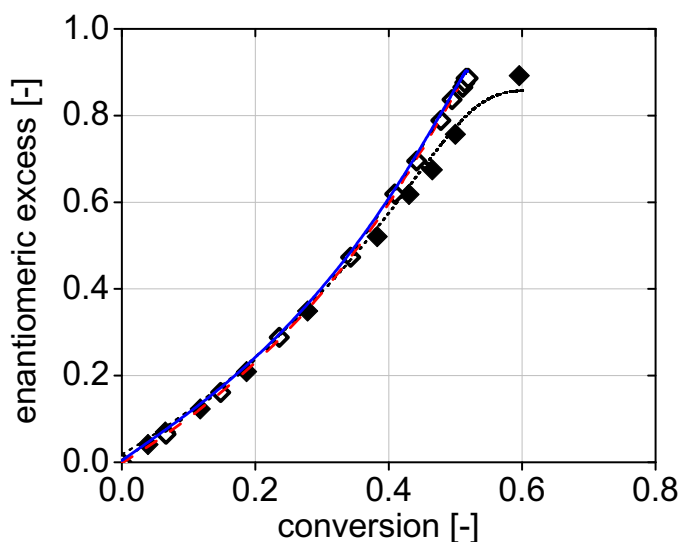


Figure 4.7: Influence of substrate ratio and uncatalyzed side reaction on enantioselectivity. \blacklozenge : experimental data, $\chi_{rac-3} = 0.33$; \diamond : experimental data, $\chi_{rac-3} = 0.67$; $(\cdot \cdot \cdot)$: simulation using kinetic model including side reaction, $\chi_{0,rac-3} = 0.33$; $(- -)$: simulation using kinetic model without side reaction, $\chi_{0,rac-3} = 0.33$; $(-)$: simulation using kinetic model with and without side reaction, $\chi_{0,rac-3} = 0.67$. $0.152 \text{ g}_{N435} \text{ g}^{-1}$, 60°C .

4.2 Stability of Novozym 435

In many industrial applications, catalyst costs represent a major factor determining the overall economics of a process. Large quantities of product formed per unit of catalyst expressed by a high total turnover number ttn are highly desired, while at the same time high space-time yields should be reached. Therefore, enzyme stability is crucial in process optimization and temperature a decisive physical parameter. On the one hand, high temperature is known to cause partial or complete enzyme denaturation and thus loss of catalytic activity. On the other hand, enzyme activity generally increases with temperature by a factor of 2-3 per 10°C [42]. Immobilized *Candida antarctica* lipase B is considered a very robust enzyme for which applications of up to 160°C can be found in literature [98]. Continuous processes carried out at $60\text{-}80^\circ \text{C}$ have been described without significant loss of activity after several thousand hours of operation [2]. Apart from temperature and pressure⁵, further physicochemical parameters of the solvent, ionic strength, pH in aqueous systems or polarity of an organic solvent affect the stability by interacting with the amino acid side chains of the protein or by stripping of essential water molecules from the enzyme surface. In this study, the stability of Novozym 435

⁵See chapter 7.3 on page 85 for pressure effects on stability

4 Biocatalytic aminolysis

was tested under reaction conditions by incubation in a solvent-free system at a molar fraction of $\chi_{rac-3} = 0.5$ in the range from 60-75 °C (Figure 4.8). The deactivation constant k_{deact} was determined by exponential fitting of the residual activity vs. time using Equation 4.2.

$$[Enz.] = [Enz.]_0 \cdot e^{-k_{deact} \cdot t} \quad (4.2)$$

A deactivation constant of $k_{deact} = 0.007 \text{ h}^{-1}$ was found at 60 °C, which corresponds to a half-life time of about 100 days. Towards higher temperatures a significantly increasing thermal deactivation was observed.

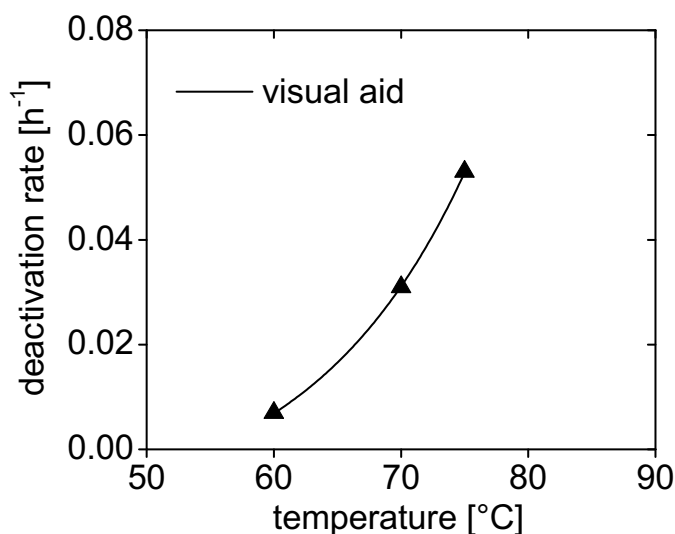


Figure 4.8: Temperature dependence of stability of Novozym 435 in solvent-free system. $\chi_{rac-3} = 0.5$.

Additionally, the stability of lipase Novozym 435 under reaction conditions by incubation in solvent-free substrate mixtures of different composition was tested. At low mole fractions of *rac-3* a rapid loss of activity was observed. No activity was recovered after incubation of Novozym 435 for 15 min in pure benzylamine. Both the increased polarity and basicity of the substrate benzylamine may be responsible for the observed inactivation, as more polar solvents increasingly strip water molecules that are essential for activity from the enzyme surface [149]. Maximal stability under the applied conditions was found around $\chi_{rac-3} = 0.67$, where after two days a loss of less than 10 % of the initial activity was observed. A less dominant but noticeable decrease of stability towards higher concentrations of *rac-3* was observed somewhat unexpectedly. It may be speculated that the effect can be attributed to the formation of low concentrations of the corresponding acid when the concentration of benzylamine as the target nucleophile is reduced and the hydrolytic side reaction with residual water as a competing nucleophile becomes more significant. Hollmann et al. reported the irreversible inactivation of CALB by strong acids with pK_a values below 4.8 [45]. No data on the pK_a -value of the potentially formed β -(benzylamino)butanoic acid is available in literature. However, reported pK_a -values for β -alanine and γ -aminobutyric acid for example are 3.6 and 4.28,

respectively, indicating that the value for the formed acid here may well be below 4.8.⁶ Comparing both thermal and medium effects on stability, the latter is certainly more predominant. Below $\chi_{rac-3} = 0.4$ the deactivation constant k_{deact} quickly rises an order of magnitude above the deactivation constant noted at 75 °C.

$$k_{deact} = e^{6.7 - 38.7 \cdot \chi_{rac-3} + 28.0 \cdot \chi_{rac-3}^2} \quad (4.3)$$

An empirical exponential function with 3 parameters (Equation 4.3) was used to fit the experimental data on k_{deact} as a function of the substrate mole fraction. In combination with Equation 4.2, this correlation can be implemented into kinetic models for prediction of reactor performance under varying conditions. This has been done in section 4.6 on page 46 for an estimation of the performance of a fed batch reactor and in section 6.3 on page 73 for a continuous packed bed reactor.

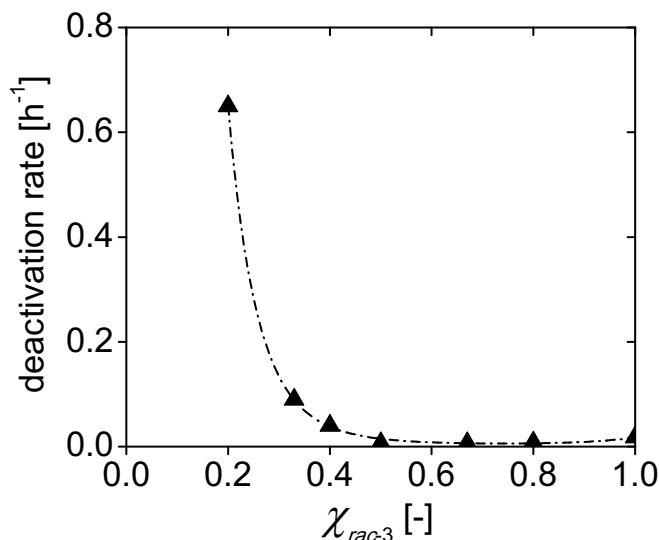


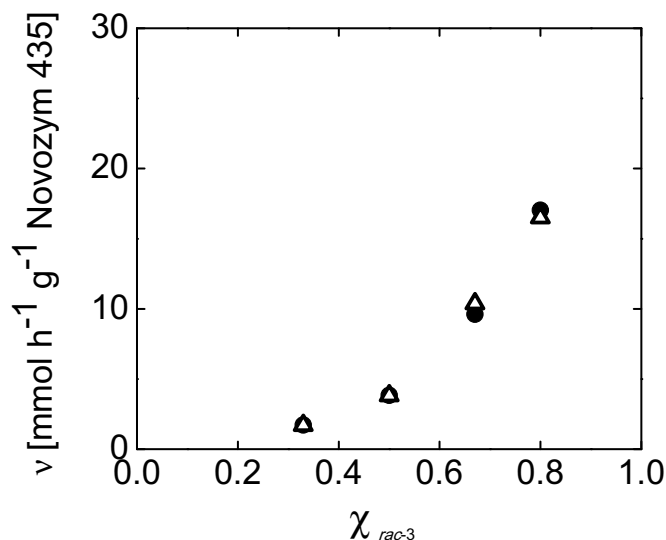
Figure 4.9: Stability of Novozym 435 as function of initial substrate mole fraction in solvent-free system at 60 °C.

4.3 Diffusion limitation

External and internal diffusion limitations may be observed when heterogenous biocatalysts immobilized on porous supports are used. A possible internal diffusion limitation in the Novozym 435-catalyzed aminolysis of *rac-3* with **1** was examined by carrying out experiments using pestled Novozym 435 and subsequent comparison with the reaction rates observed using intact Novozym 435. Figure 4.10 shows similar reaction rates for both pestled and intact Novozym 435 for all tested substrate mole fractions. A possible external diffusion limitation was minimized by magnetic stirring. Therefore, diffusion limitation was excluded as a rate limiting factor.

⁶Data from "Dawson, R.M.C. et al., Data for Biochemical Research, Oxford, Clarendon Press, 1959".

Figure 4.10: Investigation of diffusion limitation by comparison of initial reaction rates in Novozym 435-catalyzed aminolysis of *rac*-**3** using intact (●) and pestled (△) enzyme carrier.



4.4 Enzyme kinetics

In order to optimize the reaction, detailed knowledge of the factors influencing enzyme kinetics in the given system is required. Several attempts have been made to study the kinetics of solvent-free, enzyme catalyzed reactions [6, 78, 136, 145]. In the majority of such synthetic examples, the investigated reactions systems are esterifications and transesterifications using immobilized lipases. However, up to this point no generally valid strategy for the determination of intrinsic enzyme kinetic parameters has been established. Blackmond recently described a valuable procedure for the determination of kinetic properties of even complex bio- and chemocatalytic systems [7]. The approach allows to extract a large amount of information from only a limited number of experiments by investigating the full reaction progress rather than focusing on initial rates. An *in situ* method for the continuous collection of experimental data is required. Additionally, the necessary "excess" experiments⁷ are limited to solvent systems and cannot be applied directly in a solvent-free system.

On the other hand, much effort has been put on the description of enzyme action in organic solvents. Particularly, many attempts have been made to correlate observed effects on enzyme activity or selectivity to physicochemical properties of the solvent [18, 64]. An obvious dependency on the solvent polarity expressed by logP values was described by Laane et al. [67]. The effect could be related to an increased stripping of essential water molecules from the enzyme surface by hydrophilic solvents. At a constant level of enzyme bound water, similar activities were observed by Zaks and Klivanov [149].

The implementation of thermodynamic activities in order to account for solvation of the reactants instead of their concentrations as a concept in enzyme kinetics has been shown to allow the determination of intrinsic parameters independent of the solvent used (for selected examples see: [8, 51, 111, 112, 118, 132]). However, only initial rates

⁷In two-substrate reaction systems, experiments are carried out with the same excess of one substrate over the other, but different absolute concentrations.

were investigated in these studies. Additionally, solvent effects not accounted for by the use of thermodynamic activities were observed including possible enzyme inhibition by the solvent and altered amino acid mobility [112, 132]. It has been shown that solvent molecules may bind to enzymes at several places including the active site, thus influencing activity [31, 58].

Recently, the analysis of protein dynamics has allowed an improved insight into the importance of internal enzyme movement. Three-dimensional motions on different enzyme levels and time scales such as loop-, domain- or subunit motions may affect the catalytic properties of the enzyme even if the distance to the active site is quite large [129]. In organic solvents where enzyme motion is restricted and thought to be responsible for decreased enzyme activities, enzyme hydration has been shown to affect protein dynamics and electrostatics, thus enhancing activity [47].

In solvent-free kinetics, previously described direct and indirect effects extremely hamper the development of valid mechanistic models. While concentrations of all reactants change with conversion, so do the properties of the surrounding medium making up the "solvent", including factors such as polarity, viscosity, activity coefficients of all reagents and the ability to hydrogen bond. Thus, there are a number of unknown variables changing simultaneously. The direct evaluation of the enzyme kinetics in solvent-free media is therefore difficult. Consequently, the determination of kinetic data in an organic solvent and subsequent transfer to the solvent-free system seems to be a more promising approach and was therefore chosen in this study. It is likely, however, that upon the transfer to a different solvent- or solvent-free system further adaptation of the kinetic data is required.

As pointed out in section 1.2.2 on page 6, it is highly desired to use high substrate concentrations or even solvent-free reactions in biocatalytic processes. The kinetics of such reaction systems are of utter importance for choosing an appropriate fundamental reactor type [43]. From a practical point of view, it is wise to apply kinetic models as simple as possible that fit the experimental data sufficiently well [133]. Ideally, the model should describe the data in a broad concentration range, but most importantly must describe the reaction course accurately in the range of significance for practical application

4.4.1 Solvent polarity

Solvent properties including polarity have been proposed to affect enzyme performance both with regard to selectivity and activity [18, 64]. As described in section 4.1 on page 26, enantioselectivity largely depended on the solvent used, but was unaltered in solvent-free reactions using different substrate ratios. Activity on the other hand was observed to increase with increasing concentration of *rac*-**3** as discussed in detail in section 4.4.5. Sandoval et al. observed a linear relationship of ν_{max} to the mole fraction of two solvents (substrates in solvent-free system) or logP of the same mixtures in a lipase catalyzed esterification of oleic acid with ethanol [112]. Therefore, the polarity of the solvent-free medium was investigated. Several polarity scales have been introduced in literature. Especially the relative permittivity expressed by the dielectric

constant ε or the logP scale have been used frequently in association with biocatalytic reactions. The logP value represents the partition coefficient of the compound between a water and an octanol phase saturated with water. However, the experimental determination of logP is highly erroneous particularly in the case of basic or acidic substances. Thus, largely diverging values are found e.g. for benzylamine ranging from -2.35 to 3 in aqueous systems depending on the pH of the water phase.⁸ In addition, both the dielectric constant ε and the logP-scale take into account only bulk solvent effects. LogP values of solvent mixtures have consequently been determined using the simple relationship $\log P = \chi_A \cdot \log P_A + \chi_B \cdot \log P_B$ with χ_A and χ_B being the mole fractions of two compounds A and B [6], which by definition implies a linear relationship of $\chi_{A/B}$ and logP. However, effects on a microscopic level of the solute environment are neglected. As proposed by Reichardt, polarity covers the overall solvation capability including specific and non-specific interactions. The former include interactions such as electron-pair donor/electron-pair acceptor interactions, solvophobic interactions or hydrogen bonding interactions, but exclude those leading to definite chemical changes (protonation, oxidation, complex formation etc.) [106]. Certain compounds exhibit a pronounced change in UV absorption in different solvents caused by specific and non-specific interactions. The effect is called "solvatochromism". Reichardt's betaine dye 2,6-diphenyl-4-(2,4,6-triphenyl-1-pyridinio)-1-phenoxide, which is used to generate the $E_T(30)$ -scale⁹, or the π^* -scale¹⁰ based on 4-nitroanisole as a solvatochromic dye are the most popular scales and have been used to quantify the polarity of many different compounds [27, 56, 68, 69, 93, 106]. For a series of binary solvent mixtures, Mehranpour and Hasemnia showed that the polarity is not necessarily linear over the full mole fraction range [85]. Instead, preferential solvation of the solvatochromic dye by one of the two solvents occurred as may likewise be the case for any other compound. The observation emphasizes the importance of taking into account also specific interactions. Using Reichardt's betaine dye, no clear absorption bands were observed with benzylamine (**1**) and *rac*-**3**. Therefore, 4-nitroanisole was used as an alternative solvatochromic dye. The π^* -value for a solvent S is defined as follows:

$$\pi^*(S) = \frac{\nu(S) - \nu(cHex)}{\nu(DMSO) - \nu(cHex)} \quad (4.4)$$

$\nu(S)$ represents the frequency of the maximum of the absorption band. Cyclohexane (cHex) and dimethylsulfoxide (DMSO) function as reference solvents with $\pi^* = 0$ for cHex and $\pi^* = 1$ for DMSO. UV absorption spectra were recorded for pure benzylamine (**1**), pure *rac*-**3** and binary mixtures thereof (Figure 4.11a). The corresponding π^* -values as calculated from Equation 4.4 are shown in Figure 4.11b. A linear dependency of the polarity on the mole fraction of the two substrates in a solvent-free system was observed.

⁸Values taken from LOGKOW databank, Sangster Research Laboratories (logkow.cisti.nrc.ca/).

⁹Defined as the molar electronic transition energy of a betaine dye that was published initially with the running number 30 measured in kcal mol⁻¹ at 25 °C and atm.

¹⁰Empirical measure of the nonspecific part of van der Waals interactions, i.e. interactions other than hydrogen bonding.

This observation supports the validity of introducing a linear dependency of ν_{max}^* as in section 4.4.5 on page 42 for the development of a kinetic model in the solvent-free system.

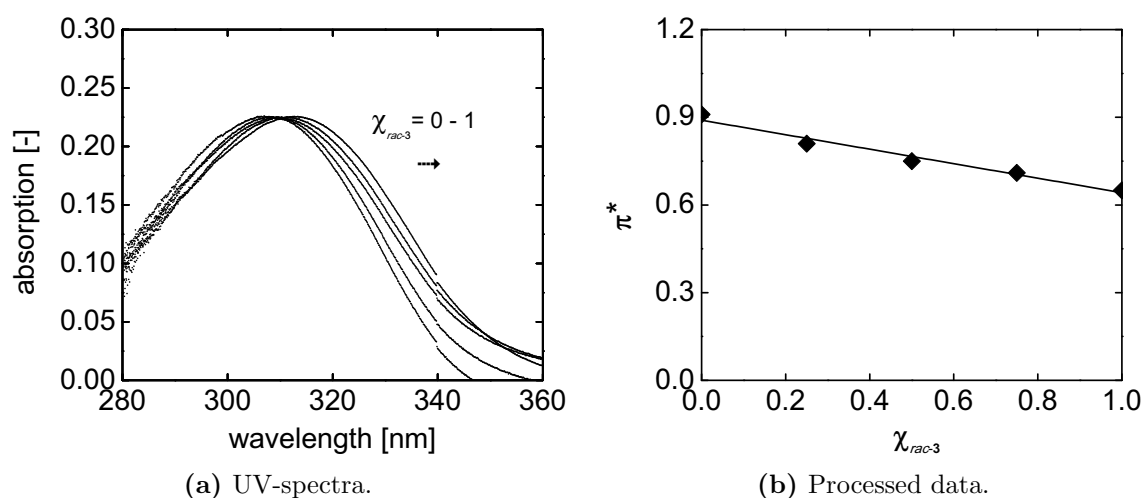


Figure 4.11: Polarity of solvent-free medium depending on substrate fraction on π^* -scale. UV-spectra were recorded at room temperature for mixtures of **1** and *rac-3* in the range from $\chi_{rac-3}=0-1$.

A linear dependency of the parameter ν_{max}^* with $\log P$ was only found for mixtures of the same two solvents in different ratios or similarly for solvent-free systems with different ratios of the two substrates by Sandoval et al. [112]. On the other hand, non-linearity was found when different solvents were tested. In order to demonstrate solvent effects, the reaction rate of the Novozym 435-catalyzed aminolysis was measured in organic solvents of different polarity. Reactions generally seemed to proceed faster in more hydrophobic solvents (Figure 4.12 on the next page). However, the observed trend is vague using the $E_T(30)$ -scale and even more so when the π^* -scale is applied. A linear dependency is not found on either scale. In the absence of hydrogen bonding (which is mostly valid for the applied solvents), main differences between the $E_T(30)$ - and π^* -scales arise from the different responses to solvent polarizability [68]. The extent of these interactions depends on both solvent and solute properties. Analogous to the specific interactions of the solvent with the solvatochromic dye, similar interactions may occur with the enzyme and affect activity. Additionally, thermodynamic activity coefficients of the substrates depend on the solvent and largely influence the rate of any reaction.

4.4.2 Water activity control

The importance of tightly bound water molecules for enzyme performance is well-recognized. The addition of small quantities of water to anhydrous systems such as organic solvents or solvent-free media can largely increase enzyme activity by several orders of magnitude [64]. Zaks and Klibanov showed for three independent enzymes from different classes that enzyme activity remained unaffected in different solvents as

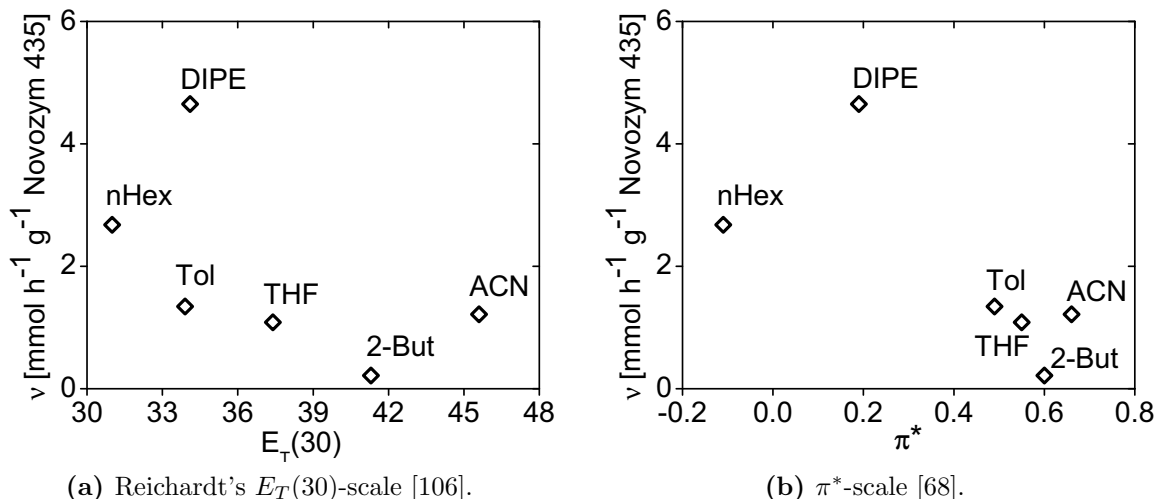


Figure 4.12: Reaction rate in organic solvents as a function of solvent polarity expressed by solvatochromic polarity scales. 0.2 M of **1** and *rac*-**3**, 45 mg_{N435} ml⁻¹, 60 °C.

long as the amount of water bound to the enzyme remained constant [149]. The thermodynamic water activity a_w was suggested as a suitable factor for the correlation of the water content to enzyme performance [36]. It is correlated with the mole fraction of water (χ_w) and the thermodynamic activity coefficient (γ_w) by $a_w = \gamma_w \cdot \chi_w$. Experimentally, the water activity can be set to defined values using saturated salt solutions which are applied for the equilibration of the respective reactants via the gas phase. In this study, LiCl ($a_w = 0.11$), KAc ($a_w = 0.22$), MgCl₂ ($a_w = 0.33$), K₂CO₃ ($a_w = 0.43$), KI ($a_w = 0.69$) and KCl ($a_w = 0.86$) were used. Figure 4.13 shows an increasing formation of a white precipitate with increasing a_w . Therefore, water concentrations were not controlled via salt hydrates but kept low as obtained from the suppliers or after MgSO₄-drying in own syntheses throughout all studies presented in this work.

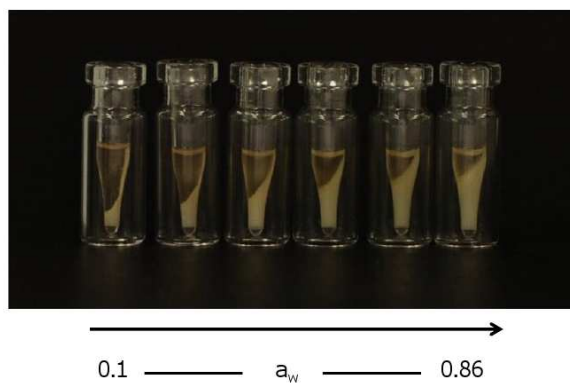


Figure 4.13: Formation of precipitate in Novozym 435-catalyzed aminolysis at defined water activities a_w .

The thermodynamic activity coefficients of water in mixtures of the substrates benzy-

lamine **1** and *rac*-**3** were calculated using COSMO-RS software (Cosmologic, Germany) under reaction conditions (60°C) on mole fraction scale. The water concentration in the substrates and adsorbed on the enzyme carrier were determined experimentally using Karl Fischer titration. The overall water concentration was nearly 0.16 mmol g⁻¹ in all reaction mixtures. Figure 4.14 shows an increasing water activity coefficient with increasing mole fraction of *rac*-**3**. In kinetic resolutions of *sec*-alcohols, *Candida antarctica* lipase B seemed to be affected only to a minor degree by water activity variations [96, 137]. Nonetheless, the shown increase must be considered as a possible reason for the observed dependency of the kinetic constant ν'_{max} value¹¹ on the applied substrate ratio χ_{rac-3} in the solvent-free Novozym 435-catalyzed aminolysis.

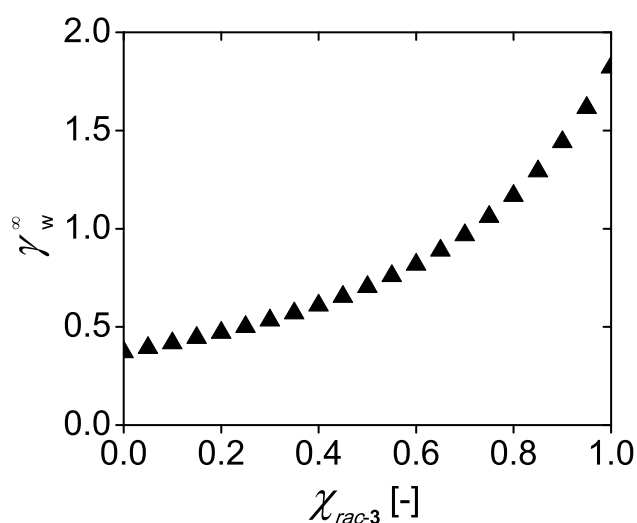


Figure 4.14: Infinite dilution water activity coefficient γ_w^∞ as a function of mole fraction of *rac*-**3** in solvent-free system with benzylamine at 60 °C. The overall water concentration was nearly 0.16 mmol g⁻¹ for all substrate mixtures.

4.4.3 Thermodynamic activity calculation

Various physicochemical parameters such as dielectric constant or hydrophobicity have been suggested for the correlation of enzyme performance in organic media. However, none of these parameters were found to be generally true [50, 132]. The use of thermodynamic activities as a generally valid concept was recognized as early as in 1974 by Bell et al. [4]. The method can be used to correct the concentrations of the reactants for solvation. The obtained thermodynamic activities are then applied in kinetic equations replacing concentrations. Kinetic parameters obtained by this method are called "intrinsic" parameters as they are independent from the organic solvent given no additional effects of the solvent on the enzyme occur [112]. However, despite the use of thermodynamic activities different parameters have been observed in literature implying that solvents can have additional effects on enzyme activity [51, 112, 132]. Such unspecified solvent effects must be additionally determined and considered in kinetic equations. Thermodynamic activities of compounds in a given solvent (or solvent-free

¹¹See Figure 4.17a on page 44 and sections 4.4.4-4.4.5 for a detailed discussion of ν'_{max} .

system with the second substrate being the "solvent") are usually determined using the UNIFAC group contribution method or more recently COSMO-RS. In this study, the molecule geometry of all solvents, substrates and products was initially determined using HyperChem[®] 8.5 (Hypercube, USA). Quantum chemical optimization of the molecule geometry and charge distribution was achieved using Turbomole[®] 5.10 (Turbomole, Germany). Figure 4.15 exemplarily shows the geometrically optimized stick model and charge distribution of (*S*)-**3** for the most abundant conformer in a pure racemic mixture of **3**. Activity coefficients of all mixtures in solvent- or solvent-free systems were subsequently calculated under reaction conditions on mole fraction scale using COSMO-RS Version C21_0110 (Cosmologic, Germany) [28].

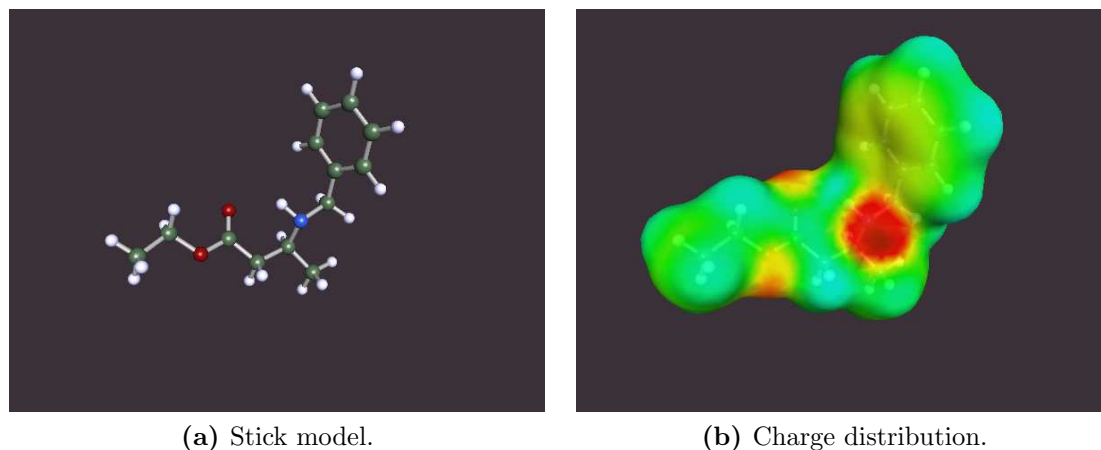


Figure 4.15: Molecule geometry and charge distribution of most abundant (*S*)-**3** conformer in racemic mixture calculated and optimized using HyperChem, Turbomole and COSMO-RS-software.

4.4.4 Kinetics in organic solvent

Despite the ultimate goal to kinetically characterize the lipase Novozym 435-catalyzed kinetic resolution of *rac*-**3** with **1** in a solvent-free system, the reaction was initially investigated by initial rate measurements in an organic solvent in order to be able to vary substrate and product concentrations individually and to obtain reliable information on the effect of each compound. As the enantioselectivity of Novozym 435 was higher in THF compared to other organic solvents and similar to the solvent-free system (section 4.1), THF was chosen as a solvent. A decreasing reaction rate was observed when increasing the concentration of the substrate **1** above a concentration of 0.1 M while the concentration of *rac*-**3** was maintained at 2 M (Figure 4.16a on page 43). In lipase-catalyzed esterification reactions, a competitive inhibition by the alcohol nucleophile has been frequently reported [51, 112]. A similar inhibiting effect is apparently caused by the amine nucleophile at elevated concentrations. In fact, substrate surplus inhibition is a common observation in reaction systems applying comparably high substrate concentrations. Noticeably, benzylamine (**1**) concentrations have been raised to a molar level

largely replacing the solvent THF. Since a decreasing activity can already be observed at approximately 0.25 M of **1** (2.5 % v/v), the effect is considered to be inhibitory rather than induced by altered solvent properties. On the other hand, a linear increase of the reaction rate was observed with increasing concentration of (*R*)-**3** at a constant concentration of **1** at 1 M (Figure 4.16b). The affinity of the substrate ester to the enzyme can therefore assumed to be small, which is expressed by a high K_m -value for the compound ($K_{m(R)-3} \gg [(R) - \mathbf{3}]$). It must be noted though, that the concentration of (*R*)-**3** was varied by addition of the racemic substrate *rac*-**3**, leaving the possibility of added effects such as a blocking of the active site by the "wrong" (*S*)-enantiomer and thus prevention of conversion of (*R*)-**3**. However, the affinity of (*R/S*)-**3** to the active site is generally low implying a minor impact of such an occupation of the active site. Given the known good enantioselectivity of Novozym 435 in this reaction, the enzymatic aminolysis of (*S*)-**3** as a side reaction does not contribute significantly to the overall conversion and could therefore be neglected ([140], this study). The equation for Michaelis-Menten double substrate kinetics including substrate surplus inhibition by **1** was considered as a model Equation 4.5.

$$\nu_{(R)-\mathbf{3}} = \frac{\nu_{max(R)} \cdot [\mathbf{1}]}{K_{m1} + (1 + \frac{[\mathbf{1}]}{K_{i1}}) \cdot [\mathbf{1}]} \cdot \frac{[(R) - \mathbf{3}]}{K_{m(R)-3} + [(R) - \mathbf{3}]} \quad (4.5)$$

With $K_{m(R)-3} \gg [(R) - \mathbf{3}]$, the latter can be neglected in the denominator of Equation 4.5 and Equation 4.6 is obtained

$$\nu_{(R)-\mathbf{3}} = \frac{\nu'_{max(R)} \cdot [\mathbf{1}] \cdot [(R) - \mathbf{3}]}{K_{m1} + (1 + \frac{[\mathbf{1}]}{K_{i1}}) \cdot [\mathbf{1}]} \quad (4.6)$$

with $\nu'_{max(R)}$ comprising $\nu_{max(R)}$ and $K_{m(R)-3}$ to a common parameter. The new parameter $\nu'_{max(R)}$ in fact is related to the enzymes catalytic efficiency which is defined as k_{cat}/K_m and likewise is a measure of the rate by which the enzyme can convert substrate into product. Addition of product *rac*-**4** to the reaction leads to a decreased reaction rate suggesting an inhibitory effect by one or both enantiomers (Figure 4.16c). Consideration of the activity coefficients of the substrates did not account for this observation. It must be stressed, however, that given the applied high product concentrations it is difficult to distinguish between weak inhibitory effects and solvent related effects reducing enzyme activity which are not covered by the use of thermodynamic activity coefficients instead of concentrations. Including product inhibition into the model leads to Equation 4.7 and can account for the observed reduced activity despite the uncertainty of its origin.

$$\nu_{(R)-\mathbf{3}} = \frac{\nu'_{max(R)} \cdot [\mathbf{1}] \cdot [(R) - \mathbf{3}]}{K_{m1} + (1 + \frac{[\mathbf{1}]}{K_{i1}}) \cdot [\mathbf{1}] \cdot (1 + \frac{[rac-\mathbf{4}]}{K_{i_{rac-4}}})} \quad (4.7)$$

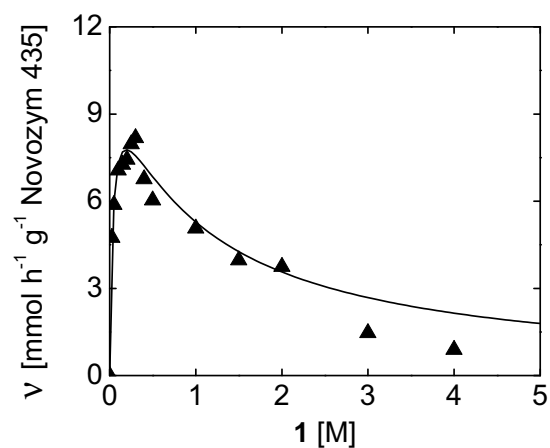
Fitting the experimental data to model Equation 4.7 using MicroMath[®] Scientist[®] software yielded the parameters summarized in Table 4.2. A good correlation of the experimental data could be obtained for both activity (not shown) and concentration based parameters (Figure 4.16). Both obtained sets of parameters are similar in order of magnitude. Since the parameters considering thermodynamic activities rather than concentrations more likely represent inherent enzyme parameters instead of apparent parameters, there is a good probability that these values allow a better transfer to other solvents or a solvent-free system and are therefore used in all following studies.

Table 4.2: Estimated kinetic parameters for Novozym 435-catalyzed aminolysis in THF at 60 °C. Parameters were determined according to model Equation 4.7 using concentrations or thermodynamic activities.

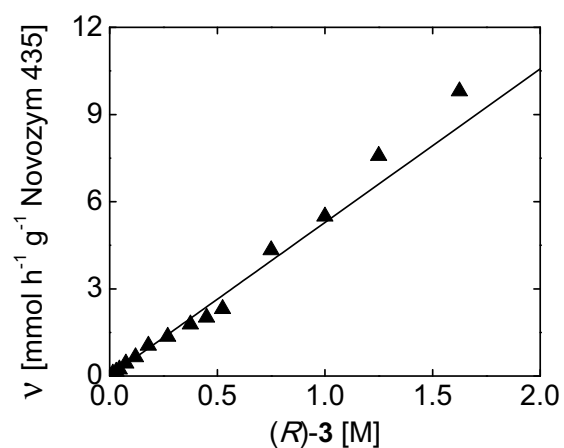
	$\nu'_{max(R)}$ [mmol · (mmol · g ⁻¹ · h ⁻¹ · g _{Novozym435} ⁻¹)]	K_{m1} [mmol · g ⁻¹]	K_{i1} [mmol · g ⁻¹]	$K_{i_{rac-4}}$ [mmol · g ⁻¹]
Conc. based	10.2 ± 0.8	0.040 ± 0.010	1.05 ± 0.17	1.32 ± 0.32
Activity based	12.9 ± 0.9	0.045 ± 0.010	0.90 ± 0.13	0.96 ± 0.17

4.4.5 Kinetics in solvent-free medium

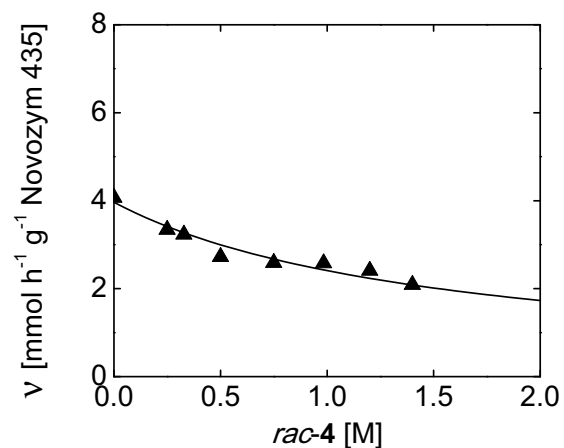
Initial reaction rates in the solvent-free reaction system strongly depend on the ratio of the two substrates used (Figure 4.17). Higher reaction rates were observed towards a higher mole fraction of *rac-3*. While the application of the kinetic model obtained from initial rate measurements in THF correctly displays the shape of the curve, it fails to predict the magnitude of the maximum reaction rate at approximately $\chi_{rac-3} = 0.95$. It is likely that solvent effects mentioned previously caused the observed deviation. As briefly mentioned above, Sandoval and co-workers introduced an adapted ν_{max}^* parameter dependent on the solvent used that corrects for solvent effects not accounted for by the use of thermodynamic activities [112]. Both in the case of binary solvent mixtures as well as in solvent-free reactions with varying mole fractions of two substrates they observed a linear dependence of ν_{max}^* on the ratio of the two solvents or substrates, respectively. As can be seen from Figure 4.17a, a similar observation was made here. The parameter can easily be calculated from Equation 4.6. In fact, introducing this linear adaptation of $\nu'_{max(R)}$ into the model allows a good description of the initial rates of the solvent-free reaction with the kinetic parameters determined previously in the solvent system (Figure 4.17b). A linear polarity change depending on the mole fraction of the substrates used was observed (section 4.4.1 on page 35) and supports the validity of introducing a linear



(a) Dependence on concentration of substrate benzylamine **1**. The concentration of (*R*)-**3** was held constant at 1 M.



(b) Dependence on concentration of substrate *rac*-**3** at constant concentration of **1** at 1 M.



(c) Dependence on concentration of product *rac*-**4** at constant concentrations of **1** at 1 M and (*R*)-**3** at 0.75 M.

Figure 4.16: Initial rate measurements of Novozym 435-catalyzed aminolysis of *rac*-**3** with benzylamine **1** in THF at 60 °C.

correction factor. Due to the observed hydrolytic side reaction, it was not possible to maintain a constant water activity using salt hydrates. Residual water contained in the substrates, however, can hardly be avoided. Even though it did not lead to significant amounts of side product, the activity coefficient of water was found to increase with an increasing concentration of *rac-3* (section 4.4.2 on page 37, Figure 4.14) and has to be considered as an additional potential reason for the observed dependence of $\nu'_{max(R)-3}$ on the substrate mole fraction.

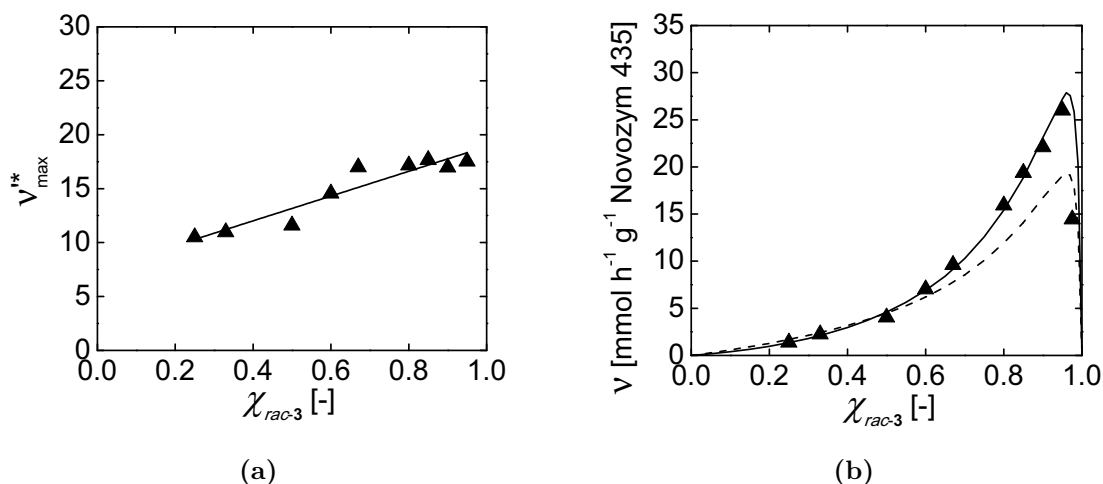


Figure 4.17: Initial rate measurements of Novozym 435-catalyzed aminolysis of *rac-3* with benzylamine **1** in solvent-free system at 60 °C. a) Linear adaption of ν'_{max} in order to account for solvent effects according to Sandoval et al., 2001 ($y = 7.42 \chi_{rac-3} + 11.48$). b) Dependence of initial rate on mole fraction of *rac-3*, simulation with model Equation 4.7 (--) and model with adapted ν'_{max} (-).

In addition to the observed strong dependency of the initial reaction rate in the Novozym 435-catalyzed kinetic resolution of *rac-3* on the concentration of the same compound, reaction temperature generally influences enzyme activity. The dependency of the reaction rate on temperature is depicted in Figure 4.18. A linear relationship of enzyme activity and temperature was found in the range from 40–80 °C. For practical application lower temperatures are not relevant due to reduced space-time yields at low reaction rates. Higher temperatures on the other hand go in hand with a significant loss of enzyme stability (see Figure 4.8 on page 32) thus causing uneconomically high catalyst costs.

4.5 Prediction of progress curve

In order to predict the full progress curve of the Novozym 435-catalyzed aminolysis in a solvent-free system, the model derived from measurements in THF (Equation 4.7) needs to be adapted by using the modified ν'_{max} parameter ν'_{max} as suggested in the previous

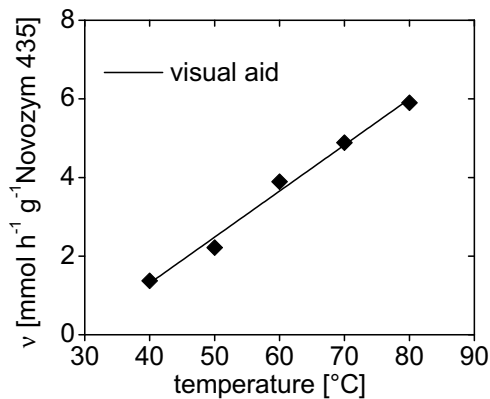


Figure 4.18: Temperature dependence of initial reaction rate in solvent-free Novozym 435-catalyzed aminolysis of *rac*-**3**. $\chi_{0, rac-3} = 0.5$, $\chi_{0,1} = 0.5$, 152 mg $g_{Novozym435}^{-1}$

section in order to account for solvent effects. The overall model including the solvent adapted parameter ν'_{maxR} as well as activity coefficients γ_i to account for solvation, the non-catalyzed background reaction and enzyme deactivation can be displayed as follows for the two enantiomers:

$$\nu_{(R)-3} = \frac{\nu'_{max(R)} \cdot \gamma_1 \cdot [1] \cdot \gamma_{(R)-3} \cdot [(R) - 3]}{K_{m1} + \left(1 + \frac{\gamma_1 \cdot [1]}{K_{i1}}\right) \cdot \gamma_1 \cdot [1] \cdot \left(1 + \frac{\gamma_{rac-4} [rac-4]}{K_{i_{rac-4}}}\right)} \quad (4.8)$$

$$\nu_{(S)-3} = \frac{\nu'_{max(S)} \cdot \gamma_1 \cdot [1] \cdot \gamma_{(S)-3} \cdot [(S) - 3]}{K_{m1} + \left(1 + \frac{\gamma_1 \cdot [1]}{K_{i1}}\right) \cdot \gamma_1 \cdot [1] \cdot \left(1 + \frac{\gamma_{rac-4} [rac-4]}{K_{i_{rac-4}}}\right)} \quad (4.9)$$

No information was gained on a parameter ν'_{maxS} for the (*S*)-enantiomer of **3** in the solvent system. In a single progress curve experiment, however, the concentrations of this enantiomer are varied automatically with increasing conversion. Numerical integration of the reaction rate equation coupled with non-linear regression can be used to extract kinetic information and thus displays a valuable tool in order to determine parameters for substrates that are difficult to obtain in a pure form [32]. Therefore, estimation of the missing parameter ν'_{maxS} was done by numerical integration of the rate equation and non-linear fitting to the experimental data of six different experiments using Matlab[®] software (see section A.3.4 on page 104). For consideration of the non-catalyzed side reaction, the kinetic rate equations introduced in chapter 3 on page 15 were implemented in the model as presented in Equations 4.10-4.11.

$$\nu_{chem.,(R)} = k_2 \cdot [1] \cdot [(R) - 3] \quad (4.10)$$

$$\nu_{chem.,(S)} = k_2 \cdot [1] \cdot [(S) - 3] \quad (4.11)$$

The respective mass balances for each compound necessary for progress curve simulation can then be introduced as in Equations 4.12-4.16.

$$\frac{d[\mathbf{1}]}{dt} = (-\nu_{(S)-\mathbf{3}} - \nu_{(R)-\mathbf{3}}) \cdot [Enz.] - \nu_{chem.,(R)} - \nu_{chem.,(S)} \quad (4.12)$$

$$\frac{d[(R)-\mathbf{3}]}{dt} = -\nu_{(R)-\mathbf{3}} \cdot [Enz.] - \nu_{chem.,(R)} \quad (4.13)$$

$$\frac{d[(S)-\mathbf{3}]}{dt} = -\nu_{(S)-\mathbf{3}} \cdot [Enz.] - \nu_{chem.,(S)} \quad (4.14)$$

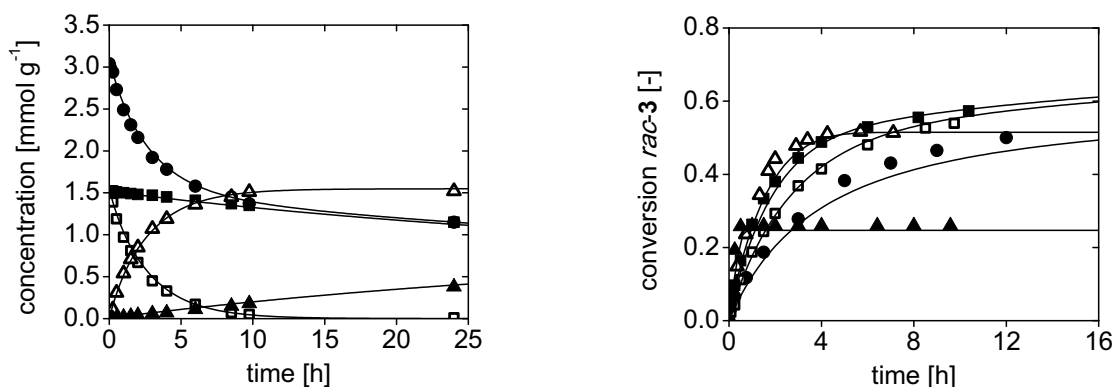
$$\frac{d[(R)-\mathbf{4}]}{dt} = \nu_{(R)-\mathbf{3}} \cdot [Enz.] + \nu_{chem.,(R)} \quad (4.15)$$

$$\frac{d[(S)-\mathbf{4}]}{dt} = \nu_{(S)-\mathbf{3}} \cdot [Enz.] + \nu_{chem.,(S)} \quad (4.16)$$

Application of the model predicts the time course over a broad range of starting mixtures of the substrates **1** and *rac*-**3** with good accuracy. Figure 4.19a exemplarily shows the concentration profile of a typical reaction along with associated conversion-time curves for runs with a starting mole fraction in the range of $\chi_{0,rac-\mathbf{3}} = 0.33 - 0.8$. The model also describes the enantiomeric excess as a function of conversion above $\chi_{0,rac-\mathbf{3}} = 0.33$, which represents the relevant range for application in a process due to excellent enzyme stabilities and increased reaction rates. The strategy to investigate the reaction in THF as a solvent first in order to reduce the number of variables and subsequently transfer the obtained data to the solvent-free system after substitution of concentrations with thermodynamic activities could thus be applied successfully. It is worth to notice though, that the activity coefficients of all substrates and products excluding water range from about 0.7 to 1.2 both in THF and in the solvent-free reactions ([123], supplemental information). The change of the actual concentrations is therefore small leading to only minor differences of the obtained parameters. Hence, parameters obtained without consideration of the thermodynamic activities could be transferred and used likewise to describe the progress curve of the solvent-free reactions.

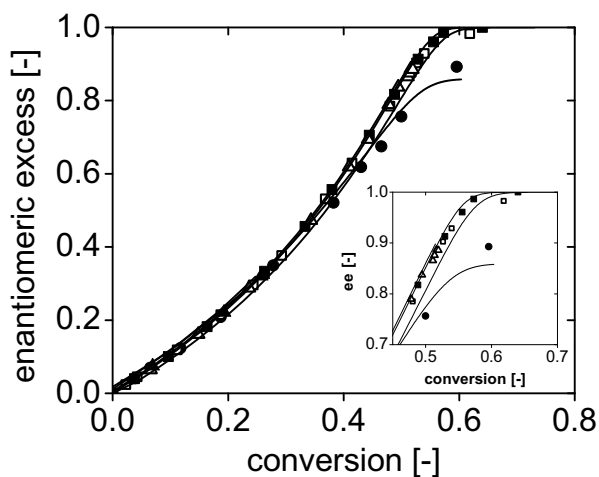
4.6 Batch vs. fed batch operation

In fed batch operation one or more substrates are fed batchwise or continuously to an otherwise discontinuously operated batch reactor. Such an operation mode usually is



(a) Experimental time course of reaction with initial substrate mole fraction $\chi_{0,rac-3} = 0.5$ and predicted data (-). Symbols: ● benzylamine **1**; □ (*R*)-**3**; ■ (*S*)-**3**; △ (*R*)-**4**; ▲ (*S*)-**4**.

(b) Conversion-time plot of experimental and predicted data of experiments with different substrate mole fractions. ● $\chi_{rac-3} = 0.33$; □ $\chi_{rac-3} = 0.5$; ■ $\chi_{rac-3} = 0.6$; △ $\chi_{rac-3} = 0.67$; ▲ $\chi_{rac-3} = 0.8$.



(c) Conversion-*ee* plot of experimental and predicted data of experiments with different substrate mole fractions. ● $\chi_{rac-3} = 0.33$; □ $\chi_{rac-3} = 0.5$; ■ $\chi_{rac-3} = 0.6$; △ $\chi_{rac-3} = 0.67$; ▲ $\chi_{rac-3} = 0.8$.

Figure 4.19: Simulation of Novozym 435-catalyzed aminolysis of *rac*-**3** with benzylamine **1** according to model Equations 4.8 - 4.16. All reactions were carried out in a solvent-free system at 60 °C with 0.152 g g⁻¹ Novozym 435.

applied for kinetic reasons, i.e. especially in the case of substrate surplus inhibition or deactivation by the substrate that is added in the course of the reaction. Using an adequate feeding strategy, the concentration of the substrate is kept low and unfavorable effects are avoided while at the same time high degrees of conversion can be reached. In kinetic resolutions, a feeding of the racemic compound leads to the increased, undesired turnover of the "wrong" enantiomer and therefore represents an unfavorable process engineering strategy. However, from the kinetic investigation carried out in a solvent-free medium (section 4.4.5), it is obvious that applying a feeding strategy for benzylamine **1** should be beneficial for an improved space-time yield. Reaction rates are much higher towards high mole fractions of *rac*-**3** as compared to **1** (Figure 4.17b on page 44). With regard to enzyme stability, a large decrease at high concentrations of **1** was observed. In the practically more relevant range towards large concentrations of *rac*-**3** only minor differences were observed (Figure 4.9) that should only be noticeable in long term continuous or repetitive batch experiments. Both batch and fed batch operation modes were therefore compared experimentally and by simulation using the kinetic model presented above (Figure 4.20). In fed batch experiments, initial concentrations after each substrate feeding step were calculated based on conversion and amount of substrate addition. The batch experiment was started with a mole fraction of $\chi_{rac-3} = 0.6$ which represents the ratio of maximum enzyme stability and at the same time allows to obtain a high $ee_{(S)-3}$ of $> 99\%$. The fed batch experiment was started with $\chi_{rac-3} = 0.88$ and proceeded with feeding of **1** in five equal amounts at distinct time points.

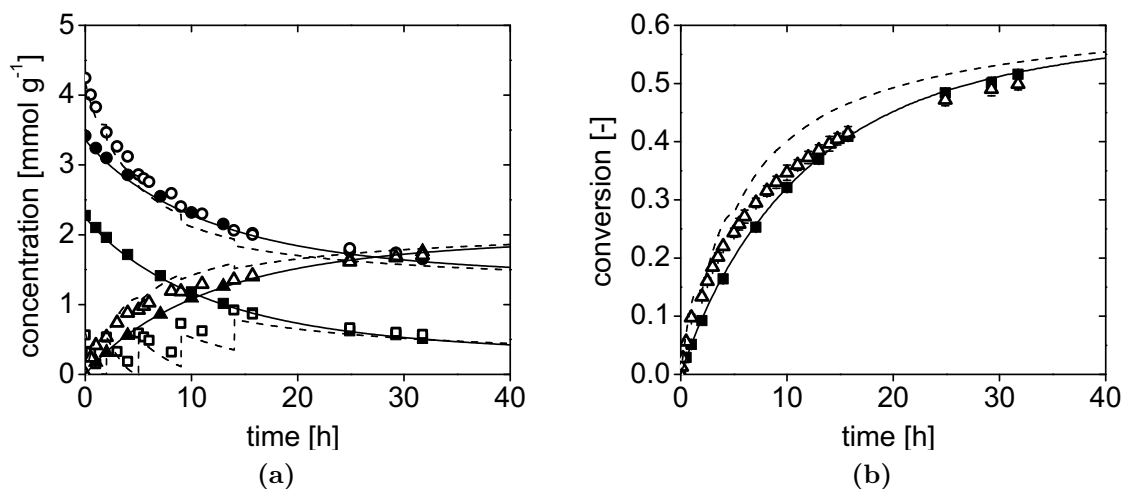


Figure 4.20: Comparison of batch and fed batch operation in Novozym 435-catalyzed kinetic resolution of *rac*-**3** with **1** by simulation (dashed lines) and experimentally (symbols). Filled symbols: batch experiment. Open symbols: fed batch experiment. (a) \circ/\bullet **1**; \square/\blacksquare *rac*-**3**; \triangle/\blacktriangle *rac*-**4**. (b) \blacksquare Conversion in batch experiment; \triangle Conversion in fed batch experiment. Batch reactions were carried out with $\chi_{0,rac-3} = 0.6$, fed batch reactions with $\chi_{0,rac-3} = 0.88$. Benzylamine was added in 5 equal portions of 0.27 mmol at 0 h, 2 h, 5 h, 9 h and 14 h. $0.152 \text{ g}_{N435} \text{ g}^{-1}$, $60 \text{ }^\circ\text{C}$.

Despite the expected higher initial reaction rates with $\chi_{0,rac-3} = 0.88$, the batch experiment with $\chi_{0,rac-3} = 0.6$ eventually outperforms the fed batch experiment. The kinetic model introduced in section 4.4.5 on the other hand predicts a faster course of the fed batch reaction. After about 15 h reaction time, it is noticed that concentrations in both batch and fed batch experiments are nearly the same. Since the compared reactions contained the same initial amount of enzyme, the only possible explanation conceivable is an unexpectedly high deactivation in the fed batch experiment. As discussed in section 4.2 the formation of the corresponding acid of the ester *rac-3* may be responsible for an increased deactivation in the case of low concentrations of the target amine nucleophile. As shown in Figure 4.13 on page 38, the acid formation rate depends of the amount of water in the system. It may be speculated that a less dry batch of Novozym 435 or substrates with a higher water content were used in this series of experiments.

4.7 Summary

This chapter covered the characterization of the Novozym 435-catalyzed kinetic resolution of *rac-3* via aminolysis with benzylamine as a nucleophile in a solvent-free system. Particular focus was laid on parameters influencing selectivity and activity. The following conclusions can be made:

- An apparent enantioselectivity E' of 32 was determined for the reaction carried out at 60 °C with $\chi_{0,rac-3} = 0.5$.
- A linear decrease of both intrinsic and apparent enantioselectivity E and E' , respectively, was found with increasing temperature in the range from 40-80 °C. The loss of selectivity is therefore attributed to an impaired enzyme performance rather than an increased thermal side reaction.
- Enantioselectivity in different solvents was tested. A decreasing selectivity with increasing logP was observed for the tested solvents. However, a larger amount of data is needed in order to claim a general trend.
- In a solvent-free system the apparent enantioselectivity E' is solely determined by the contribution of the thermal side reaction. The intrinsic value E remains fully unaffected over the analyzed range from $\chi_{0,rac-3} = 0.33 - 0.8$.
- The stability of Novozym 435 in the solvent free system is a function of temperature and substrate mole fraction. Increasing temperature and concentrations of benzylamine were found to be detrimental for enzyme stability with the latter effect being more pronounced in the analyzed range.
- Diffusion limitation was excluded as a rate-determining factor. Reaction rates of both pestled and intact Novozym 435 were alike.

4 Biocatalytic aminolysis

- A linear relationship between substrate mole fraction and polarity was found on a π^* -polarity scale. A correlation of the polarity with the linear dependence of ν_{max}^* is proposed.
- Control of water activity using salt hydrates led to an increased formation of the hydrolytic side product and was therefore avoided. The infinite dilution water activity coefficient $\gamma_{H_2O}^\infty$ of the residual water increased with increasing $\chi_{0,rac-3}$.
- Thermodynamic activity coefficients of all compounds in THF and in the solvent-free system γ_i were calculated using COSMO-RS software and incorporated into a kinetic model.
- A kinetic model based on Michaelis-Menten two substrate kinetics including substrate inhibition by benzylamine **1** and the product *rac-4* was devised. Kinetic parameters were determined in THF as a solvent using initial rate measurements.
- A linear dependence of $\nu_{max_S}^*$ on the applied mole fraction was found and integrated into the kinetic model.
- The kinetic model developed in THF as a solvent was transferred to the solvent-free system and could be used to predict conversion and *ee* with good accuracy.
- A fed batch system was investigated experimentally and via simulation. As expected, a higher initial reaction rate was found for both simulation and experiment compared to the batch system. Diverging results at higher conversion are related to an unexpectedly high enzyme deactivation in the fed batch system.

5 Inline analytics via FTIR

The Fourier transformation infrared (FTIR) absorption spectroscopy is frequently utilized for a number of applications. Most often, FTIR technology is used for product identification purposes in organic chemistry. Depending on the type of covalent bond, infrared light of a particular wavelength is absorbed and causes molecular vibrations. Two types of vibrations may be considered in this context: deformational vibrations (scissoring, rocking, wagging and twisting) or stretch vibrations (symmetric or asymmetric) [117]. Any organic compound shows a characteristic infrared spectrum composed of absorption bands from functional groups and a fingerprint region in the near mid-infrared region that can be used to designate a spectrum to a certain compound and thus to identify the substance. Due to the excellent specificity of the method a quantification of compounds in mixtures is also possible. FTIR technology therefore represents a convenient method for real-time monitoring of reactions. Both near- (NIR, 13.000 - 4.000 cm^{-1}) and mid-infrared (MIR, 4.000 - 400 cm^{-1}) regions are usually considered for this purpose. The former is cheaper and more robust towards outer interferences and is therefore more frequently used in industrial applications. The latter, however, is more sensitive and allows the direct correlation of absorption bands to functional groups thus facilitating interpretation [141]. Real-time monitoring of reactions may be carried out online or inline. By definition, *online* analytical methods may include additional filtration steps for the removal of particles or bubbles, while *inline*- or *in situ* analytics refers to the direct analysis inside the reactor [60]. Contrarily, in *offline* or *atline* methods in which the sample is taken from the reactor and analyzed in a nearby instrument, analytical data is obtained only with a time shift. In literature, *inline*, *online* and *in situ* analytics are often used analogously. The term *inline* analytics will be used throughout this work. Compared to offline analytical methods such as frequently used gas- or liquid chromatography, inline FTIR spectroscopy offers the additional advantage of being non-destructive.

ATR-FTIR spectroscopy

FTIR spectroscopy can be applied analogously to common UV-absorption spectroscopy by using transmission cells. However, for reactions that only show a limited permittivity for infrared light such as solvent-free systems or disperse media transmissional IR spectroscopy is not suited for quantification purposes. Here, attenuated total reflectance spectroscopy (ATR) represents a convenient alternative. The principle of ATR measurements is depicted in Figure 5.1a. A close-up picture of the ATR diamond probe which has been applied in all batch experiments is shown in Figure 5.1b.

Light passing through a medium with a high refraction index is reflected upon contact

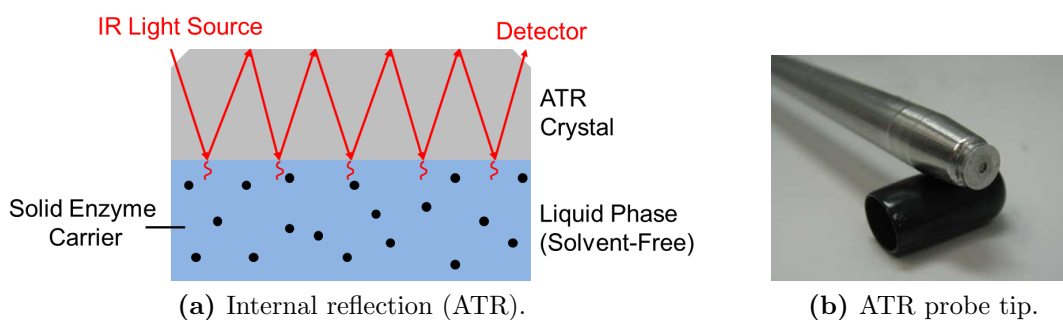


Figure 5.1: Schematic and photographic depiction of ATR crystal for FTIR spectroscopy.

with a medium of low refraction index, if the angle at which the electromagnetic wave hits the surface exceeds the critical reflection angle. To a small extent the light enters the medium of lower optical density and is partly absorbed at the interface of crystal and sample by the interaction of the electromagnetic wave with the sample. The depth by which the wave enters the sample depends on the frequency and is generally higher towards larger wavelengths (lower wavenumber). As a result, absorption bands at lower wavenumbers generally show a larger intensity. Depending on the crystal geometry used, usually 4-8 total reflections occur at the interface of the crystal leading to an improved signal-to-noise ratio. Since light is partly absorbed upon reflection, the principle is called attenuated total reflection.

Characteristic absorption of functional groups

All organic compounds (gas, liquid, solid) show characteristic IR-spectra. These may be used both for product identification, quality or purity control and for quantification. Reference spectra of the pure compounds involved in the aza-Michael addition of **1** and **2** and the subsequent biocatalytic aminolysis as outlined in chapters 3 and 4 were collected using a Mettler Toledo ReactIR 45m instrument. The respective spectra are shown on page 112 in the appendix. The wavenumber of characteristic absorption bands resulting from functional groups of the compounds **1-4** is summarized in Table 5.1 [40]. The obvious differences may be used to follow the reactions inline as described in section 5.1.1 for the aza-Michael addition and section 5.1.2 for the Novozym 435-catalyzed aminolysis.

Chemometrics

Being a relative quantification method (as opposed to absolute methods such as titrimetry or gravimetry), a calibration of all compounds needs to be carried out for quantification. Depending on the amount of compounds involved in the reaction, the necessary effort to develop a robust model allowing the precise quantification of all compounds may be quite substantial. Chemometrics as a tool in analytical chemistry for the statistical interpretation of complex spectral data obtained experimentally is nowadays routinely applied. However, the field has been introduced relatively recently in analytical chemistry due to both the necessary computing capacity and rapidly enhancing measuring

Table 5.1: Characteristic IR absorption bands of compounds **1-5**.

Compound	Functional group	Wavenumber of IR absorption
1	-C ₆ H ₆	770 - 735 cm ⁻¹
2	-RCH=CHCOOR-	1750 - 1725 cm ⁻¹
3	-C ₆ H ₆ -RCOOR-	770 - 735 cm ⁻¹ 1750 - 1735 cm ⁻¹
4	-C ₆ H ₆ -RCONHR-	770 - 735 cm ⁻¹ 1680 - 1630 cm ⁻¹

techniques [24]. Analogous to commonly applied calibration methods (such as Lambert-Beer's Law in UV-spectroscopy), a correlation between spectral data obtained from FTIR measurements and concentrations measured offline (e.g. HPLC, GC, etc.) can be achieved by the aid of chemometric models. The correlated inline and offline data is initially verified internally using the same experiments and subsequently applied to further experiments that may have been carried out under different reaction conditions in an external validation procedure. The general methodology is depicted in Figure 5.2.

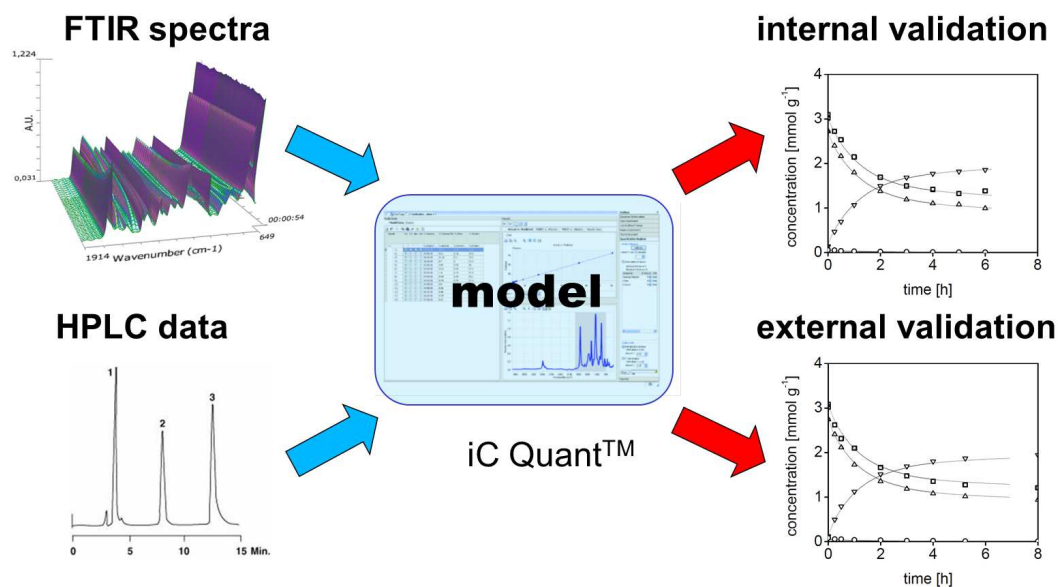


Figure 5.2: Schematic depiction of general procedure in chemometric modelling.

Initially, a number of spectra of reference compounds with varying known concentra-

tions are collected. The respective absorption spectra can be transformed into a matrix as follows with m being the wavenumber of absorption and n being the number of spectra 5.1:

$$A = \begin{pmatrix} A_{11} & A_{12} & \cdots & A_{1m} \\ A_{21} & A_{22} & \cdots & A_{2m} \\ \vdots & \vdots & \ddots & \vdots \\ A_{n1} & A_{n2} & \cdots & A_{nm} \end{pmatrix} \quad (5.1)$$

Multiplication of the matrix A with a vector containing the model parameters allows the transformation of the spectral data to concentrations. The vector can be determined mathematically by either univariate or multivariate regression [87]. In univariate analysis, variables are analyzed independently. In multivariate regression analysis, several variables are analysed at the same time and thus, interdependencies of the variables can be detected and considered in the model. In this study, several compounds were detected in each reaction at the same time and overlapping IR absorption peaks were found for both substrates and products in nearly all regions of the spectrum (see Figure B.2 and B.3 on page 112 in appendix). Therefore, multivariate analysis was applied. The respective chemometric methods as well as statistical evaluation tools necessary for determination of the validity of the derived model parameters are integrated in the iC Quant Modeling Package[®] from Mettler Toledo that was applied throughout this study. Partial Least Square regression (PLS) as a chemometric method which is based on the Principal Component Analysis (PCA) technique is commonly used as a standard algorithm in multivariate data analysis of highly correlated and intercorrelated data sets. While a detailed discussion on PLS and other regression algorithms can be found in literature [24], it is important to notice that the number of principal components should be kept as low as possible. The ideal number of principal components must be determined empirically.

5.1 Inline monitoring in batch processes

Solvent-free reactions in batch mode were carried out in thermostated glass vessels at 60 °C with magnetic stirring. The FTIR-probe was inserted directly into the reaction medium. All FTIR spectra were recorded using a Mettler Toledo ReactIR 45m instrument equipped with a liquid nitrogen cooled MCT detector, a silver halide optical fiber and a diamond crystal ATR probe. The FTIR instrument was constantly purged with 3 L min⁻¹ of dry nitrogen in order to avoid disturbing water vapour or carbon dioxide detection. Spectra were recorded with 256 scans per spectrum at defined time intervals. The reaction setup is depicted schematically in Figure 5.3.

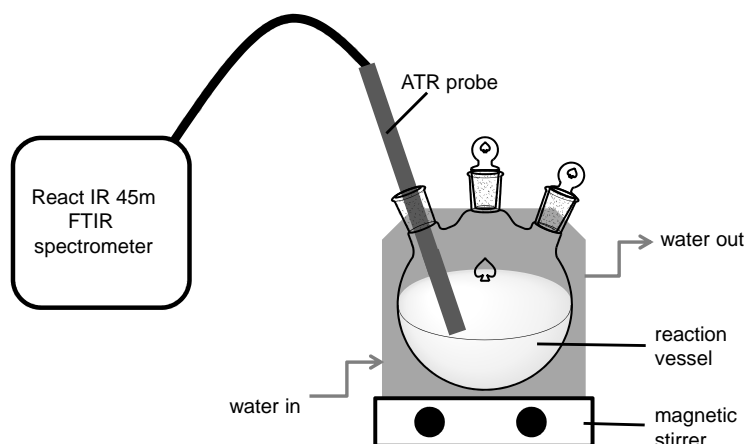


Figure 5.3: Experimental setup for inline monitoring of aza-Michael addition via ATR-FTIR spectroscopy.

5.1.1 aza-Michael addition

Figure 5.4 shows a 3-dimensional plot of FTIR-spectra vs. time recorded for the solvent-free aza-Michael addition of the substrates **1** and **2** at an initial molar ratio of 1:1. Changes caused by substrate depletion and product formation are obvious throughout the whole spectrum, while an interference of the depletion of the characteristic absorption for the α,β -unsaturated ester **2** at $1750 - 1725 \text{ cm}^{-1}$ and formation of the ester peak of *rac*-**3** at $1750 - 1735 \text{ cm}^{-1}$ clearly show the need for application of chemometric modelling. Additionally, mathematical spectrum transformations by computation of 1st or higher order derivatives often improves the resolution of the absorption peaks in such cases.

The development of a chemometric model for calibration is possible by measuring defined mixtures of substrates and products from pure compounds. However, in order to avoid the elaborate purification of the not commercially available compounds **3** and **4** and the erroneous preparation of calibration samples of defined composition, experiments analyzed both inline and offline were used directly for calibration. The chemometric models were validated based on an internal/external-validation procedure for batch experiments using the ATR-probe. In experiments performed with a Mettler Toledo DS Micro Flowcell, which is designed for the inline monitoring of continuous processes, a more broadly applicable and robust model was developed using an internal/external-validation procedure (section 5.2 on page 58). Such a strategy is commonly applied in chemometrics.[23]

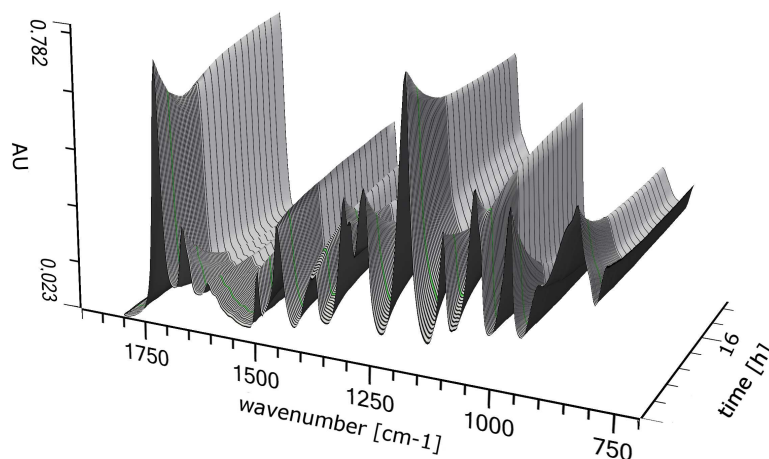


Figure 5.4: 3-Dimensional depiction of FTIR spectra vs. time in thermal aza-Michael addition of **1** and **2**. Characteristic absorption of α,β -unsaturated ester (**2**): 1750 - 1725 cm^{-1} , characteristic ester absorption (*rac*-**3**): 1750 - 1735 cm^{-1} .

Internal and external validation

In order to prove the general applicability of FTIR spectroscopy for the inline monitoring of the solvent-free aza-Michael addition, a reaction was carried out with an initial ratio of 2.2 mole equivalents of benzylamine (**1**) and 1 mole equivalent of *trans*-ethyl crotonate (**2**) as described above. Figure 5.5a shows the experimental data of the reaction analyzed offline using HPLC and the respective FTIR-data as predicted by the model. An excellent fit of the experimental data was achieved as expressed by low root mean square errors of calibration (RMSEC) for all compounds (see Table B.2 on page 113 in appendix).

External validation was then performed by applying the obtained chemometric model on a second set of experimental data obtained from a reaction carried out under equal conditions. Validation of the predicted data was again achieved using HPLC as an independent offline analytical method. Figure 5.5b shows the inline FTIR data as predicted from the model and the offline data as obtained from HPLC analysis. Again, an excellent fit of predicted and experimental data was observed. It should be noted, however, that in this set of experiments only a single type of experiment with fixed initial concentrations of substrates **1** and **2** was compared, thus limiting a more broad application of the model. Relevant statistical data for the development of the chemometric model is summarized in Table B.2 in the appendix.

5.1.2 Biocatalytic aminolysis

An analogous procedure as used above for the aza-Michael addition was applied for the biocatalytic aminolysis of *rac*-**3** with **1**. The reactions were carried out as a solvent-free one-pot process directly after the aza-Michael addition without prior purification of the intermediate products using 50 mg mmol^{-1} Novozym 435. Thus, small amounts

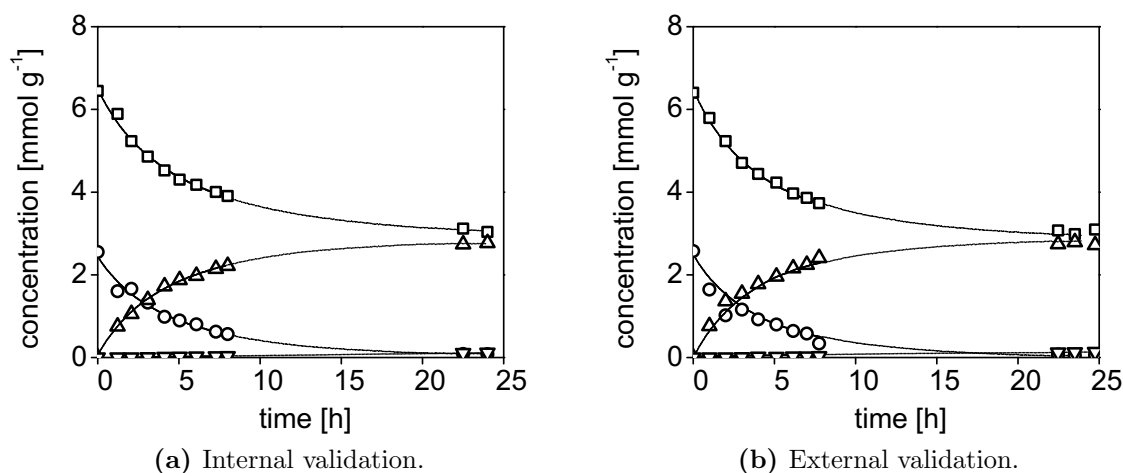


Figure 5.5: Offline HPLC-data (symbols) and inline FTIR spectroscopic data (dots) as interpreted using chemometric model in aza-Michael addition of substrates **1** (\square) and **2** (\circ) forming *rac-3* (\triangle) and *rac-4* (∇). 60 °C, 2.2:1 mole eq. of **1** and **2**.

of unreacted ester substrate **2** and amide product *rac-4* were present initially in the reaction and considered in the chemometric model. FTIR-spectra recorded over time clearly indicate the formation of an amide peak at approximately 1650 cm^{-1} and the depletion of the ester peak at 1730 cm^{-1} (Figure 5.6).

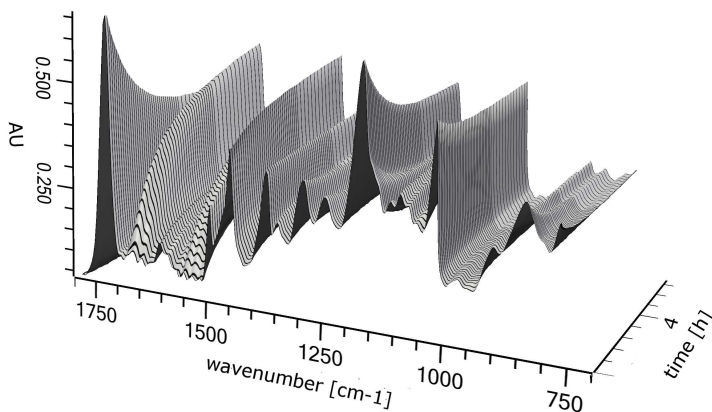


Figure 5.6: 3-Dimensional depiction of FTIR spectra vs. time in Novozym 435-catalyzed aminolysis of *rac-3* and **1**. Characteristic ester absorption (*rac-3*): $1750 - 1735\text{ cm}^{-1}$, characteristic absorption of amide (*rac-4*): $1690 - 1630\text{ cm}^{-1}$.

The developed chemometric model allows a good description of the experimental data collected offline via HPLC (Figure 5.7a). The model was externally validated by a second reaction carried out analogously. The predicted data is also in very good agreement with the data collected offline via HPLC (Figure 5.7b). The results prove the robustness of

FTIR spectroscopic analysis in the given system.

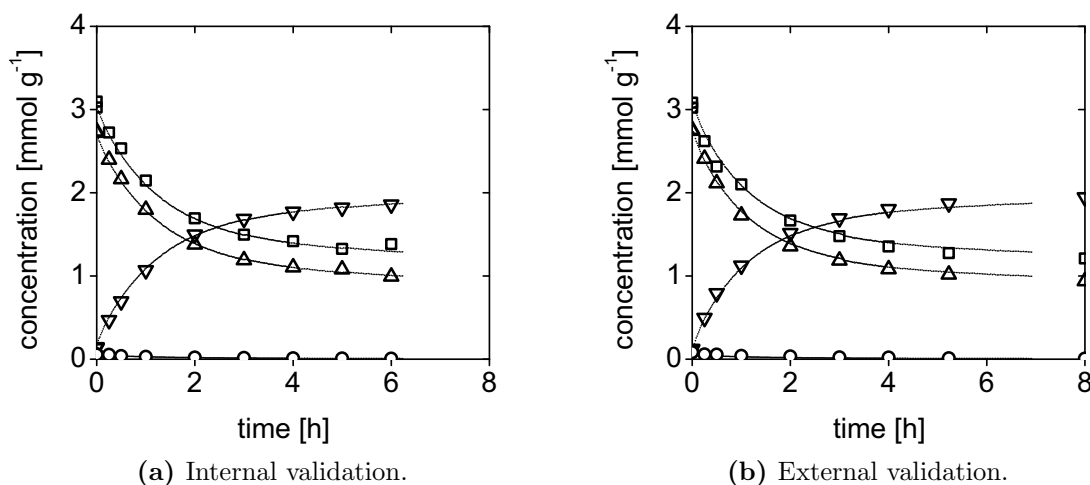


Figure 5.7: Offline HPLC-data (symbols) and inline FTIR spectroscopic data (dots) as interpreted using chemometric model in Novozym 435-catalyzed aminolysis of *rac-3* and **1**. **1** (\square); **2** (\circ); *rac-3* (\triangle); *rac-4* (∇). Reactions were carried out directly after aza-Michael addition with 2.2:1 mole eq. of **1** and **2** without prior purification of intermediates. 60 °C, 50 mg mmol⁻¹ Novozym 435.

5.2 Inline monitoring in continuous processes

Continuous flow chemistry is a rapidly growing field in organic chemistry and the pharmaceutical industry with numerous processes having been reported in recent years applying chemo- or biocatalysts [147]. The availability of real-time data on reactor performance is crucial for continuous processes in order to react towards changes in conversion. Here, FTIR can be applied as a very useful technology for inline monitoring as documented by a number of recent publications in the field of flow chemistry [19, 20, 101]. In this study, the recently developed DS Micro Flowcell from Mettler Toledo was tested for applicability in the continuous chemoenzymatic process under investigation. Analogous to the silver halide optical fiber probe described in section 5 on page 51, the flowcell is based on ATR spectroscopy. The lack of need for an optical fiber allows to achieve higher signal intensities and a more stable process setup that is less prone to signal alterations caused by positional- or temperature changes as in the case of FTIR optical fiber probes. The flowcell is characterized by a low dead volume of 50 μl , pressure stability up to 50 bar and temperature control up to 60 °C.

5.2.1 aza-Michael addition

A batch reactor setup with bypass analytics was applied for feasibility studies as depicted in Figure 5.8. The reactions were carried out in batch mode while the reactants

were continuously pumped in a loop through the flowcell, thus simulating a continuous process. A bubble trap was installed prior to the micro flowcell in order to avoid signal fluctuations caused by bubbles in the flow cell. The flowcell is sensitive to pressure changes. Signal intensities decrease upon pressure drops. The effect can partly be compensated by chemometric modeling and mathematical spectrum transformation. Alternatively, a pressure maintenance valve can be installed in order to avoid signal fluctuations.

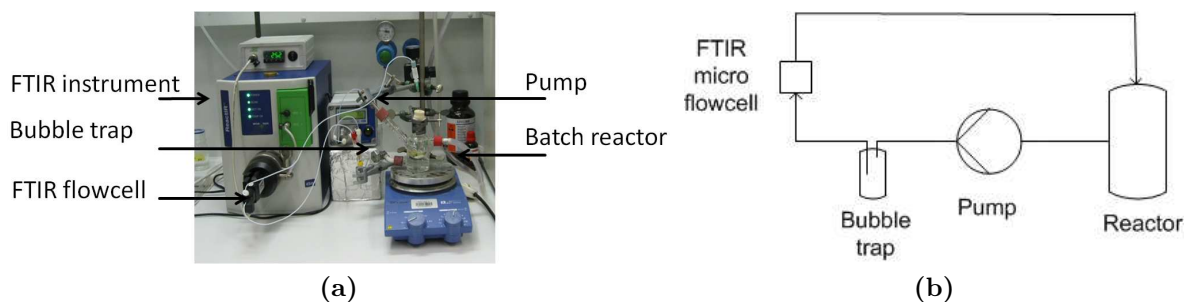


Figure 5.8: Batch reactor setup with bypass analytics for the inline reaction monitoring of the solvent-free aza-Michael addition of **1** and **2** applying an FTIR flowcell. (a) photographic. (b) schematic.

In order to develop a robust chemometric model that is applicable over a large range of substrate ratios of the solvent-free system, an internal/external validation procedure was applied. A total of four experiments applying substrate ratios of benzylamine **1** and *trans*-ethyl crotonate **2** of 1.5:1, 1.77:1, 3:1 and 4:1 mole equivalents were carried out and integrated into a single chemometric model. The data obtained from offline HPLC measurements was described with good accuracy in all cases. Figure 5.9a exemplarily shows the inline data obtained from FTIR measurements and the offline HPLC data for the substrates **1** and **2** as well as the main product *rac*-**3**. The predictive reliability of the developed chemometric model was verified by external validation. This was achieved by carrying out an experiment with an initial molar ratio of the two substrates **1** and **2** of 2:1 mole equivalents, which had not been used for model calculation. The predicted data obtained from inline FTIR monitoring is in good agreement with the data obtained from offline HPLC data (Figure 5.9b). Deviations at the beginning of the reaction may have been caused by a non-equilibrated system with regard to constant temperature, pressure and flow rate and are less likely to result from model inaccuracy. Relevant statistical data and information on the procedure applied for the development of the chemometric model are summarized on page 114 in the appendix. The chemometric model for the real-time conversion and concentration prediction may be applied in a continuous reactor setup as described in chapter 6 on page 65.

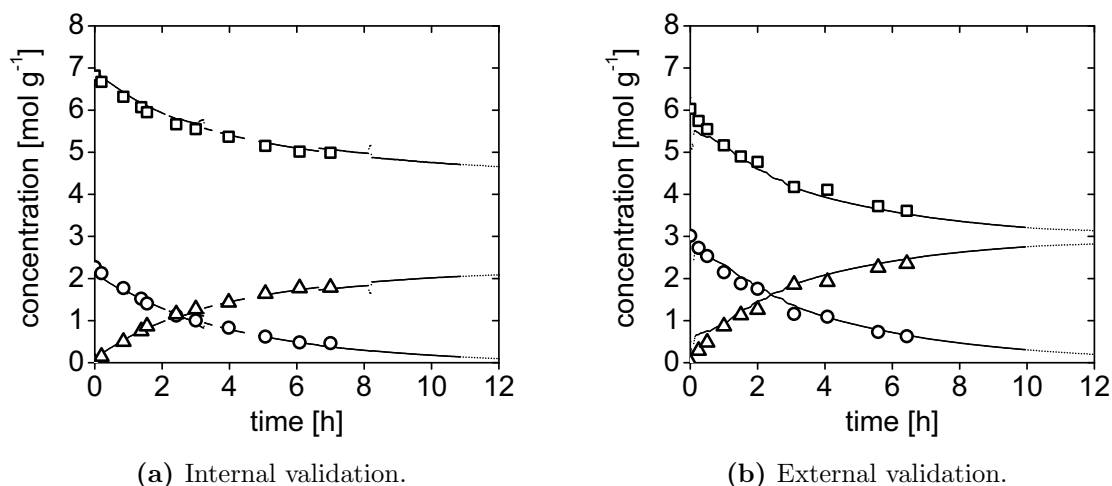


Figure 5.9: Internal and external validation of regression model for the prediction of concentrations in aza-Michael addition of **1** and **2** monitored inline using FTIR flowcell. Offline HPLC data is represented by symbols, inline FTIR data by dots. **1** (\square); **2** (\circ); *rac*-**3** (\triangle). 60 °C, flow rate 0.25 ml min⁻¹, integration time of FTIR spectrum collection: 1 min. The aza-Michael addition reactions were carried out with (a) 3:1 mole eq. of **1** and **2** and (b) 2:1 mole eq. of **1** and **2**, respectively.

5.2.2 Biocatalytic aminolysis

Analogously, a batch reactor setup with bypass analytics was used for the FTIR inline monitoring of the biocatalytic aminolysis of *rac*-**3** and **1** with the flowcell. The experimental setup is shown in Figure 5.10. The reactants are circulated continuously from a substrate reservoir through a packed bed reactor containing the immobilized enzyme Novozym 435. The FTIR flowcell was connected at the outlet of the packed bed reactor. A bubble trap was installed prior to the flowcell to avoid signal fluctuations caused by bubbles.

Three experiments were used for the development of a chemometric model in an internal validation procedure. The products of aza-Michael additions carried out in a solvent-free system and without purification of the reactants were used as substrates for the Novozym 435-catalyzed aminolysis. Starting molar fractions of benzylamine **1** and the ester *rac*-**3** were approximately 1:2, 2:1 and 3:1 mole equivalents. An excellent agreement of the experimental data obtained offline via HPLC was achieved using the chemometric model for calibration in the internal validation procedure (Figure 5.11a). The same model applied for the prediction of a reaction carried out with a starting molar ratio of 1:1 mole equivalents of **1** and *rac*-**3** yielded an excellent prediction of the concentrations of substrate *rac*-**3** and product *rac*-**4** (Figure 5.11b). The relevant degree of conversion of *rac*-**3** can be calculated easily from these two compounds alone. Larger deviations were observed for the substrate **1**, despite a correct display of the trend of the reaction course. This observation may result from the IR absorption characteristics of benzylamine, which lacks a similarly predominant absorption band of functional ester

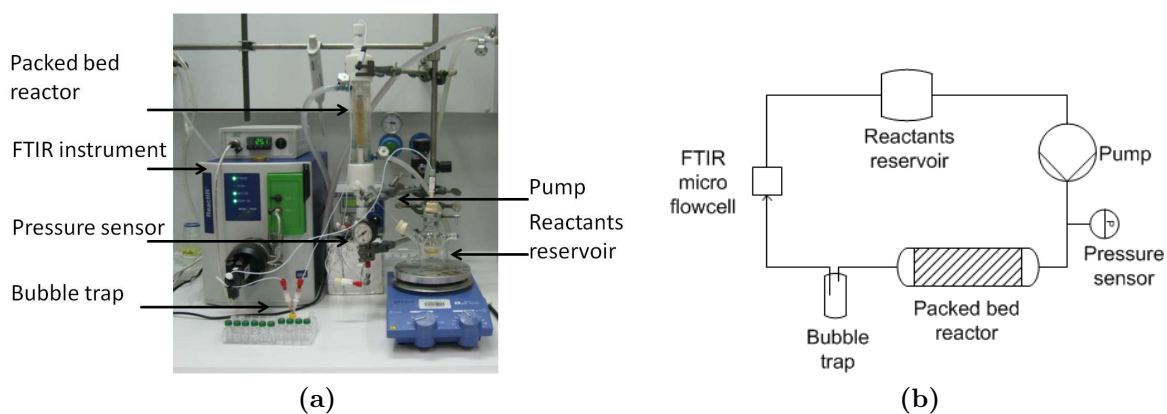


Figure 5.10: Batch reactor setup with bypass analytics for the inline reaction monitoring of the solvent-free Novozym 435-catalyzed aminolysis of *rac*-**3** and **1** applying an FTIR flowcell. (a) photographic. (b) schematic.

or amide groups as in the case of compounds **3** and **4**. Relevant statistical data and information on the procedure applied for the development of the chemometric model is summarized on page 114 in the appendix. As in the case of the aza-Michael addition, a chemometric model for the real-time conversion and concentration prediction could be established that may be used to monitor inline the biocatalytic aminolysis in a continuous reactor setup as outlined in chapter 6 on page 65.

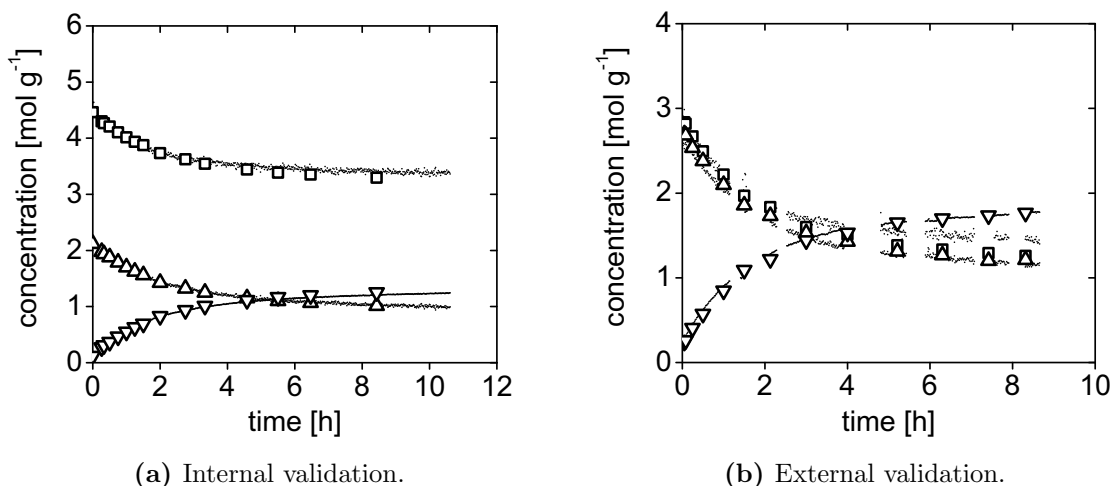


Figure 5.11: Internal and external validation of regression model for the prediction of concentrations in biocatalytic aminolysis of *rac*-**3** and **1** monitored inline using FTIR flowcell. Offline HPLC data is represented by symbols, inline FTIR data by dots. **1** (□); *rac*-**3** (Δ); *rac*-**4** (∇). 60 °C, 0.27 g g⁻¹ Novozym 435, flow rate 0.25 ml min⁻¹, integration time of FTIR spectrum collection: 1 min. Aminolysis reactions were carried out directly after aza-Michael addition with (a) 3:1 mole eq. of **1** and **2** and (b) 2:1 mole eq. of **1** and **2**, respectively, without prior purification of intermediates.

5.3 Summary

In this chapter, the applicability of FTIR spectroscopy for the inline monitoring of both the aza-Michael addition and the Novozym 435-catalyzed aminolysis was investigated. A fiber probe with diamond tip was applied in batch experiments and a Micro flowcell in batch experiments with bypass analytics. The experiments can be summarized as follows:

- The feasibility of applying FTIR spectroscopy for the accurate real-time monitoring of both aza-Michael addition and biocatalytic aminolysis was demonstrated.
- A chemometric model was developed using the Mettler Toledo ICQuant software. Internal - and external validation of the model was carried out. An accurate prediction of the data collected offline via HPLC was achieved applying the model.
- A high signal to noise ratio was observed in the solvent-free system, allowing even the precise prediction of low concentrations of the side product *rac*-**4** in the aza-Michael addition.
- An ATR flowcell could be applied similarly with excellent signal intensity.
- Signal fluctuations caused by pressure drops could largely be avoided installing a pressure maintenance valve.

- A chemometric model was developed based on several experiments. Internal validation of the model showed good accuracy in all experiments for both aza-Michael addition and aminolysis.
- External validation for the prediction of a reaction with starting concentrations not used for model development was carried out. Inaccuracy of the predictive capability of the model was only observed for benzylamine in the biocatalytic aminolysis. Concentrations of all other compounds were predicted with good accuracy.

6 Continuous chemo-enzymatic process

Continuous processes represent an attractive approach applied in the chemical and pharmaceutical industry. Major advantages lie in the possibility to achieve high space-time yields by making efficient use of substrates and catalysts, improved safety aspects and a significantly reduced physical space requirement as opposed to conventional batch reactors [20]. Additionally, a decreased labor input of skilled workers is required in case of stable processes with long operation times. The stability of the process, however, is often limited by catalyst deactivation or wash-out, contamination in the case of bioprocesses, or mechanic failure of pumps, valves, membranes or pipes (depending on process e.g. caused by precipitate formation, membrane fouling etc.).

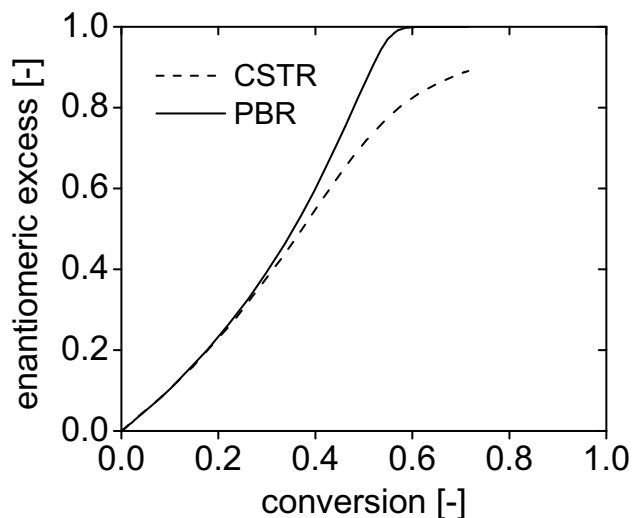
This chapter covers the development of a reactor setup for the continuous chemoenzymatic production of (*S*)-ethyl 3-(benzylamino)butanoate ((*S*)-**3**) in a solvent-free system based on the experimental results covered in chapter 3 for the aza-Michael addition and chapter 4 for the Novozym 435-catalyzed aminolysis. As a coupled reaction carried out in continuous flow, the process belongs to the class of fourth generation processes according to the classification introduced in Section 1.4 on page 10.

Reactor Design: Theoretical Aspects

While numerous reactor layouts exist that are specifically adapted to a given reaction system, only two general ideal reactor types exist for the realization of a continuous operation mode: continuous stirred tank reactors (CSTR) and plug flow reactors (PFR). Characteristics of the reaction system determine the layout suited best for the achievement of e.g. maximum selectivity, total turnover or productivity. The aza-Michael addition of **1** and **2** under investigation here was found to yield the product *rac*-**3** as the main product. However, in a slow successive side reaction, the aminolysis of *rac*-**3** to form *rac*-**4** was observed. While a CSTR would favor the formation of the final product (*rac*-**4**) and thus lead to decreased yields, maximal formation of the intermediate product *rac*-**3** can be achieved using a PFR [70]. Similarly, the Novozym 435-catalyzed aminolysis of *rac*-**3** may be carried out in a CSTR or a PFR in the form of a packed bed reactor (PBR). For kinetic reasons, the latter reactor type is favored in order to achieve maximal yields of the desired chiral product with high enantiomeric excess. In a CSTR, the continuous operation at high conversion of the "correct" enantiomer necessarily leads to operation at high concentration of the "wrong" enantiomer, thus kinetically favoring its conversion and causing decreased yields. The effect becomes obvious when plotting

the enantiomeric excess as a function of conversion for both PBR and CSTR (Figure 6.1).

Figure 6.1: Simulation of enantiomeric excess as a function of conversion in PBR and CSTR reactor in the Novozym 435-catalyzed kinetic resolution of *rac*-**3** with **1**. The simulation was based on the kinetic model introduced in section 4.5. Initial concentrations for each compound were as obtained from an aza-Michael addition carried without prior purification of intermediates. $[\mathbf{1}]_0 = 2.15 \text{ g g}^{-1}$, $[(R)\text{-}\mathbf{3}]_0 = 1.50 \text{ g g}^{-1}$, $[(S)\text{-}\mathbf{3}]_0 = 1.50 \text{ g g}^{-1}$, $[(R)\text{-}\mathbf{4}]_0 = 0.69 \text{ g g}^{-1}$, $[(S)\text{-}\mathbf{4}]_0 = 0.069 \text{ g g}^{-1}$.



The depicted simulation was based on the kinetic model introduced in section 4.5 on page 44 and clearly demonstrates the advantage of a PBR reactor as compared to a CSTR reactor in the kinetic resolution investigated in this study. Taking these aspects into account, a coupled reactor design comprising a tube reactor for the aza-Michael addition and a packed bed reactor for the Novozym 435-catalyzed aminolysis was envisioned as depicted in Figure 6.2.

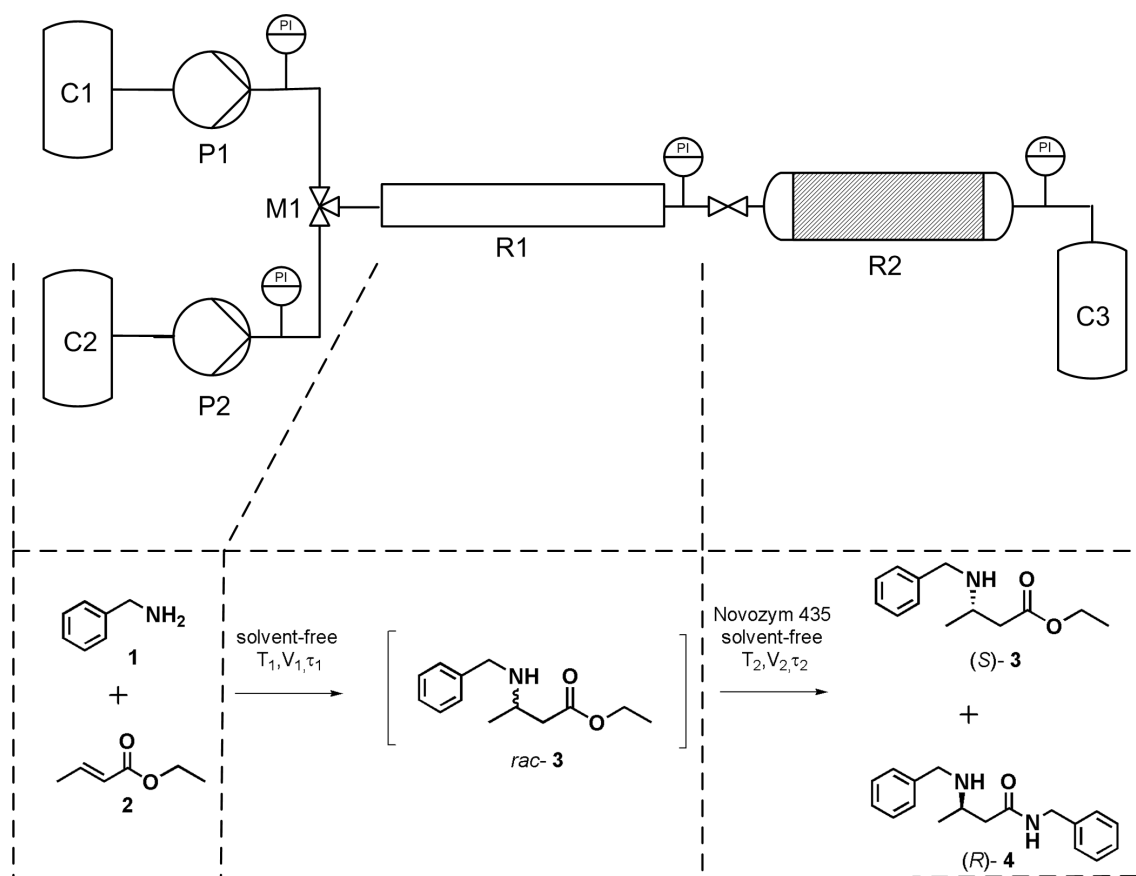


Figure 6.2: Schematic depiction of coupled reactor setup for the chemoenzymatic production of (*S*)-ethyl 3-(benzylamino)butanoate. C1, C2: substrate containers. C3: product container. M1: mixing tee. R1: tube reactor. R2: packed bed reactor.

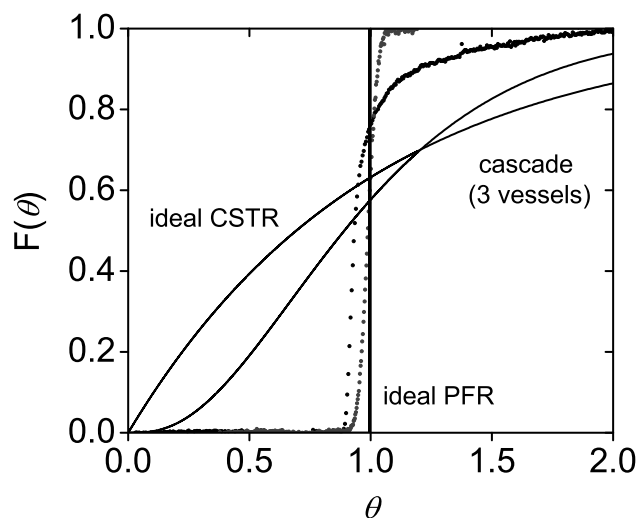
6.1 Continuous aza-Michael addition in tube reactor

With the kinetic and thermodynamic data of the aza-Michael addition from batch experiments in hand (chapter 3), a transfer of the system to a continuously operated plug flow reactor can be realized. In an ideal PFR backmixing or turbulent flow profiles do not occur. The reaction time in a batch process and the residence time τ in a PFR are used analogously. In an otherwise identical mathematical description of the two reactors, these two dimensions are exchanged [11]. Consequently, in a PFR the concentration changes with the length of the reactor instead of time as in a batch reactor.

6.1.1 Flow characteristics

In order to verify, if the assumption of an ideal reactor is true for envisioned reactor geometries, a residence time distribution analysis was carried out [70]. Plug flow reactors of two different dimensions were tested using water as a model system with 3.0 mM benzaldehyde as a tracer substance that can be detected using an Ocean Optics UV Flowcell for continuous monitoring ($\lambda = 280$ nm). $F(\theta)$ with θ being the number of residence times is directly obtained after simple transformation of the UV signal as described in Section A.3.3 on page 102. The $F(\theta)$ curves for two tube reactors of identical volume but different inner diameter d_i imply an almost ideal flow behaviour (Figure 6.3). Both curves resemble the ideal behaviour of a PFR and show a significantly decreased residence time distribution as compared to a 3-stage cascade reactor. Thus, despite the fact that an aqueous model system has been used here instead of the solvent-free system, potential backmixing can most likely be neglected and a laminar flow is seemingly observed.

Figure 6.3: Residence time distribution ($F(\theta)$ -curve) in tube reactor. Grey dots: PTFE reactor, $V = 41.6$ ml, $L = 13.25$ m, $d_i = 2.0$ mm. Black dots: PTFE reactor, $V = 41.6$ ml, $L = 82.7$ m, $d_i = 0.8$ mm. Lines are numerically simulated using model equations for ideal reactors.



For tube or pipe reactors, however, a turbulent flow is usually desired in which small vortices cause a local, lateral mixing of the liquid phase. The Reynolds number Re as

a dimensionless number is usually used to characterize flow characteristics in a tube reactor. For tubes or pipes it is defined as

$$Re = \frac{\rho_f \cdot u_f \cdot d_i}{\eta_f} \quad (6.1)$$

with ρ_f being the density of fluid, u_f the mean velocity of the fluid, d_i the inner diameter of the tube and η_f the dynamic viscosity of the fluid. While no data on the dynamic viscosity of *rac-3* is available in literature, Re numbers for the pure substrates were calculated to be $Re = 1.5$ for benzylamine (**1**) and $Re = 2.8$ *trans*-ethyl crotonate (**2**) in a tube with an inner diameter $d_i = 0.8$ mm and a flow velocity $u_f = 6.3$ m h⁻¹. Below a critical Reynolds number of $Re_{crit} \approx 2300$, the flow can be considered laminar. Due to the very low flow velocities used here in order to allow long reaction times and thereby sufficiently high degrees of conversion, it is not surprising to find a laminar flow regime in the given reactor. In fact, this is a common problem encountered for slow reactions in continuous flow necessitating several hours reaction time. In the absence of vortices in an entirely laminar flow regime, a non-ideal flow profile within the tube is caused by friction of the fluid and the tube wall. Consequently, the fluid velocity is slowed down towards the tube wall while higher velocities are found in the center of the tube. However, effects such as channeling or stagnant regions reduce the performance of the reactor and should be avoided [70]. This is seemingly observed in Figure 6.4a, where conversion in an ideally mixed batch reactor is compared to the conversion obtained in a tube reactor. Dean vortices can be used to circumvent the problem of channel wall effects. Such vortices are generated in a curved pipe by a pressure driven flow of the fluid when the higher velocity stream in the center experiences a greater centripetal force and is hence directed outward [46].

In Figure 6.4b, conversion in a coiled steel capillary reactor is plotted as a function of the flow rate at a constant residence time of $\tau = 4$ min. With increasing flow rate an increased conversion is observed. The improved mixing resulting from Dean vortices is likely to be responsible for the effect. In a microreactor setup, Howell et al. observed Dean vortice formation starting at Reynolds numbers between 1-10 that became stronger with increasing flow velocity [46]. Again, Reynolds numbers cannot be given for the system under investigation here, because no literature data is available on the dynamic viscosity and density of a 1.7:1 mole eq. mixture of the substrates **1** and **2**. The Reynolds number for pure benzylamine at 60 °C was calculated to be approximately $Re = 21$ at 0.75 ml min⁻¹ in the given reactor setup and is expected to increase sharply with temperature.¹ Unfortunately, similarly high flow velocities and hence Reynolds numbers cannot be realized easily in a tube reactor setup without at the same time drastically reducing the reaction time or increasing the length of the tube.

¹A Reynolds of $Re=45$ is calculated for benzylamine at 140 °C assuming linear density decrease with temperature.

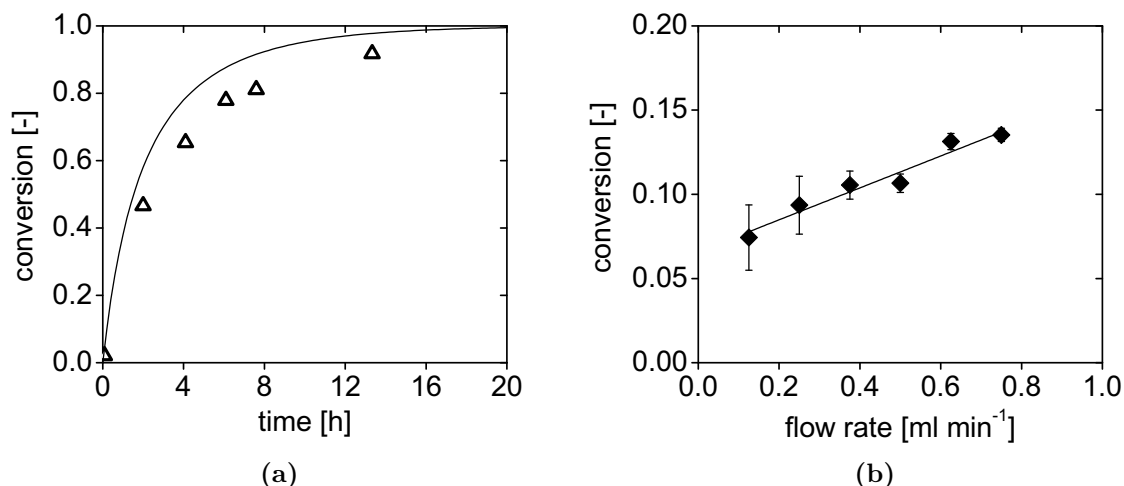


Figure 6.4: Aza-Michael addition of **1** and **2** in a plug flow reactor. (a) Prediction of conversion based on kinetic model (–) and experimental results (Δ). Tube reactor (PTFE), $V=41.6$ ml, $L=82.7$ m, $d_i=0.8$ mm. $T=80$ °C. (b) Conversion as a function of the flow rate at constant residence time $\tau=4$ min using plug flow reactors of constant diameter but increasing length. Tube reactor (stainless steel), $V=0.5$ -3 ml, $L=1$ -6 m, $d_i=0.75$ mm, $R=2.5$ cm. $T=140$ °C.

6.1.2 Temperature dependence in tube reactor

Generally short reaction times and consequently smaller reactor volumes are desirable. In particular for chemical reactions, this is usually achieved by increasing temperature. Safety issues resulting from high temperature and pressure are substantially avoided using continuously operated microreactors [142]. Therefore, high temperatures were tested using a steel capillary reactor at temperatures up to 180 °C. Despite a significant increase of the conversion rate (data not shown), selectivity is drastically reduced upon exposure to increased temperature (Figure 6.5). As suggested in chapter 3 for batch reactions, a compromise between high reaction rate and selectivity must be considered also for the continuous aza-Michael addition.

Minnich et al. developed a nested-pipe reactor to address problems encountered for slow reactions in continuous flow [88]. Improved characteristics were found with regard to heat transfer properties, dispersion characteristics and pressure drop as compared to coiled capillary or multi-tube reactors. Microreactors with improved mixing by microstructural elements may be considered and have been used previously for the Michael addition of secondary amines to α,β -unsaturated carbonyl compounds [74]. Alternatively, Taylor reactors may allow to achieve a well mixed continuous reactor with near-ideal plug flow characteristics as well. The reactors are composed of two cylinders in which mixing is provided by rotation of the inner cylinder. Selection of a suited rotation speed defining the Taylor number allows to define the residence time distribution from near-ideal CSTR to PFR. Such reactors have, for example, been used for polymerization

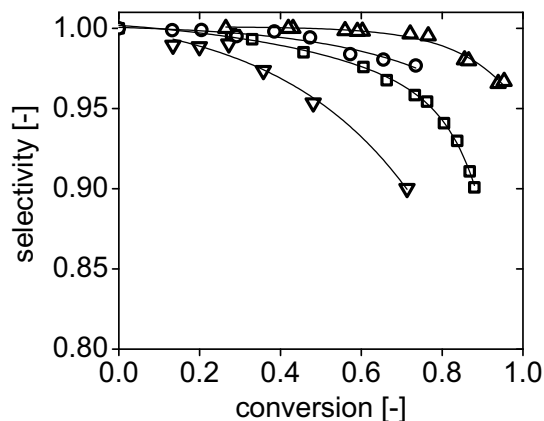


Figure 6.5: Temperature dependence of selectivity in thermal aza-Michael addition carried out with 1.7:1 mole eq. of **1** and **2** in plug flow reactor. 70 °C (Δ); 100 °C (○); 140 °C (□); 180 °C (▽). Flow rate: 0.035 - 0.75 ml min⁻¹.

reactions, but also for enzymatic conversions [34, 59].

6.2 Biocatalytic aminolysis in packed bed reactor

In order to transfer previous results from batch experiments to a continuous packed bed reactor setup, geometrical parameters of reactor and catalyst must be considered. A borosilicate glass reactor of $d_i=1$ cm was chosen as a suitable PBR due to its chemical resistance and flexibility with regard to adjustment of reactor length. The heterogeneous catalyst Novozym 435 according to the manufacturer has a bulk particle density of

$$\rho_{bp} = \frac{m_{p,tot}}{V_{PB}} = 430 \frac{kg}{m^3} \quad (6.2)$$

With a Sauter mean diameter of the particles of 498 μm and an average mass of a single particle of $\bar{m}_p = 6.095 \cdot 10^{-5} g$, the density of the carrier material is calculated to

$$\rho_p = \frac{\bar{m}_p}{\frac{\pi}{6} \cdot d_p^3} = 946 \frac{kg}{m^3} \quad (6.3)$$

The porosity ε describing the void volume in the reactor may be calculated as

$$\varepsilon = 1 - \frac{\rho_{bp}}{\rho_p} = 0.543 \quad (6.4)$$

The data was used to estimate residence times depending on the amount of catalyst and the volumetric flow rate. However, deviations were observed comparing calculated and experimentally determined bulk particle density and porosity, which in turn impact parameters such as void and total volume and the residence time (see Table 6.1 on page 75). All calculations and simulations were based on experimentally determined parameters.

Long reaction times of the aza-Michael addition described in the previous section necessitate low flow rates. However, in reactions carried out with enzymes immobilized

on porous carriers, external mass transfer or internal diffusion limitations are a common problem. For batch reactions, such limitations could be excluded (Section 4.3 on page 33). The potential presence of diffusion limitation can be determined experimentally for packed bed reactors by comparing the conversion of two PBRs with different amounts of catalyst. Equal residence times in both reactors of different catalyst loading can be achieved by varying the flow rate. Similar conversion levels at equal residence times are expected in case no diffusion limitation is present. A decreased degree of conversion in the reactor that is operated at lower flow rates (lower catalyst load) on the other hand indicates the presence of diffusional limitations. Figure 6.6a shows the conversion as a function of residence time for two PBRs of 3.5 ml (PBR₁) and 7 ml (PBR₂) void volume. Additionally, the conversion for a batch reaction known to be not limited by mass transfer phenomena is shown. The respective values were calculated from reactions carried out with a lower catalyst concentration as compared to PBR experiments. Negligible differences are visible comparing batch reactor and larger PBR₂. In Figure 6.6b, conversion is plotted as a function of the volumetric flow rate at constant residence time. Each curve represents a different residence time. Only minor differences can be observed for PBR₁ and PBR₂ indicating weak diffusion limitation.

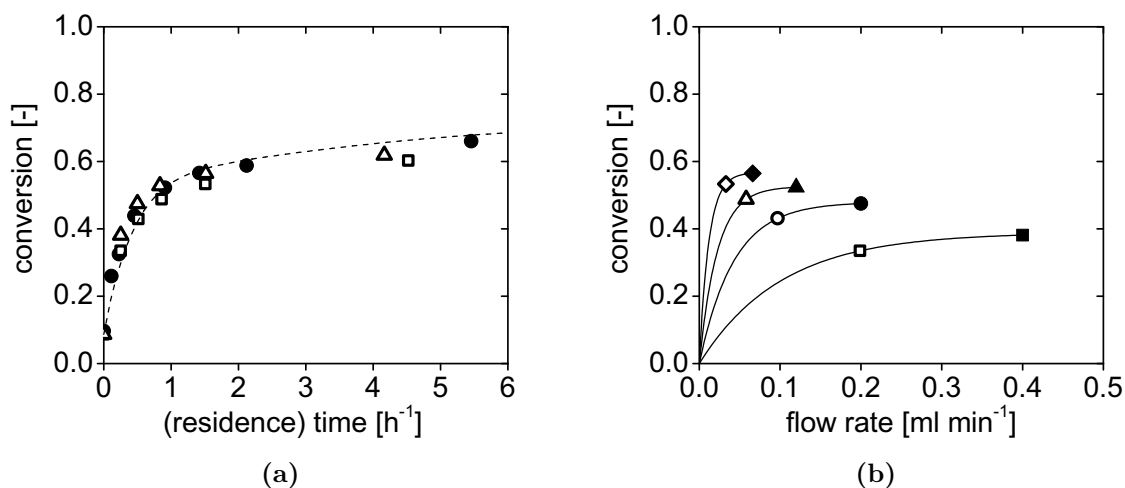


Figure 6.6: Diffusion limitation in packed bed reactor for Novozym 435-catalyzed aminolysis. (a) Comparison of conversion of benzylamine **1** as a function of residence time in batch reactor and two packed bed reactors. $T=60\text{ }^{\circ}\text{C}$, $\chi_{0,rac-3} = 0.62$. Batch reactor (\bullet); PBR₁, $V_1=3.5\text{ ml}$ void volume (\square); PBR₂, $V_2=7\text{ ml}$ void volume (\triangle); simulation based on kinetic model introduced in Section 4.5 on page 44 (---). (b) Comparison of conversion of *rac-3* in two PBR of different void volume and equal residence time. Open symbols: PBR₁, $V_1=3.5\text{ ml}$. Filled symbols: PBR₂, $V_2=7\text{ ml}$. $\tau=0.25\text{ h}$ (\blacksquare/\square); $\tau=0.50\text{ h}$ (\bullet/\circ); $\tau=0.85\text{ h}$ (\blacktriangle/\triangle), $\tau=1.5\text{ h}$ (\blacklozenge/\lozenge).

6.3 Coupled reactor setup for the continuous production of (S)-ethyl 3-(benzylamino)butanoate

A coupled reactor setup according to scheme 6.2 on page 67 comprising both the tube reactor for the aza-Michael addition (stage 1) and the packed bed reactor for the subsequent Novozym 435 catalyzed aminolysis (stage 2) must be based on thermodynamic and kinetic information obtained from batch experiments. Optimization of the overall reactor performance mainly depends on the enzymatic reaction carried out in the PBR. A high operational stability of the biocatalyst and a good turnover frequency are crucial in order to develop any economically attractive process. Important aspects to consider with respect to the substrate ratio effects in the biocatalytic aminolysis are therefore summarized graphically in Figure 6.7.

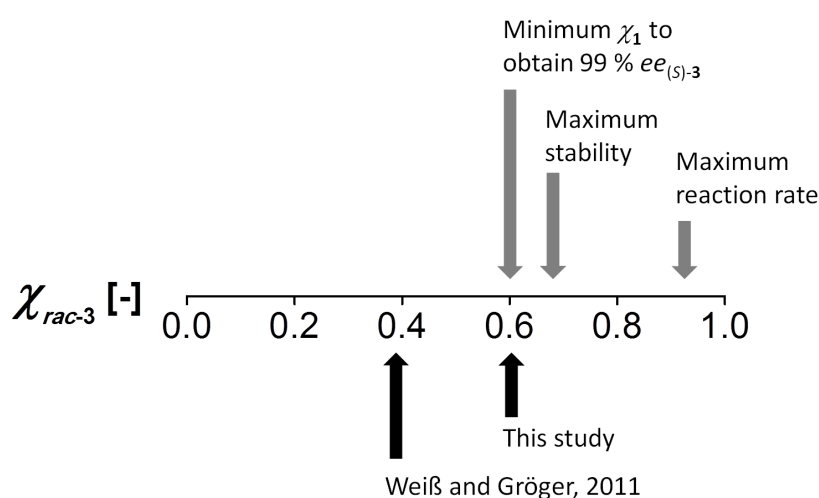


Figure 6.7: Summary of optimized parameters as obtained from batch experiments (chapters 3 and 4).

A high enantiomeric excess of ideally >99 % of the product *rac-3* is a prerequisite in order to achieve a value added product, for which approximately 60 % conversion of *rac-3* are necessary given the intrinsic selectivity of Novozym 435. Consequently, benzylamine **1** as a remainder from stage 1 must be available as a substrate in sufficient amounts in stage 2. At the same time, the excess of **1** should be kept as low as possible for kinetic, stability and atom efficiency reasons. Taking into consideration that due to non-ideal flow conditions in the PFR (stage 1), 92 % conversion can be achieved in a reasonable time frame ($\tau = 13.3$ h, $T = 80$ °C), the requirements can be fulfilled best using an initial molar ratio of approximately 1.7:1 of substrates **1** and **2**.

Based on the concentration of each compound, the kinetic model derived in chapter 4.4 on page 34 was used to simulate $ee_{(S)-3}$ and conversion as a function of residence time with a fixed amount of 6.3 g of Novozym 435 assuming no impact of diffusional limitation. Figure 6.8 shows that a residence time τ of approximately 2.7 h is necessary

to obtain 99 % *ee* at 58 % conversion.

Figure 6.8: Simulation of conversion (—) and enantiomeric excess (---) as a function of residence time in a packed bed reactor ($m_{\text{Novozym435}} = 6.3 \text{ g}$, $60 \text{ }^\circ\text{C}$). Initial substrate concentrations used for simulation were as obtained in previous experiments from aza-Michael addition carried out in a PFR with an initial substrate ratio of 1.7:1 for **1** and **2** ($\tau = 13.3 \text{ h}$, $T = 80 \text{ }^\circ\text{C}$, conversion = 92 %).

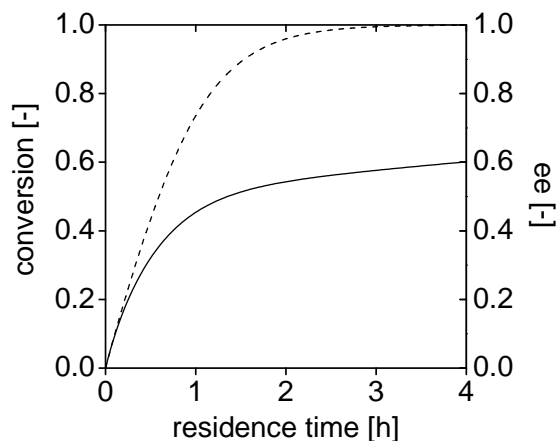


Table 6.1 summarizes calculated and observed data characterizing the geometric reactor data and operational parameters such as volume flow and residence time for two PBRs that were coupled in series in the continuous reactor setup. The coupling of two reactors allowed to determine the conversion/*ee*-data at different degrees of conversion within a single experiment. Slightly lower flow rates were observed for the second reactor due to a density increase from approximately 1.00 g ml^{-1} at ambient temperature at the inlet of the first PBR to about 1.06 g ml^{-1} at ambient temperature at the inlet of the second PBR due to ongoing conversion in the solvent-free system.

A photographic depiction of the coupled reactor setup for the continuous production of *rac-3* is shown in Figure 6.9. The helical winding of the tube reactor for the aza-Michael addition that was applied in the coupled reactor setup is shown in Figure 6.10.



Figure 6.9: Photographic depiction of reactor setup for the continuous aza-Michael addition and subsequent Novozym 435-catalyzed aminolysis.

6.3 Coupled reactor setup for continuous production

Table 6.1: Calculated and observed data characterizing the packed bed reactor used in a coupled, continuous flow reactor setup.

#	d_i [cm]	m_{N435} [g]	V_{total} [ml]	V_{void} [ml]	L [cm]	\dot{v} [ml·min ⁻¹]	u [cm·min ⁻¹]	τ [h]	ρ_{bp} [g·ml ⁻¹]	ε [-]
calculated^a										
1	1	4.3	10.0	5.4	12.7	0.052	0.12	1.7	0.43	0.54
2	1	2.0	4.7	2.5	5.9	0.052	0.12	0.8	0.43	0.54
observed^b										
1	1	4.3	11.9	7.8	15.2	0.052	0.10	2.5	0.36	0.65
2	1	2.0	5.1	3.4	6.5	0.049	0.09	1.2	0.39	0.67

^aValues with grey background as expected according to porosity and bulk particle density (provided by manufacturer) for given amount of Novozym 435. ^bValues with grey background as determined experimentally for given amount of Novozym 435. See Appendix A.3.3 on page 103 for further details on experimental procedures.

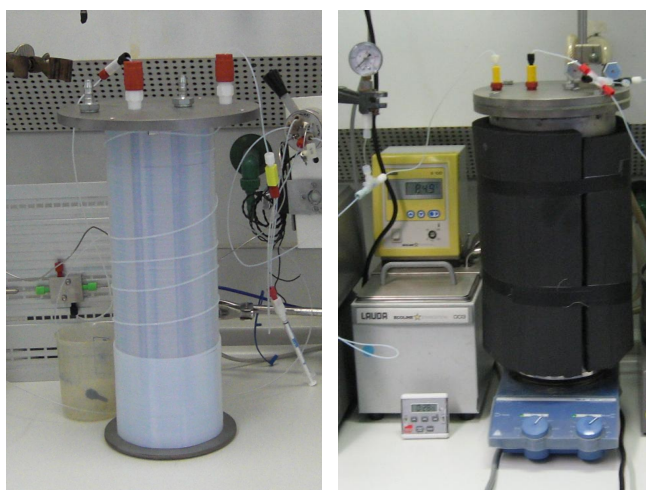


Figure 6.10: Photographic depiction of helically wound tube reactor for the aza-Michael addition as applied in the coupled reactor setup (left). The reactor was incubated in a steel pot connected to a thermostat for temperature control (right).

The reactor was continuously operated for 88 h without significant loss of activity. With a residence time $\tau=2.5$ h a conversion of 55 % at $ee_{(S)-\mathbf{3}}=0.97$ was achieved (Figure 6.11a). A further elongation of the residence time to $\tau=3.7$ h led to an increased conversion of 59 % and an average $ee_{(S)-\mathbf{3}}$ of 0.98 (Figure 6.11b). With regard to conversion, the results for both residence times are in good agreement with the simulated data based on the kinetic model introduced in chapter 4. The enantioselectivity is slightly lower as expected. Enzyme deactivation was not observed to a significant degree in the time frame of operation. Diffusional limitations were not regarded in the kinetic model despite earlier observations indicating the presence of weak limitations (Section 6.2 on page 71). The presence of such a limitation should be more predominant at lower conversion. At high conversion of the preferred substrate (*R*)-**3**, the overall reaction rate is very low leading to minor differences in conversion. This becomes obvious comparing the only slightly increased conversion after $\tau=3.7$ h as opposed to after $\tau=2.5$ h. Thus, a potential effect of diffusion limitation may be within the error of analysis and therefore not detectable. The operation of the process was aborted after 88 h due to blocked capillaries and sampling valves caused by a colorless precipitate. The precipitate may have been formed from benzylamine, which upon exposure to carbon dioxide forms the corresponding carbamic acid salt [41] or the corresponding acid of *rac*-**3** after enzyme-catalyzed hydrolysis with residual water contained in the substrate solutions.

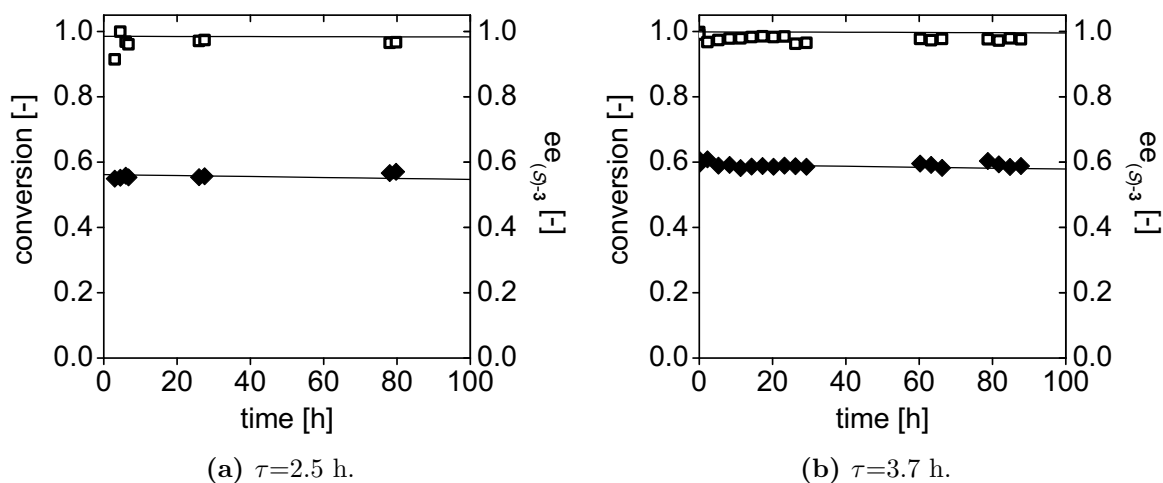


Figure 6.11: Conversion and ee as a function of reaction time in coupled reactor for the continuous aza-Michael addition of **1** and **2** and subsequent Novozym 435 catalyzed aminolysis. Symbols represent experimental data: Conversion of *rac*-**3** (\blacklozenge). $ee_{(S)-\mathbf{3}}$ (\square). Lines represent predicted data as obtained from simulation based on kinetic model (see Sections 4.4-4.5). PTFE tube reactor: 80 °C, $V = 41.6$ ml, $L = 82.7$ m, $d_i = 0.8$ mm. Packed bed reactor: 60 °C, $V_{total} = 17$ ml, $L_{total} = 21.7$ cm, $d_i = 1$ cm, 6.3 g Novozym 435. Flow rate for substrates **1** and **2**: $\dot{v}_1 = 0.303$ mmol min^{-1} , $\dot{v}_2 = 0.180$ mmol min^{-1} .

6.3 Coupled reactor setup for continuous production

Parameters characterizing the performance of the process are summarized in Table 6.2 for the aza-Michael addition and Table 6.3 for the Novozym 435-catalyzed aminolysis. The achieved results are compared to those obtained by Weiß [138] using non-optimized conditions. In PFR experiments, the STY was improved by a factor of almost 2. The applied substrate ratio of 1.7:1 was kinetically less favorable for the aza-Michael addition as compared to a 2.2:1 ratio, but the effect was compensated by the use of a higher temperature. For the PBR, a STY of $1.8 \text{ kg L}^{-1} \text{ d}^{-1}$ was obtained at about 59 % conversion, 98 % *ee* and a catalyst productivity *Q* of $4.8 \text{ kg kg}_{N435}^{-1} \text{ h}^{-1}$. Compared to Weiß, the results correspond to an improvement by almost 40 % for the STY and about 32 % for the catalyst productivity *Q*. The total turnover number *ttn* was significantly enhanced by a factor of 5.4, which in turn leads to catalyst costs reduced by the same factor. The higher *ttn* can be attributed to the increased stability of Novozym 435 under the applied optimized conditions.

Table 6.2: Comparison of the PFR performance for the aza-Michael addition as carried out by Weiß, 2011 [138] and under optimized conditions (this study).

	Molar ratio^a [-]	T [°C]	τ [h]	X [-]	STY [kg L ⁻¹ d ⁻¹]
Weiß, 2011 [138]	2.2:1	60	24	0.91	0.7
this study	1.7:1	80	13.3	0.92	1.2

^aMolar ratio of benzylamine **1** and *trans*-ethyl crotonate **2**.

Table 6.3: Comparison of the PBR performance for the Novozym 435-catalyzed aminolysis as carried out by Weiß, 2011 [138] and under optimized conditions (this study).

	χ_{rac-3} [-]	T [°C]	τ [h]	X [-]	ee [-]
Weiß, 2011 [138]	0.38	60	4.25	0.54	0.95
this study	0.53	60	3.67	0.59	0.98

	STY^a [kg L ⁻¹ d ⁻¹]	Q [kg kg _{N435} ⁻¹ d ⁻¹]	ttn^b [-]	spec. ttn [mol kg _{N435} ⁻¹]	cat. costs [€ mol ⁻¹]
Weiß, 2011 [138]	1.3	3.7	29000	44	32.0
this study	1.8	4.9	158000	239	5.8

^abased solely on the volume of the PBR. ^bexpected according to stability determined in batch experiments. Calculation according to B.7 on page 109. ^c1400 € kg⁻¹ (Novozymes, Denmark).

6.4 Summary

This chapter covered the characterization of the coupled, continuous reactor for the continuous production of (*S*)-**3** via aza-Michael addition in a tube reactor and subsequent Novozym 435-catalyzed aminolysis in a packed bed reactor from benzylamine and *trans*-ethyl crotonate as starting materials. The results can be summarized as follows:

- A tube reactor is suited for carrying out the solvent-free aza-Michael addition of **1** and **2** in continuous mode. However, a lower conversion rate was observed compared to batch reactions. As a consequence of the slow reaction the reactor was operated at low Reynolds numbers ($Re=1-3$). This probably causes a reduced flow velocity near the tube wall and thus non-ideal flow characteristics, which may account for the observed deviation.
- The formation of Dean vortices at high flow rates leads to an improved conversion. However, such flow rates are difficult to realize for slow reactions when high conversions are needed.
- The reaction rate of the aza-Michael addition increases with temperature. A substantial loss of selectivity towards high temperatures is observed in the PFR leading to formation of *rac*-**4** as a side product.
- Only weak diffusional limitations were observed operating the PBR containing porous Novozym 435 as a heterogenous catalyst.
- The coupled reactor was operated for 88 h without significant loss of activity. A high enantiomeric excess of 98 % could be achieved at 59 % conversion and a residence time τ of 3.7 h. The simulation based on the kinetic model without consideration of diffusional limitation predicted the experimental data with good accuracy.
- The process was aborted after blocking of capillaries caused by precipitate formation. This may have been caused by hydrolysis *rac*-**3** to the corresponding acid or by carbamic acid salt formation from benzylamine and CO₂.
- A space-time yield of 1.8 kg L⁻¹ d⁻¹ was achieved, which represents an improvement by almost 40 % compared to results obtained by Weiß. A specific total turnover number ttn of 239 mol kg_{N435}⁻¹ was calculated leading to an estimated catalyst price of 5.8 € mol⁻¹.

7 High pressure reaction

The application of high pressure has already found industrial relevance as a nonthermal technology for food processing and preservation in the early 1990s. Whole organisms as well as isolated enzymes can be inactivated by pressure or a combination of pressure and temperature [104]. In a recent publication, Aertsen et al. reviewed the effect of high pressure on diverse biological systems ranging from proteins and enzymes to viruses, microorganisms, mammalian cells and tissues, emphasizing the large range of application of high pressure technology [1]. In enzyme-catalyzed reactions, high pressure has been investigated as an alternative physical engineering parameter besides e.g. temperature or pH [79]. Particular focus has been put on studying the pressure-induced effect on selectivity, stability of biocatalyst and reactants, kinetics and thermodynamic equilibrium. Interesting applications include amongst others enantioselective esterifications with lipases or the thermolysin catalyzed synthesis of pharmacological peptides [65]. In the continuous effort to find new reaction media with improved characteristics for enzymatic conversions, reactions carried out in supercritical CO_2 have shown interesting opportunities (for selected examples see [13, 80–82]). Such reactions necessarily have to be carried out under high pressure conditions around 10 MPa or higher in order to maintain CO_2 in a supercritical state.

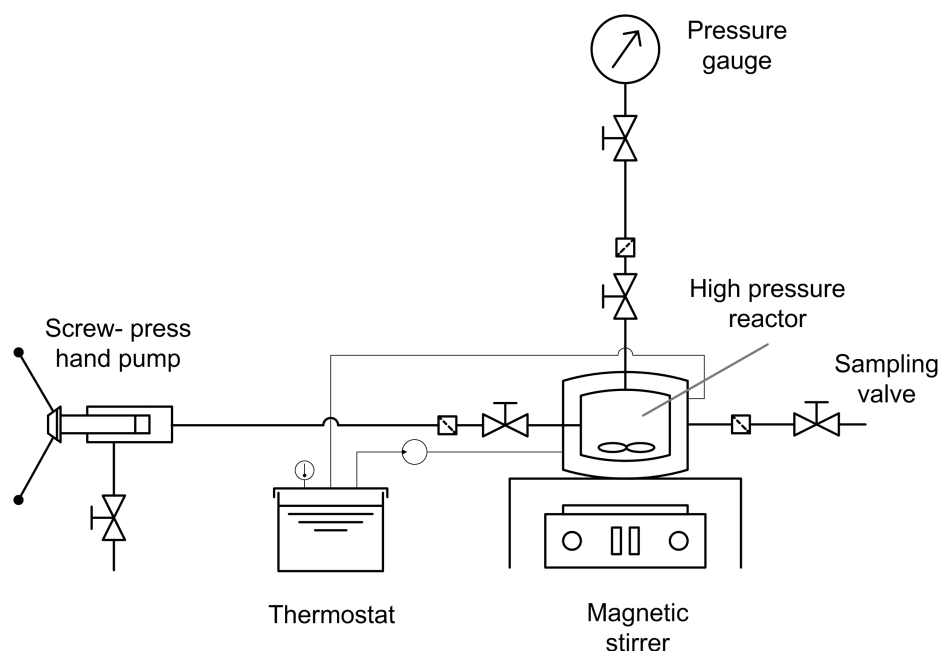


Figure 7.1: Schematic depiction of high pressure batch reactor.

7 High pressure reaction

In this study, the pressure induced effect on enantioselectivity of the Novozym 435-catalyzed kinetic resolution of *rac*-**3** with **1** was investigated (see Scheme 4.1 on page 25).¹ Additionally, the reaction rate and stability of the biocatalyst were analyzed. The reactions were carried out in tetrahydrofuran (THF) or diisopropylether (DIPE) as organic solvent. The solvent systems were chosen mainly because of a facilitated handling and cleaning, as well as a decreased usage of the not commercially available substrate *rac*-**3** in the high pressure reactor ($V = 25$ ml). A schematic representation of the high pressure reactor used is shown in Figure 7.1.

The reactor was operated in batch mode and thermostated at 60 °C. Mixing was ensured by magnetic stirring. All high pressure reactions were carried out at 200 MPa. Before each reaction, the screw-press hand pump (see Figure 7.2b on page 80) and the connecting capillary to the reactor were pre-filled with pure organic solvent. The reactor ($V = 25$ ml) was subsequently filled with organic solvent and 50 mM of substrates **1** and *rac*-**3**. Reactions were started by addition of lipase Novozym 435 at atm pressure. Only afterwards pressure was applied to the system using the screw-press hand pump. The procedure of closing the reactor and compression of the medium lasted approximately 5 min. Taking into account the low conversion observed after this time interval (see Figure 7.5 on page 84) a potential impact on enantioselectivity was neglected. A photographic depiction of the high pressure batch reactor is shown in Figure 7.2.

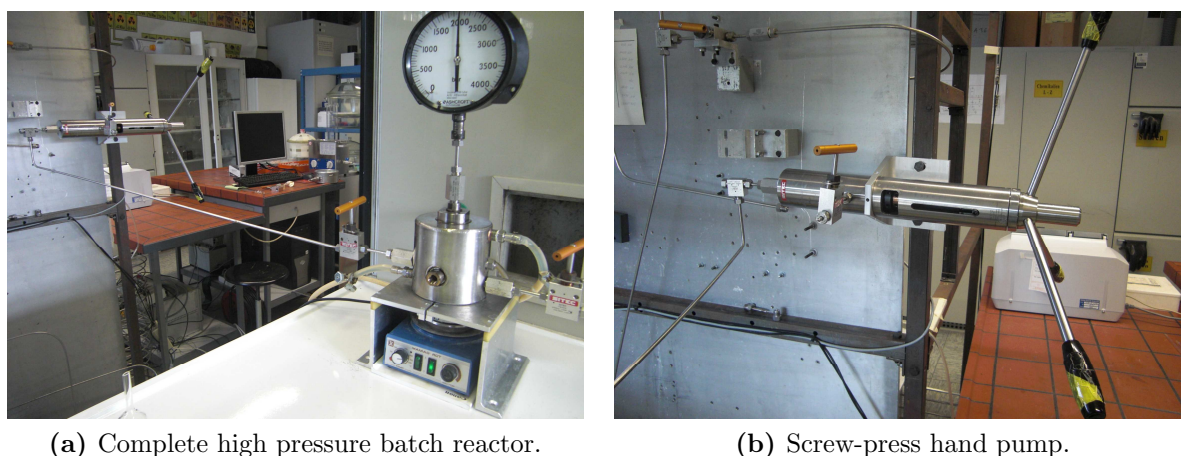


Figure 7.2: Photographic depiction of thermostated high pressure batch reactor at Process Engineering Institute, Helmut Schmidt University, Hamburg, Germany, including screw-press hand pump, pressure gauge, sampling valve and magnetic stirrer.

¹All high pressure reactions were carried out with kind support from Dipl.-Ing. (FH) D. Herbst and Prof. Dr.-Ing. B. Niemeyer at the Process Engineering Institute, Helmut Schmidt University, Hamburg, Germany.

7.1 Selectivity at high pressure

A number of publications document on structural changes of enzymes upon pressure application. Primary and secondary structures of proteins are usually not affected by pressures up to 1000 MPa, whereas pressures below 100-200 MPa are sufficient to dissociate protein oligomers [116]. Weak non-covalent forces relevant for maintaining the protein's tertiary structure such as London dispersion forces are destabilized at high pressure [90]. Intramolecular ion pairs may dissociate when pressure is applied leading to conformations with reduced volume [10]. Water molecules have been demonstrated to exert an important role in conformational changes at high pressure affecting e.g. hydrogen-bonding, compressibility, water penetration into the interior of the protein and altered conformational fluctuations. The influence of conformational changes on activity or stability has been analyzed frequently [86]. Surprisingly, only relatively few studies report on the effect of pressure on enantioselectivity [5, 55, 57, 81]. Berheide and Kara investigated the enantioselectivity of benzoylformate decarboxylase catalyzed C-C bond forming reactions at high pressure [5, 57]. They observed a pressure dependency of enantioselectivity that even rendered an enzyme with preference for the (*S*)-enantiomer into an (*R*)-selective enzyme. Thus, pressure besides enzyme- or reaction medium engineering can be considered as an alternative strategy to influence selectivity.

The effect of pressure on enantioselectivity was therefore investigated here for the kinetic resolution of *rac*-**3** with **1** in two different solvents. THF was chosen as a rather hydrophilic and DIPE as a hydrophobic solvent (see Section 4.4.1 on page 35). Preliminary results had shown an increased enantioselectivity in THF as compared to DIPE (Figure 4.6 on page 30), while at the same time the reaction rate was reduced (Figure 4.12 on page 38).

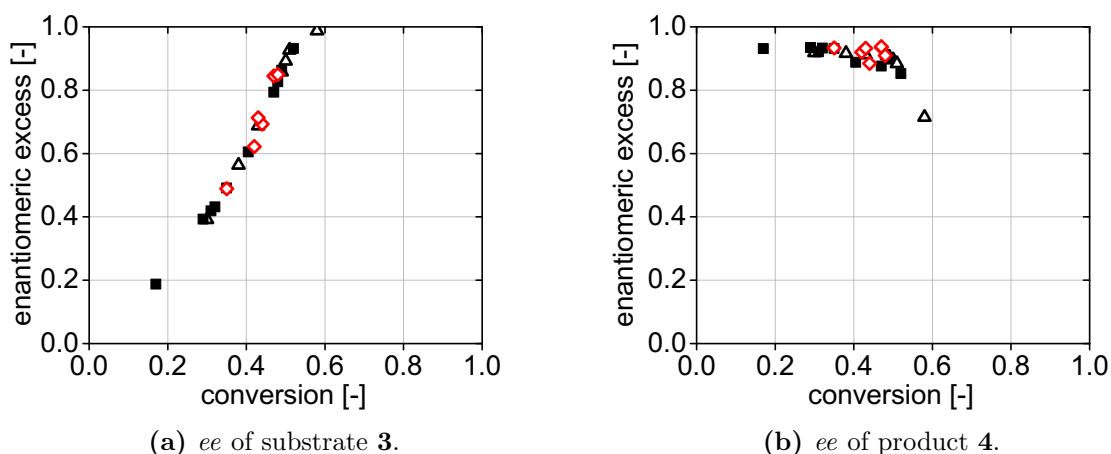


Figure 7.3: Enantioselectivity of Novozym 435-catalyzed aminolysis of *rac*-**3** with **1** in THF at atm pressure in a glass (Δ) or steel reactor (\diamond) and at 200 MPa (\blacksquare). T = 60 °C, 50 mM of substrates **1** and *rac*-**3**, 20 mg ml⁻¹ Novozym 435.

7 High pressure reaction

The enantiomeric excess of the substrate **3** and the product **4** as a function of conversion are compared for atmospheric and high pressure (200 MPa) experiments carried out in THF in Figure 7.3. Each data point of the high pressure reaction represents a new experiment. In order to exclude potential effects caused by dissolution of metal ions from the steel reactor, reactions at atmospheric pressure were conducted both in a glass reactor under reflux of the solvent and in a closed steel reactor. No obvious differences were detected in the conversion - *ee* plots in Figure 7.3. The application of high pressure therefore did not significantly render the enantioselectivity of the lipase in the investigated reaction in THF.

The data obtained in DIPE as a solvent was collected from a single experiment. Sampling was accomplished using the sampling valve (see Figure 7.1). Inevitable loss of pressure caused by the volume reduction was compensated by solvent addition using the screw-press hand pump. The sample size was approximately 2 ml. Therefore, sampling from the reactor with a total volume of 25 ml was accompanied by an approximate dilution of 5-10 V-% for each sample. The enantiomeric excess of substrate **3** and product **4** are compared in Figure 7.4.

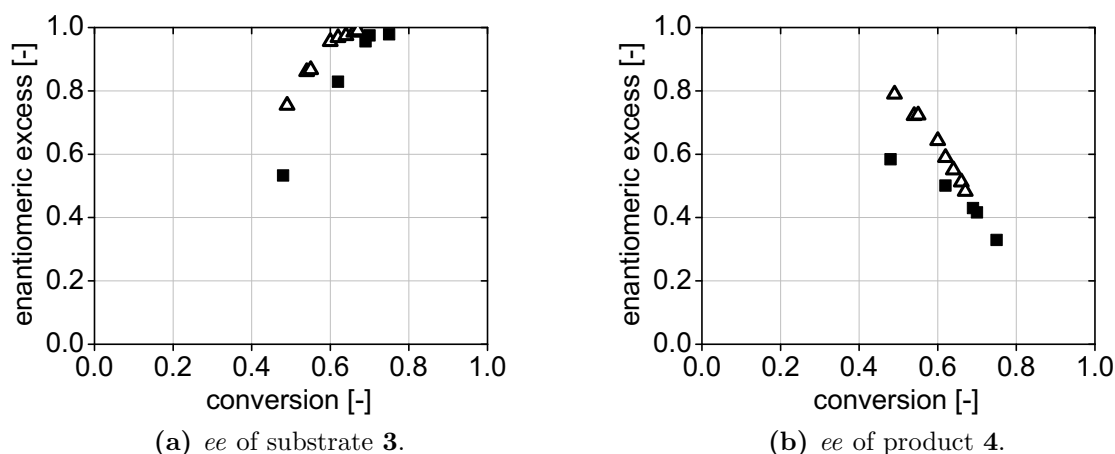


Figure 7.4: Enantioselectivity of Novozym 435-catalyzed aminolysis of *rac*-**3** with **1** at atmospheric pressure (Δ) and 200 MPa (\blacksquare) in DIPE.

A significant reduction of enantioselectivity at high pressure was observed using DIPE as a solvent. Similarly, Kahlow et al. observed a decreasing enantioselectivity with increasing pressure up to 10 MPa in the *Candida rugosa* lipase-catalyzed kinetic resolution of (\pm)-menthol with propionic acid [55]. By molecular modelling studies, they could demonstrate that an accumulation of water molecules in a cavity occurred, eventually opening the cavity to form a water tunnel and causing a decreased selectivity. Similarly, a movement of side chains may be responsible for the observed lowered selectivity in the lipase-catalyzed reaction here.

Since the sampling procedure necessitated a considerable dilution of the reactants, a substrate concentration effect must be taken into account as well. A dependency of the

enantioselectivity of enzymes on substrate concentrations has been reported previously [48, 49, 57]. Guo et al. described a mechanism of partial noncompetitive inhibition of the (*R*)-enantiomer and pure noncompetitive inhibition for the (*S*)-enantiomer as the reason for an enantioselective inhibition by chiral amines in the lipase-catalyzed asymmetric hydrolysis of a variety of racemic arylpropionic and (aryloxy)propionic esters [38]. However, the obvious differences in selectivity in Figure 7.4 are already observed in the first samples where no or negligible dilution has occurred. Additionally, previous kinetic studies (see Section 4.4.4 on page 40) have revealed a rather low inhibition by the substrate benzylamine **1** ($k_i = 0.9 \pm 0.13 \text{ mmol g}^{-1}$) and the product **4** ($k_i = 0.96 \pm 0.17 \text{ mmol g}^{-1}$). Thus, the observed changes in enantioselectivity are mainly attributed to high pressure effects. A non-catalyzed aminolysis side-reaction was not detected in control reactions in either solvent.

Most studies on pressure-induced effects on proteins that can be found in literature have been carried out in aqueous solvent systems, despite the observation that pressure can have a larger impact in organic media than in water [61]. Hydration of the protein plays a crucial role in all non-covalent interactions outlined above that are relevant for catalysis under high pressure such as stabilization of transition states or conformational changes. Therefore, pressure effects are expected to have a greater impact when the hydration level is more susceptible to changes. While in aqueous systems, water molecules are rapidly exchanged between enzyme and bulk solvent, hydration levels are especially prone to change in polar organic solvents. The experimental observations shown above do not confirm this expectation, since no effect was observed in the more polar solvent THF. On the other hand obvious differences occurred in more hydrophobic DIPE. The results suggest that solvent polarity may not be a suitable indicator to predict selectivity changes upon high pressure application. No studies could be found in literature studying the relationship between enantioselectivity, logP values of organic solvents and pressure. Matsuda and coworkers observed a decrease of the E-value in an enantioselective Novozym 435-catalyzed esterification with increasing pressure in supercritical CO₂ [80–82]. Further organic solvents, however, were only analyzed at atmospheric pressure. The elucidation of pressure induced effects in organic solvents and their effect on enzyme enantioselectivity remain a "hot topic" for further investigation in the near future.

7.2 Reaction rate at high pressure

The influence of high pressure on enzyme kinetics has been reported to depend on the activation volume (ΔV^\ddagger) and on conformational changes of the enzyme [10]. The activation volume is defined as the overall molar volume change between ground and activated states [90]. In the case of a negative activation volume change pressure accelerates the reaction. On the other hand, structural changes induced by pressure are mainly related to hydration changes. Such changes may affect the substrate binding affinity expressed by an altered K_M value. Water penetrating the active site under pressure may additionally result in weakened substrate binding caused by disruption of ion pairs between enzyme and substrate [10]. Due to the number of both positive and negative effects

7 High pressure reaction

contributing to enzyme activity under pressure, a non-linearity of enzyme activity with pressure has been observed. Depending on the enzyme, the reaction and the scale of the applied pressure increased or decreased activities may be found [89].

The time course of reactions carried out under atmospheric pressure and at 200 MPa were therefore compared (Figure 7.5). As mentioned above, only a single reaction was set up in DIPE as a solvent leading to a dilution of 5-10 % each sampling. Since the rate of the enzyme-catalyzed reaction is concentration dependent, especially late samples may not accurately represent the real time course in Figure 7.5b. The effect is more predominant at low conversion and thus may be considered negligible here due to the already high conversion after two samplings.

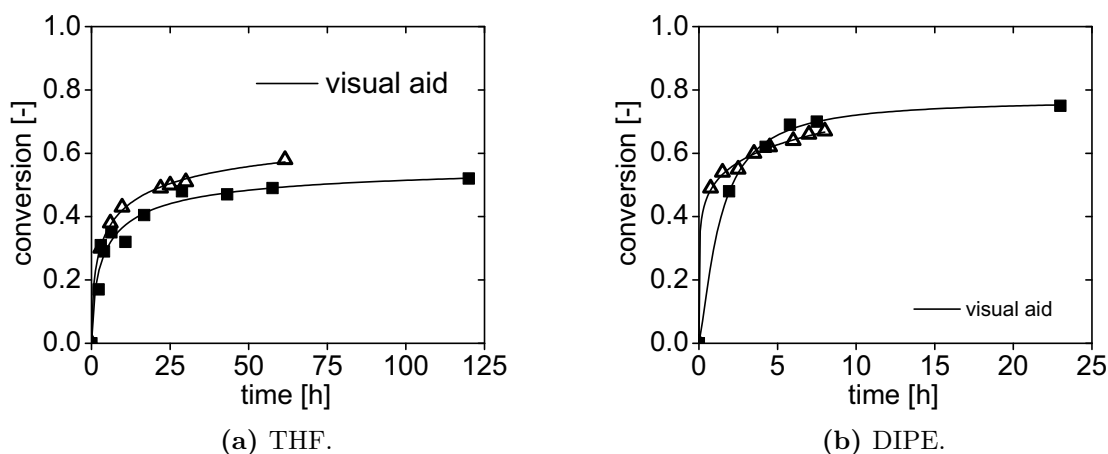


Figure 7.5: Comparison of reaction rate of Novozym 435-catalyzed aminolysis of *rac*-**3** with **1** at atm pressure (Δ) and at 200 MPa (\blacksquare). $T = 60\text{ }^{\circ}\text{C}$, 50 mM of substrates **1** and *rac*-**3**, 20 mg ml⁻¹ Novozym 435.

Both in THF as well as DIPE, reactions at atmospheric pressure seem to proceed faster. Both structural modifications as well as a positive activation volume may account for this observation. Taking into account the observed similar enantioselectivity in THF (Figure 7.3 on page 81), significant structural modifications of the active site of CALB in THF are unlikely. Consequently, a positive activation volume, i.e. a positive volume difference between transition and ground states may be anticipated.

In addition to a reduced enantioselectivity of the lipase-catalyzed kinetic resolution of (\pm)-menthol under pressure, Kahlow et al. reported a decreased reaction rate in the lipase-catalyzed kinetic resolution of menthol with increasing pressure [55]. A displaced side chain relevant for substrate binding caused by the pressure-induced insertion of a water molecule between two amino acids was found to provoke converging reaction rates for both (+)- and (-)-menthol and, therefore, reduced enantioselectivity. Likewise, side chain movements may have led to the same effect in the kinetic resolution of *rac*-**3** in DIPE.

7.3 Protein stability at high pressure

High pressure technology is applied especially in the food industry for sterilization and enzyme deactivation. Most proteins denature at high pressure either reversibly or irreversibly. On the other hand, enzymes have been described that tolerate a remarkable magnitude of pressure, with some even showing an increased stability [86]. In particular, thermal unfolding caused by fluctuations at higher temperature has been discussed to be reduced by high pressure. Since fluctuations can also be caused by pressure, the effect is, however, not observed for such enzymes. Several examples of enzymes with limited stabilization of enzymes against thermal inactivation within a certain pressure range can be found [10]. The addition of stabilizing cosolvents or organic solvents may also increase the thermobarostability of enzymes, which is particularly interesting for industrial applications [79].

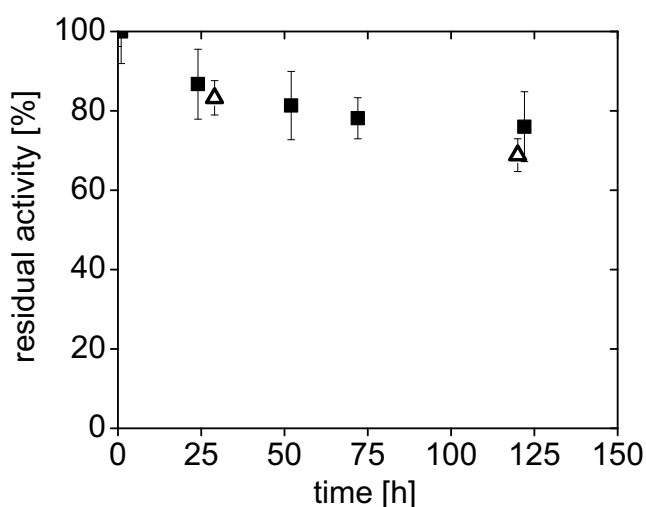


Figure 7.6: Stability of lipase Novozym 435 at atm pressure (■) and 200 MPa (△) in THF at 60 °C.

The stability of the immobilized lipase (Novozym 435) was tested under reaction conditions, i.e. in the presence of 50 mM of benzylamine (**1**) and *rac*-**3** in THF, at atmospheric pressure and 200 MPa and 60 °C. The heterogenous catalyst was separated from the reaction and tested for residual activity at atmospheric pressure. No significant differences were observed for the stability of Novozym 435 in THF at atmospheric pressure and 200 MPa. Abrasion by magnetic stirring and high pressure led to a visible, partial destruction of the heterogenous catalyst. However, internal diffusional limitations were not observed in a solvent-free system (4.3 on page 33), and are therefore most likely not present in THF as a solvent. While the unchanged enantioselectivity implies that no significant conformational changes in THF as a solvent have occurred, the reduced reaction rate combined with the unchanged stability at atmospheric and high pressure may indicate a reversible structural modification. These structural changes may have equally affected the reaction rates for the conversion of (*R*)- and (*S*)-**3** and therefore did not alter the enantioselectivity. In DIPE as organic solvent, the carrier material was fully pulverized and no reliable activity could be determined.

7.4 Summary

The high pressure experiments can be summarized as follows:

- The enantioselectivity in THF remains unchanged at atm pressure or 200 MPa.
- A decreased enantioselectivity probably resulting from conformational changes was observed at 200 MPa as compared to atm pressure in DIPE as a solvent.
- Reactions were slowed down under pressure in both solvents hinting at positive activation volumes for the reaction.
- A similar stability was observed in THF at atm and high pressure. In combination with the finding of a reduced reaction rate, reversible changes in the protein structure are anticipated.
- Because of pulverization of the carrier material in DIPE both at atm and high pressure, no reliable information on enzyme stability could be gained in the respective solvent.

8 Discussion and outlook

The experimental results have already been discussed in the respective chapters. The aim of this chapter is now to critically discuss the overall outcome of this study. Comparisons with alternative approaches will be presented as well as perspectives for future optimization.

The stereoselective synthesis of β -amino acids is of great interest both in research and industry, which is documented by the large number of original papers, reviews and even books entirely devoted to β -amino acid synthesis. The large effort is mainly driven by the versatility and ease of modification of the compounds on the one hand and the number of biologically active compounds available on the market¹ on the other hand. The diversity of β -amino acids is enormous: up to two substitutions may be added at the β^2 and β^3 position, while the type of substitution may be aromatic, aliphatic or a functional group. A total of 15 different structurally relevant groups of β -amino acids have been summarized [54]. It therefore does not surprise to find such a large number of synthetic entries towards this class of compounds from the field of asymmetric heavy-metal, organic and enzyme catalysis.

The chemoenzymatic reaction sequence developed by Weiß and Gröger, which has been investigated in detail in this work, is a useful and "green" method for the synthesis of short-chain aliphatic β -amino acids [140]. The number of alternative, scalable methods towards the asymmetric synthesis of this specific class of compounds is limited. An optimized downstream processing strategy for the conversion of the β -amino acid ester (*S*)-**3** to the free β -amino acid (*S*)-aminobutanoic acid via hydrogenation and hydrolysis has been published [139]. A satisfying environmental E-factor² of 41 was calculated for the overall process including isolation. The reactions were carried out as a one-pot process with an excess of 2.2:1 for the substrates benzylamine and *trans*-ethyl crotonate as opposed to 1.7:1 in the optimized process in this study. A recently published chemical approach towards the same compound (*S*)-aminobutanoic acid proved efficient in terms of achieved yields and *ee* [25]. However, raw material consumption and costs as well as health issues are better in the chemoenzymatic sequence investigated here including downstream processing [29].

In this study, the coupled solvent-free reaction system for the synthesis of optically pure β -amino acid esters was characterized. In line with common strategies for the optimization of bioprocesses, both the aza-Michael addition and the biocatalytic aminolysis

¹e.g. Sitagliptin, Taxol, Ezetimibe

²Defined as the weight of waste produced per weight of product.

were investigated in detail with regard to kinetics and thermodynamics of the reaction on the one hand, and catalyst characteristics on the other hand. The obtained results were subsequently applied for the numerical simulation and optimization of the process. The aza-Michael addition could be described by simple second-order kinetics and the respective kinetic parameters determined by numerical integration of the corresponding rate equations combined with nonlinear regression of the experimental data. Due to the added complexity of the enzyme catalyzed reaction in a solvent-free system, such a straightforward approach did not allow the statistically significant determination of the hence large number of kinetic parameters. Starting in an organic solvent and subsequently transferring the kinetic data to a solvent-free system including a phenomenological rather than mechanistic model derivation was chosen as an approach instead and proved to be expedient for modelling of the reaction over a broad substrate range. The procedure thus represented an effective, target-driven method for the optimization of the process. Suitable conditions for an increased reaction rate and stability of the catalyst could be identified. The process could be operated for more than 80 hours without significant loss of activity. A STY of $1.8 \text{ kg L}^{-1} \text{ d}^{-1}$ ($128 \text{ g L}^{-1} \text{ h}^{-1}$) was achieved. According to Straathof et al. [121], industrial processes for the production of fine chemicals range in between 0.1 and $130 \text{ g L}^{-1} \text{ h}^{-1}$. For comparison, α -amino acids are produced at 30 - $130 \text{ g L}^{-1} \text{ h}^{-1}$. The productivity of the process presented here is thus comparable to established industrial processes. Additionally, the reduced waste formation by using a lower excess of benzylamine as compared to the original process should lead to a slightly lower E-factor due to less unconverted substrate in the product stream. According to Weiss et al. [139], benzylamine adds by $1.9 \text{ kg}_{\text{waste}} \text{ kg}_{\text{product}}^{-1}$ to the overall E-factor of $41 \text{ kg}_{\text{waste}} \text{ kg}_{\text{product}}^{-1}$ for the whole process including downstream processing. A reduction of the necessary amounts of organic solvent and aqueous solutions can be conceived as well, but would need to be studied experimentally.

8.1 Evaluation of process economics

The efficiency of the continuous process has been discussed in Section 6.3. Important process parameters such as STY ($1.8 \text{ kg L}^{-1} \text{ d}^{-1}$), productivity Q ($4.9 \text{ kg kg}_{\text{Novo435}}^{-1} \text{ d}^{-1}$) and spec. ttn ($239 \text{ mol kg}_{\text{Novo435}}^{-1}$) were given that lie in a range commonly found for industrial processes [121]. However, in order to determine the prospects for industrial application, the economics of the process must be evaluated. In biocatalytic processes, enzyme costs are a key factor governing the economic feasibility of the process [121]. The price for the biocatalyst Novozym 435 was calculated to be about $5.8 \text{ € mol}_{(S)-\mathbf{3}}^{-1}$.

Costs for the production of 1 kg of the final product (*S*)- β -aminobutanoic acid was estimated to be 782 €. The calculation included costs for substrates, enzymes as well as solvents and further reagents required for downstream processing.³ The amounts necessary for downstream processing were based on the mass balance as published by Weiß corrected for the lower amount of benzylamine applied in this study [139]. It was

³See Appendix B for details on the calculation of manufacturing costs.

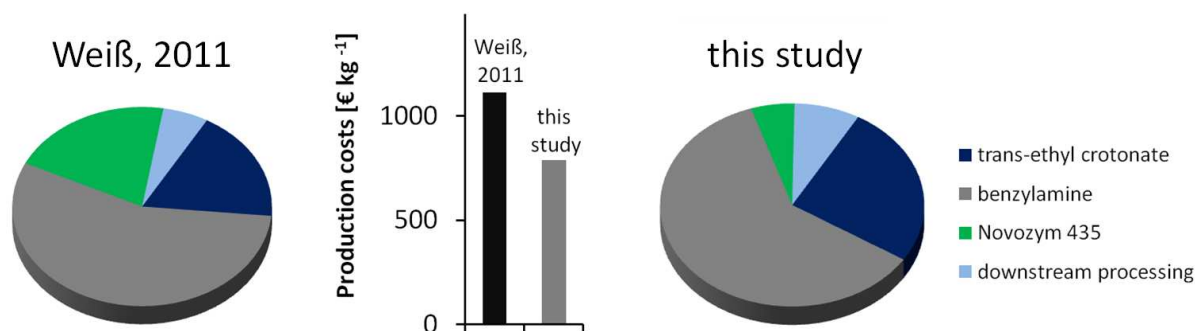


Figure 8.1: Estimation of cost distribution in optimized chemoenzymatic synthesis of (*S*)-aminobutanoic acid hydrochloride. Downstream processing costs were estimated from Weiß [139].

assumed that equal quantities of all reagents necessary for work-up are required. Not considered in the calculation were costs for energy, capital costs, water, waste treatment and reusable material involved in the downstream processing such as ion-exchanger and solvents. Cheapest available prices for all compounds were taken from Sigma-Aldrich (Taufkirchen, Germany). The distribution of costs is analyzed in Figure 8.1. The substrates benzylamine and *trans*-ethyl crotonate accordingly make up 87 % of the overall costs in the solvent-free process as carried out in this study. The biocatalyst only adds by 5 % to the overall costs and the downstream processing by 7 %. Compared to the process carried out under conditions reported by Weiß and Gröger⁴ [140], a cost reduction of almost 30 % was achieved. The improved process economics can be attributed to both a reduced substrate usage and an enhanced total turnover number of the catalyst. The estimation of the process costs shows that further improvements of the process are possible mainly by improving the yield of the target product. As discussed above, this can only be achieved by asymmetric catalysis of the aza-Michael addition coupled to the Novozym 435-catalyzed kinetic resolution.

The current market price for (*S*)- β -aminobutanoic acid could unfortunately not be determined. The price for the racemic compound (*R/S*)-3-aminobutanoic acid is 5640 € kg⁻¹ on a 25 g scale at Sigma-Aldrich (Taufkirchen, Germany). The actual price for the chiral *N*-Boc-protected (*S*)- β -aminobutanoic acid is 30600 € kg⁻¹ on a 1 g scale at Sigma-Aldrich. Even though the market price for bulk quantities is certainly much lower, it can be assumed that the optimized continuous process meets economic requirements.

8.2 Perspectives for optimization

Despite a good environmental performance of the reaction system and excellent STY for the continuous process, several aspects may be improved mainly with regard to the aza-Michael addition as the first step of the chemoenzymatic sequence. Both the re-

⁴A substrate ratio of 2.2:1 of benzylamine and *trans*-ethyl crotonate was applied. The respective enzyme deactivation constant expected at this ratio was taken from this study.

action itself and the (continuous) process may be addressed. High yields of up to 95 % can be achieved in the non-catalyzed thermal aza-Michael addition in batch mode. However, the reaction proceeds quite slowly. Several hours of reaction time are necessary which reduces the space-time yield and complicates the efficient continuous operation. As discussed in Chapter 6, inefficient mixing and wall effects at low Reynolds and Dean numbers lead to lowered conversion rates in continuously operated tube reactors as compared to well-mixed batch reactions. Alternative reactor types such as a nested-pipe reactor or Taylor reactor may lead to improved results.

A conceptually perhaps more interesting approach is the combination of chemocatalysis with biocatalysis. In fact, the introduction of an enantioselective catalyst for the aza-Michael addition would lead to two major improvements: firstly, reaction times could be reduced allowing a facilitated transfer to continuous reactor technology. Secondly, the yield and atom efficiency of the process could be enhanced resulting in a reduction of substrate costs as the main cost contribution factor (see Figure 8.1). The intrinsic limitation to a maximum yield of 50 % in fact represents the major drawback in any kinetic resolution. Even a relatively low enantioselectivity in the aza-Michael addition would therefore lead to improved yields of the final product while high *ee*-values can still be achieved by adding the biocatalytic kinetic resolution as a second step of the sequence. The amount of side products resulting from formation of (*R*)-4 would be reduced leading to an improved E-factor of the process and thus reduced costs for raw material, downstream processing and waste disposal. The combination of chemo- and biocatalysts in a (continuous) reaction sequence thus represents a powerful approach towards enantiomerically pure compounds. The methodology is depicted schematically in Figure 8.2.

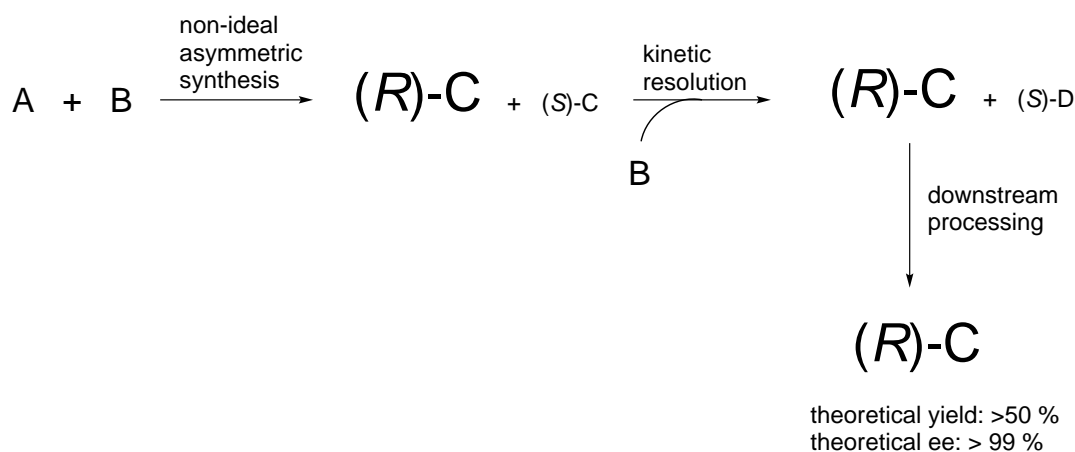


Figure 8.2: Combinatorial approach including asymmetric synthesis and kinetic resolution for the achievement of high enantiomeric excesses in non-ideal asymmetric syntheses.

The approach may actually be applied for a number of chemocatalytic reactions with insufficient selectivity for industrial application, that combined with kinetic resolution lead to enantiomerically pure compounds with good to high yields. Major challenges

lie in the finding of suitable reaction conditions that allow the sequential operation. Reaction medium engineering can be considered a key tool towards this goal. The feasibility of combining chemo- and biocatalysis was e.g. demonstrated by Burda et al., who combined a palladium-catalyzed Suzuki-cross-coupling reaction in aqueous medium with an alcohol dehydrogenase catalyzed asymmetric reduction [14]. The approach may also be regarded as an alternative tool where dynamic kinetic resolutions (DKR) are not applicable. While a DKR in principle allows to obtain 100 % yield, it can only be applied in such cases where the target product is the reacting and not the unconverted enantiomer. A DKR is therefore not feasible for the system under investigation in this study.

A drawback of the system under investigation is the intrinsic limitation to products of only one configuration at its stereogenic center as determined by the selectivity of the lipase. An access to the opposite enantiomer, e.g. by inversion of the selectivity via protein engineering, is not easily achieved. Additionally, the substrate spectrum of *Candida antarctica* lipase B is limited in the given solvent-free reaction system [138]. E-values of 48 and 83 were determined for CF₃- and ethyl-side chains at the β³-position. Further elongation of the aliphatic chain, however, led to decreased selectivities. Reaction rates were reduced in all cases compared to a methyl group at the β³-position as in *rac*-**3**. For increasing chain length of the ester moiety, best results were achieved with an ethyl moiety while increasing or decreasing chain length led to decreased enantioselectivity in the kinetic resolution.

8.3 Conclusion

The chemoenzymatic reaction sequence optimized in this work represents a useful, scalable synthetic route towards the production of chiral, short-chain aliphatic β-amino acids. Both the aza-Michael addition and the biocatalytic aminolysis could be carried out efficiently in a coupled, continuous reactor system. The reactions were carried out in a solvent-free system, which led to the achievement of an exceptionally high space-time yield of 1.8 kg L⁻¹ d⁻¹ for the chiral β-amino acid ester. Opposed to common prejudices of rapid enzyme deactivation, the stability of the biocatalyst proved to be excellent as expressed by a high total turnover number of 158000. This is particularly interesting as the solvent-free medium seemingly causes harsh conditions for an enzymatic reaction. Additionally, elevated temperatures of 60 °C were applied. The economic viability of the process was estimated based on costs for substrates, biocatalyst and reagents needed for downstream processing. Estimated costs for manufacturing of the final product (*S*)-β-aminobutanoic acid were well below current market prices for the N-Boc-protected compound, indicating the competitive capability of the process for industrial application.

9 Summary

The following results have been achieved within this study:

- The aza-Michael addition of benzylamine and *trans*-ethyl crotonate to form *rac*-ethyl 3-(benzylamino)butanoate proceeded irreversibly. A slow successive side-reaction led to the formation of the amide side product via aminolysis of the ester. Kinetic constants for both aza-Michael addition and subsequent aminolysis were determined via numerical integration of second order rate equations combined with non-linear regression of the experimental data from batch experiments.
- The temperature dependence of the kinetic constants and their influence on the process parameters conversion, selectivity and yield was analyzed. Selectivity and yield were observed to decrease with increasing temperature due to side product formation. The applicability of heat to accelerate the reaction is thus limited.
- Kinetic rate constants for the Novozym 435-catalyzed aminolysis were determined in tetrahydrofuran as an organic solvent by using initial rate studies. A phenomenological rather than mechanistic model was devised. The proposed model included inhibition by the substrate benzylamine and weak inhibition by the product amide. The Michaelis-Menten constant K_m for the ester (*R*)-ethyl 3-(benzylamino)butanoate was found to be large compared to its concentration. A new parameter ν'_{max} was therefore introduced that comprises ν_{max} and K_m for the compound and is related to the catalytic efficiency defined as k_{cat}/K_m .
- The kinetic model was transferred to the solvent-free system by introduction of thermodynamic activities instead of concentrations. Additionally, a linear dependence of ν_{max} on the concentration of the ester (*R*)-ethyl 3-(benzylamino)butanoate was observed and accounted for in the kinetic model. The adapted model was used to predict the progress curve of solvent-free batch reactions over a broad range of substrate ratios with good accuracy.
- The influence of physicochemical parameters on the enantioselectivity *E* of Novozym 435 in the kinetic resolution of *rac*-3-ethyl-3-(benzylamino)butanoate with benzylamine was studied. A decreased *E*-value was seemingly found with decreasing polarity of tested solvents and with increasing temperature. High pressure of 200 MPa had no effect on enantioselectivity in tetrahydrofuran as a solvent, whereas in diisopropylether a significant reduction of *E* was observed.
- The applicability of FTIR technology for the inline monitoring of both solvent-free aza-Michael addition and Novozym 435-catalyzed aminolysis was demonstrated.

9 Summary

An ATR fibre probe was used in batch experiments. The applicability of FTIR technology for the monitoring of continuous flow reactions was demonstrated in batch reactions with bypass FTIR analytics using an ATR micro flowcell.

- A continuous reactor setup for the two-step chemoenzymatic process was developed comprising a plug-flow reactor for the thermal aza-Michael addition and a packed-bed reactor for the Novozym 435-catalyzed aminolysis to produce (*S*)-ethyl 3-(benzylamino)butanoate. The coupled reactors were operated continuously for a time period of 4 days without significant loss of enzyme activity.
- The target β -amino acid ester was obtained at 92 % conversion in the plug-flow reactor and 59 % conversion in the packed bed reactor with high enantiomeric excess of > 98 %. A space-time yield of $1.8 \text{ kg L}^{-1} \text{ d}^{-1}$ and a total turnover number of the biocatalyst of 158000 were calculated.
- In order to judge the economic viability of the process, costs for reaction and downstream-processing were estimated. Based on the current market price for Novozym 435, biocatalyst costs were estimated to result in about 5.80 € mol^{-1} . Costs for the chiral β -amino acid (*S*)-3-aminobutanoic acid as the final product after downstream processing were estimated at about 782 € kg^{-1} , which is well below the current market price for comparable products.

A Materials and methods

A.1 Applied equipment

HPLC

Agilent 1100 Series HPLC System	Agilent Technologies, Waldbronn, Germany
Sykam S HPLC System	Sykam, Fürstenfeldbruck, Germany
High-pressure pump K-1001	Knauer, Berlin, Germany
Gilson-ABIMED Dilutor 401	ABIMED GmbH, Langenfeld, Germany
Gilson ABIMED 231XL autosampler	ABIMED GmbH, Langenfeld, Germany
Nucleodur [®] C ₈ ec, 250×5 μm	Machery Nagel, Düren, Germany
LiChrospher [®] RP8-Select B, 250×5 μm	Merck, Darmstadt, Germany
Chiralcel [®] OD-H, 250×5 μm	Daicel, Tokyo, Japan
Nucleocel [®] α S, 250×5 μm	Machery Nagel, Düren, Germany

FTIR online analytics

React IR 45m equipped with Silver Halide (AgX) FiberConduit TM , DiComp TM diamond probe tip, DS Micro Flowcell	Mettler Toledo, Columbus, OH, USA
---	-----------------------------------

Detectors and sensors

ASL1600-20 liquid flow sensor	Sensirion, Staefa ZH Switzerland
DH-2000-BAL with UV-VIS-NIR lightsource	Ocean Optics, Dunedin, FL, USA
UV-detector K-2501	Knauer, Berlin, Germany
UvikonXL spectrophotometer	Bio-Tek Instruments, Bad Friedrichshall, Germany

Continuous reactions

mzr [®] S05	HNP Mikrosysteme, Parchim, Germany
Pharmacia LKB SuperFrac Fraction Collector	Pharmacia, Uppsala, Sweden
Pharmacia LKB HPLC Pump 2248	Pharmacia, Uppsala, Sweden
Superformance [®] 150-10 LC column	Merck, Darmstadt, Germany

Centrifuges

5415D	Eppendorf AG, Hamburg, Germany
-------	--------------------------------

A Materials and methods

Avanti J-25
Minifuge T

Beckman-Coulter, Fullerton, USA
Heraeus Sepatech, Berlin, Germany

Balances

PC 440
Sartorius CP224S

Mettler Toledo, Gießen, Germany
Sartorius, Göttingen, Germany

Thermostats

E100 Ecoline Star Edition 003
MGW Lauda RC6 CS

Lauda, Hamburg, Germany
Lauda, Hamburg, Germany

Other labware and equipment

Alugram[®] SIL/UV254 nm TLC Sheets
Christ Alpha 2-4 Lyophilizer
Glassware
Magnetic stirrer
PTFE tubing and fittings
Rotavapor R-200
with V-805 vacuum controller
Steel capillaries
Ts1 thermoshaker
Vortex (MS2 Minishaker)
VTR 5022 vacuum oven

Carl Roth, Karlsruhe, Germany
Christ, Osterode am Harz, Germany
Carl Roth, Karlsruhe, Germany
IKA Werke, Staufen, Germany
Bohlender, Grünsfeld, Germany
BÜCHI Labortechnik, Flawil,
Switzerland
Latek, Heidelberg, Germany
Biometra, Göttingen, Germany
IKA Werke, Staufen, Germany
Heraeus, Hanau, Germany

A.2 Applied chemicals

Benzylamine (99.5 %, $\leq 0.3\%$ water K.F.) and *trans*-ethyl crotonate (96%) were obtained from Acros Organics (Geel, Belgium). Commercial Novozym 435 (*Candida antarctica* lipase B immobilized on acrylic resin) was obtained from Novozymes (Bagsvaerd, Denmark). The water content of the enzyme preparation stored at room temperature was determined to be 1.1% (K.F.). THF as a solvent in biocatalytic reactions was obtained from Carl Roth (Karlsruhe, Germany) with 99.9% purity and 0.005% water K.F. All other chemicals were of analytical grade purity and purchased from Carl Roth, Acros Organics, Fluka (Buchs, Switzerland), Merck (Darmstadt, Germany) or Sigma-Aldrich (Schnelldorf, Germany).

Physical properties of substrates

Physical properties (density δ and dynamic viscosity η) of the substrates used in this work are given below.

Benzylamine 1 (MW=107.15 g mol⁻¹):

	δ [g ml ⁻¹]	η [mPa·s]
61 °C	0.98	0.912
141 °C	0.88 ^a	0.394

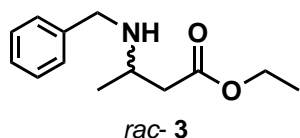
^acalculated based on available literature data (up to 50 °C) assuming linear temperature dependency of density.

***trans*-Ethyl crotonate 2** (MW=114.14 g mol⁻¹):

	δ [g ml ⁻¹]	η [mPa·s]
60 °C	0.918	0.488

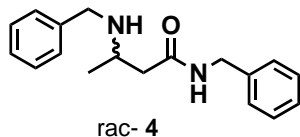
Synthesis of substrates and reference materials

ethyl 3-(benzylamino)butanoate (*rac*-3): Benzylamine (**1**, 120 mmol), *trans*-ethyl crotonate (**2**, 72 mmol) and 1,8-diazabicyclo[5.4.0]undec-7-en (60 mmol) were refluxed in acetonitrile (180 mL) for 20 h. After cooling down to room temperature, acetonitrile was evaporated in vacuo and the remaining oil was taken up in ethyl acetate. The organic phase was extracted with 8×50 mL of 1% (v/v) aqueous HCl. After adjustment to pH 8 using saturated NaHCO₃ the aqueous phase was extracted using 8×50 mL ethyl acetate. The combined organic phases were dried over MgSO₄ and evaporated to yield a yellow oil. Yield: 21.4 g (80 mol-%). Water content (measured by Karl Fischer titration (K.F.)): 0.12%.



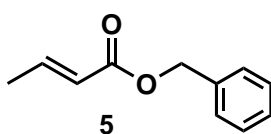
¹H-NMR: (300MHz, CDCl₃): δ_{cs} (ppm) = 1.18 (d, ³J=6.4 Hz, 3H), 1.27 (t, ³J=7.1 Hz, 3H), 1.92 (br s, 1H), 2.40 (dd, ²J=15.1 Hz, ³J=5.9 Hz, 1H), 2.52 (dd, ²J=15.1 Hz, ³J=7.9 Hz, 1H), 3.19 (sext., ³J=6.4 Hz, 1H), 3.79, 3.87 (2d, ²J=13.0 Hz, 2H), 4.15 (q, ³J=6.1 Hz, 2H), 7.24-7.36 (m, 5H).

***N*-benzyl-3-(benzylamino)butanamide (*rac-4*):** Benzylamine (**1**, 40 mmol), *rac-3* (2 mmol) and ammonium chloride (1 mmol) were stirred for 24 h at 120 °C. The product was purified by silica flash chromatography (ethyl acetate/isopropanol, 95:5 (v/v), 0.2% DEA). Yield: 0.29 g (51 mol-%).



¹H-NMR: (400MHz, CDCl₃): δ_{cs} (ppm)=1.22 (d, ³J=6.5 Hz, 3H), 1.55 (br s, 1H), 2.29 (dd, ²J=15.9 Hz, ³J=3.6 Hz, 1H), 2.49 (dd, ²J=15.9 Hz, ³J=7.6 Hz, 1H), 3.14 (m, 1H), 3.72, 3.82 (2d, 2H, ²J=12.6 Hz), 4.45 (d, 2H, ³J=5.6 Hz), 7.127.31 (m, 10H), 8.49 (br s, 1H). Water content (K.F.): <0.10%.

(*E*)-benzyl but-2-enoate (5**):** Crotonyl chloride (17.2 mmol) was dissolved in 40 ml of dry THF and kept on ice (0 °C). 2 mg of hydroquinone were added as radical scavenger. Benzylamine (**1**, 43.1 mmol) was dissolved in 25 ml dry THF and added dropwise to the dissolved acid chloride while the solution was stirred magnetically. Stirring was continued after addition of benzylamine for 1 h at 0 °C and an additional 0.5 h at ambient temperature.



The produced solid crystals were separated from the solvent by filtration. The product was purified twice via crystallization in water/methanol as a solvent. The purity of the product was controlled by HPLC with UV-detection and comparison of the spectrum to reference material obtained from Weiß.¹ Yield: 1.69 g (56 mol-%).

A.3 Methods

A.3.1 Analytical methods

Determination of conversion

Conversions of all reactions were analyzed by HPLC on an Agilent system equipped with a diode array detector (215 nm) and a Nucleodur C₈ ec column (5 μ m, 25 cm, 0.46 cm; Macherey-Nagel, Germany). A mixture consisting of 47.5/52.5 (v/v) MeOH/ sodium phosphate buffer (50 mM, pH 6.5) was used as the eluent at a flow rate of 1 ml min⁻¹. Retention times: **1**: 3.9 min, **2**: 8.5 min, *rac-3*: 15.5 min, *rac-4*: 18 min, **5**: 6.1 min.

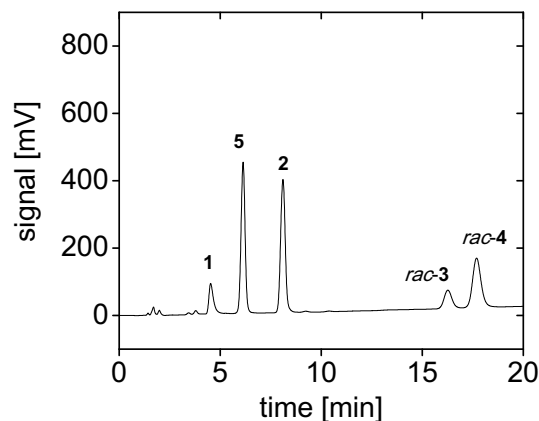


Figure A.1: Exemplary HPLC spectrum for the determination of conversion. Retention times: 1: 3.9 min, 2: 8.5 min, *rac*-3: 15.5 min, *rac*-4: 18 min, 5: 6.1 min.

An exemplary HPLC spectrum is shown in Figure A.1.

Determination of enantiomeric excess

The enantiomeric excess of **3** was determined using a Chiralcel OD-H column (5 μm , 25 cm, 0.46 cm; Daicel, Japan) cooled down to 10 $^{\circ}\text{C}$ and UV detection at 223 nm. *i*-Hexane/*i*-propanol 95/5 (v/v), 0.2 % DEA was used as the eluent at a flow rate of 0.75 ml min^{-1} . Retention times: (*R*)-3: 10 min, (*S*)-3: 12 min. The *ee* of the product **4** was measured on a Nucleocel α S, column (5 μm , 25 cm, 0.46 cm; Macherey-Nagel, Germany) at 20 $^{\circ}\text{C}$ and UV detection at 258 nm. A mixture consisting of *n*-Hexane/*i*-propanol 95/5, 0.2 % DEA was used as the eluent at a flow rate of 0.8 ml min^{-1} . Retention times: (*S*)-4: 29 min, (*R*)-4: 32 min. Representative spectra of racemic mixtures of both compounds are shown in Figure A.2.

Inline analytics via FTIR

All FTIR reference spectra were collected using a ReactIR 45m instrument from Mettler Toledo (Columbus, OH, USA) equipped with a Silver Halide (AgX) FiberConduitTM with a DiCompTM diamond probe tip or a DS Micro Flowcell. The instrument was constantly purged with dry nitrogen at 3 L min^{-1} . Liquid nitrogen was used for cooling of the MCT detector. The Mettler Toledo iC IR software and the integrated iC Quant Modeling Package[®] were used for monitoring, data handling and quantification of all experiments. Details on the experimental setup are given in Chapter 5.

¹Dr. M. Weiß, Department of Chemistry, University of Erlangen-Nuremberg.

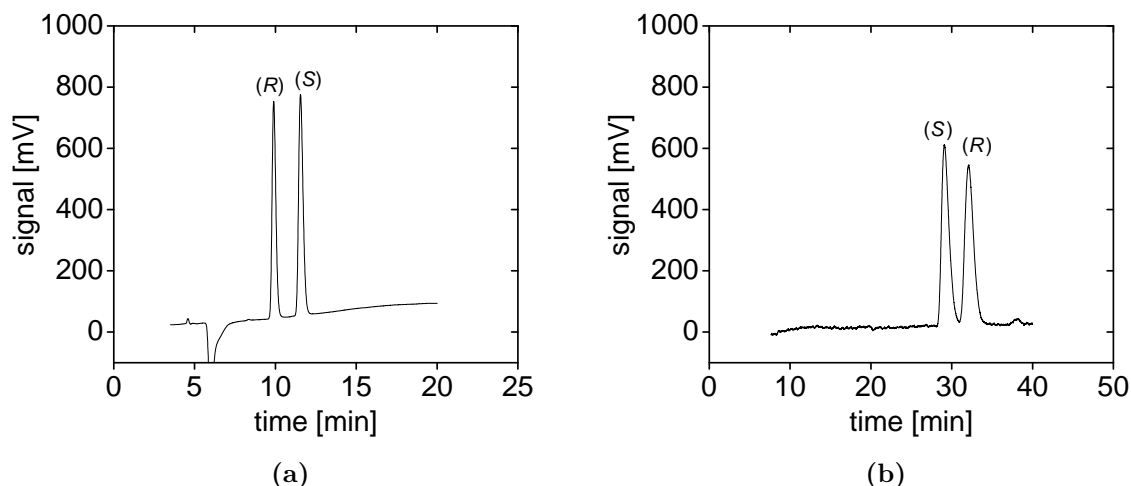


Figure A.2: HPLC analysis of enantiomeric excess of (a) (*R/S*)-**3** and (b) (*R/S*)-**4** on chiral stationary phases.

A.3.2 Analyses in batch mode

Progress curve analysis of solvent-free aza-Michael addition

The solvent-free aza-Michael addition of **1** to **2** was carried out in sealed glass vials at a controlled temperature in the range from 40-70 °C. While varying the mole fractions of both substrates the total molar amount was kept at 6 mmol. Samples were withdrawn automatically every 2 hours using a Gilson autosampler. Reactions were stopped by dilution in glass vials containing 1,3-dioxolane.

Biocatalytic aminolysis

Solvent-free reactions were carried out in glass vials using 152 mg g⁻¹ of the lipase Novozym 435 with varying mole fractions of **1** and **3** at a constant total substrate mass of 0.59 g. All reactions were carried out at 60 °C and magnetically stirred in order to overcome external diffusion limitations. Samples free of the heterogenous catalyst were withdrawn manually at various times and diluted in 1,3-dioxolane for stopping of the reaction. Reactions in THF as a solvent were carried out similarly using 10-20 mg ml⁻¹ Novozym 435 and a total reaction volume of 0.5-1 ml. Initial reaction rates in both THF and the solvent-free system were determined at conversions below 10 % in order to maintain initial reaction rate conditions. Performance of the reactions at controlled water activity (a_w 0.16-0.84, see below for experimental procedure) led to a hydrolytic side reaction, thus forming the corresponding acid from the ester **3** in the form of a precipitate. Therefore, water concentrations of substrate solutions were kept low as obtained from the suppliers or after MgSO₄-drying in own syntheses.

Determination of enzyme stability

The lipase Novozym 435 (152 mg ml⁻¹) was incubated in solvent-free reaction media of different molar fractions of **1** and *rac*-**3** as described in the previous section at 60 °C. After given time intervals the reaction mixture was removed using a syringe, the carrier washed 3 × using THF and dried at room temperature under vacuum. Potential leaching was checked and found to be negligible since constant activities (± 4 %) were detected after each washing step. The lipase was subsequently used in a standard activity test containing 50 mM of **1**, 100 mM of *rac*-**3** in THF with 20 mg ml⁻¹ of lipase Novozym 435. All activity tests were magnetically stirred and performed in closed glass vials at 60 °C for 30 minutes. It should be noted that constant conditions cannot be maintained when incubating Novozym 435 in the solvent-free system. An effect of the alternating conditions on stability can therefore not be excluded.

Determination of solvent polarity

The polarity of the substrates benzylamine (**1**) and ethyl 3-(benzylamino)butanoate (*rac*-**3**) was determined using nitroanisole as a solvatochromic agent. Benzylamine was directly used as obtained from the supplier (Acros Organics, Geel, Belgium). *Rac*-**3** was distilled prior to used in order to remove UV active impurities of the slightly yellow oil as obtained from the synthetic procedure described above ($T_b=91$ °C, 0.24 mbar). Approximately 0.2 mM of nitroanisole was dissolved in **1** and distilled *rac*-**3**, respectively, and the UV spectra recorded in the range from 280-400 nm.

Investigation of diffusion limitation in batch experiments

A possible internal diffusion limitation in the Novozym 435 catalyzed aminolysis of *rac*-**3** with **1** was examined by carrying out experiments using pestled Novozym 435 and subsequent comparison with the reaction rates observed using intact Novozym 435. 30 mg ml⁻¹ of Novozym 435 were added to mixtures of varying mole fractions of substrates **1** and **3** at a constant total substrate mass of 0.29 g. Further reaction conditions were as described above for the solvent-free biocatalytic aminolysis.

Control of water activity

The influence of the water activity on the Novozym 435 catalyzed aminolysis of *rac*-**3** with benzylamine **1** in solvent-free reactions was tested. In order to obtain a defined water activity a_w all substrates and catalysts were pre-equilibrated for 7 days in closed containers over saturated salt solutions. The salts used in this work are: LiCl ($a_w = 0.11$), KAc ($a_w = 0.22$), MgCl₂ ($a_w = 0.33$), KCO₃ ($a_w = 0.43$), KI ($a_w = 0.69$) and KCl ($a_w = 0.86$). All reactions were carried out using 1.35 mmol of **1**, 2.02 mmol of *rac*-**3** and 80 mg of Novozym 435, 60 °C and magnetic stirring.

A.3.3 Analyses in continuous flow

Residence time distribution analysis of tube reactor

The tube reactor (reactor 1: PTFE, L = 82.7 m, d_i = 0.8 mm, V = 41.6 ml; reactor 2: PTFE, L = 13.25 m, d_i = 2.0 mm, V = 41.6 ml) was pre-filled with distilled water. Benzaldehyde (3.0 mM) was used as a tracer substance. An Ocean Optics UV Flowcell was attached at the outlet of the reactor for continuous monitoring of the UV absorption at 280 nm. Water was pumped through the reactor at a flow rate of 0.05 ml min⁻¹ using a Pharmacia 2248 HPLC pump. At time t_0 , the input flow was switched from water to 3.0 mM benzaldehyde. The UV signal can directly be converted into the normalized $F(\theta)$ curve using Equation A.1

$$F(\theta) = \frac{E_{\Delta t} \cdot \Delta t}{E_F \cdot \bar{\tau}} \quad (\text{A.1})$$

where Δt is the time interval between time t and t_0 of the tracer input, $\bar{\tau}$ is the mean residence time, $E_{\Delta t}$ is the absorption after time Δt and E_F the absorption of the flow of the tracer solution. The mean residence time $\bar{\tau}$ was determined using the Zwickel interpolation method.

$F(\theta)$ curves for ideal reactors can be calculated using Equation A.2 for a CSTR or cascade thereof comprising n vessels.

$$F(\theta) = 1 - e^{-n\theta} \left(1 + n\theta + \frac{(n\theta^2)}{2!} + \dots + \frac{(n\theta^{n-1})}{(n-1)!} + \dots \right) \quad (\text{A.2})$$

General procedure for aza-Michael addition in tube reactor

The substrates **1** and **2** were mixed prior to reaction in order to avoid changes in substrate composition due to backpressure changes and pump inaccuracies upon change of flow rates. The premixed substrates were stored on ice/NaCl (-15 °C) in order to largely prevent an ongoing reaction. Substrates were subsequently pumped through a temperature controlled tube for the continuous reaction using a Pharmacia 2248 HPLC pump. Flow rates and temperature were adjusted as specified in Section 6.1. A PTFE tube (V=41.6 ml, L = 82.7 m, d_i = 0.8 mm) coiled around a custom-made steel spindle (d =cm) and inserted into a thermostated cylinder was applied at temperatures up to 80 °C. Coiled stainless steel capillaries (V= 0.5-3 ml, L = 1-6 m, d_i = 0.075 mm, R =2.5 cm) were applied for temperatures \geq 100 °C. Temperature control was achieved by immersing the steel capillary reactor into a thermostat filled with silicon oil. Samples for quantification were collected at the outlet of the reactor and quenched in 1,3-dioxolane as described above.

General procedure for Novozym 435-catalyzed aminolysis in packed bed reactor

Continuous reactions require large quantities of substrates. In order to avoid the laborious synthesis of pure *rac*-**3** in large amounts, substrate mixtures consisting predominantly of **1** and *rac*-**3** were obtained from the solvent-free aza-Michael addition of **1**

and **2**. An exemplary batch reaction for preparative substrate synthesis was carried out using 0.98 mol benzylamine and 0.58 mol *trans*-ethyl crotonate at 60 °C for 26 h in glass flasks. At 95 % conversion the composition of the product representing the substrate feed solution for the biocatalytic aminolysis was 2.3 mol g⁻¹ benzylamine (**1**), 0.152 mol g⁻¹ *trans*-ethyl crotonate (**2**), 3.031 mol g⁻¹ *rac*-**3** and 0.117 mol g⁻¹ *rac*-**4**. A borosilicate glass reactor (Superformance[®], Merck, Germany) of d_i=1 cm was filled with Novozym 435 and thermostated at 60 °C. Substrates were subsequently pumped through the packed bed reactor using a Pharmacia 2248 HPLC pump at flow rates \dot{v} of 0.02 - 0.4 ml min⁻¹. Pressure was monitored at the reactor inlet using an analogous pressure gauge.

Full reactor setup for continuous production of (S)-3

The PTFE tube reactor (V = 41.6 ml, L = 82.7 m, d_i = 0.8 mm) and packed bed reactor (V_{total} = 17 ml, L_{total} = 21.7 cm, d_i = 1 cm, 6.3 g Novozym 435) were coupled for the continuous production of (*S*)-ethyl 3-(benzylamino)butanoate according to Scheme 6.2 on page 67. Two Pharmacia 2248 HPLC pumps were used for the continuous supply of substrates **1** (0.303 mmol min⁻¹) and **2** (0.180 mmol min⁻¹). Pressure retention valves set to 2 bar were installed at the pump outlet in order to improve the performance of the pumps and maintain constant flow velocities. Mixing was achieved using a mixing tee prior to the reactor inlet. The tube reactor for the aza-Michael addition was thermostated at 80 °C. The temperature of the packed bed reactor was maintained at 60 °C. Analogous pressure gauges and sampling valves were installed before and after both reactor units. An autosampling unit was installed for the timed collection of fractions at the outlet of the reactor.

A.3.4 Computational methods

Determination of activity coefficients²

The molecule geometry of all solvents, substrates and products was initially determined using HyperChem[®] 8.5 (Hypercube, USA). Quantum chemical optimization of the molecule geometry and charge distribution was achieved using Turbomole[®] 5.10 (Turbomole, Germany). Activity coefficients of all mixtures were subsequently calculated under reaction conditions on mole fraction scale using COSMO-RS Version C21.0110 (Cosmologic, Germany) [28]. The water concentration in substrate solutions and adsorbed on the enzyme carrier was determined experimentally using Karl Fischer titration. The overall water concentration of nearly 0.16 mmol g⁻¹ for all substrate mixtures was considered in the calculation of activity coefficients.

²All calculations were performed with kind support from Dipl. Ing. T. Ingram and Prof. Dr. I. Smirnova, Institute of Thermal Separation Processes, Hamburg University of Technology

Kinetic parameter estimation

Scientist[®] software Version 2.0 (MicroMath[®], USA) was used for kinetic parameter estimation of the enzymatic reactions carried out in the solvent system. Numerical integration of the rate equations combined with non-linear regression of the experimental data of time course experiments for the determination of kinetic parameters of both the solvent-free aza-Michael addition and biocatalytic aminolysis was performed using the inherent ode45 and lsqnonlin algorithms of MATLAB[®] (MathWorks, USA). Exemplary scripts applied in this work using Scientist[®] and MATLAB[®] are presented below.

Scientist[®] script

```
IndVars: a, b
DepVars: v
Params: k1, kma, ki

// Michaelis Menten derived model
v = k1*a*b/(kma+(1+a/ki)*a)

// Initial parameters
k1 = 10.2
kma = 0.04
ki = 1.059
***
```

MATLAB[®] script

Data in- and output

```
%% Initialization
init = struct;
addpath C:\Users\Simon\Matlab\matlab;
addpath C:\Users\Simon\Matlab\scripts;
init.filename_in='Kinetik_08b.txt';
init.file_path='C:\Users\Simon\Matlab\experimental_data\activity_based';
init.ode_opts = odeset('RelTol',1e-13);
init.ls_opts_in = optimset('Display','iter','MaxIter',1000,'TolFun',1e-8,'TolX',1e-10);
init.ls_opts_out = optimset('Display','iter','MaxIter',1000,'TolFun',1e-8,'TolX',1e-10);

%% Ind and weight cell for data_cell generation
init.ind = 0,'%n %n %n %n %n %n',13;
           1,'%n %n %n %n %n %n',13;
           2,'%n %n %n %n %n %n',13;
           3,'%n %n %n %n %n %n',13;
```

```

init.w_cell=ones(13,1) ones(13,1) ones(13,1)*10 ones(13,1) ones(13,1)*10;
            ones(13,1) ones(13,1) ones(13,1)*10 ones(13,1) ones(13,1)*10;
            ones(13,1) ones(13,1) ones(13,1)*10 ones(13,1) ones(13,1)*10;
            ones(13,1) ones(13,1) ones(13,1)*10 ones(13,1) ones(13,1)*10;
init.f_vec=[1, 1, 1, 1, 1, 1];

%% Generate data cell
init.data_cell=fdata2cell(init);
init.N=count_data(init);

%% Plot generated data_cell
plot_data(init.data_cell,[1,2,3,4,5],'ob');

%% Define starting set of parameters
init.pars_in =[0.3];

init.pars_out=[3.049, 1.52, 1.52,0, 0,...
               2.28, 1.71, 1.71,0, 0,...
               1.82, 1.82, 1.82,0, 0,...
               1.01, 2.02, 2.02, 0, 0];
init.w_pars=[1];
init.parind_in=[1;
               1;
               1;
               1];
init.parind_out=[1, 2, 3, 4, 5;
                6, 7, 8, 9, 10;
                11, 12, 13, 14, 15;
                16, 17, 18, 19, 20];
init.pars_in_lb = [0.0001];
init.pars_in_ub = [100];

init.pars_out_lb = [2.95, 1.48, 1.48,0, 0,...
                   2.23, 1.67, 1.67,0, 0,...
                   1.80, 1.79, 1.79,0, 0,...
                   0.96, 1.97, 1.97,0, 0];
init.pars_out_ub = [3.1, 1.58, 1.525,0.01, 0.01,...
                   2.32, 1.76, 1.76,0.01, 0.01,...
                   1.86, 1.86, 1.82,0.01, 0.01,...
                   1.06, 2.07, 2.07,0.01, 0.01];
init.y0 = @(y0) [y0(1) y0(2) y0(3) y0(4) y0(5)];

init.const = [0.59, 0.193, 0.554, -0.030, 1.079, -0.038, 1.131, 0.0232, 0.8292, -0.0016,
              0.9196,...

```

A Materials and methods

```
0.59, 0.193, 0.554, -0.030, 1.079, -0.038, 1.131, 0.0232, 0.8292, -0.0016,
0.9196,...
0.59, 0.193, 0.554, -0.030, 1.079, -0.038, 1.131, 0.0232, 0.8292, -0.0016,
0.9196,...
0.59, 0.193, 0.554, -0.030, 1.079, -0.038, 1.131, 0.0232, 0.8292, -0.0016,
0.9196];
init.cind = [1, 2, 3, 4, 5, 6, 7, 8, 9, 10, 11;
12, 13, 14, 15, 16, 17, 18, 19, 20, 21, 22;
23, 24, 25, 26, 27, 28, 29, 30, 31, 32, 33;
34, 35, 36, 37, 38, 39, 40, 41, 42, 43, 44];

%% NLS estimation of parameters in loop init.sigma=0;
init.cycle=10;
[new_pars,resnorm,residual,jacobian] = optimize_loop(init);
p=[new_pars1 new_pars2];
j=[jacobian1 jacobian2];
ci=nlparci(p,residual1,'jacobian',j);
delta=ci(:,2)-p';
result=[p' delta];

%% Plot obtained solutions
tspan=0:0.025:5;
data_cell_old=init.data_cell;
init.data_cell=cell(4,5);
for i=1:numel(init.data_cell)
init.data_cell(i)=[tspan', ones(length(tspan),1)];
end
data_cell_new=simF(new_pars1,1,new_pars2,init);
plot_data(data_cell_old,[1,2,3,4,5],'ob');
plot_data(data_cell_new,[1,2,3,4,5]','-g');
title('Novozym 435 catalyzed aminolysis of rac-3 and 1','Fontweight','bold');
xlabel('Time [h]');
ylabel('Conc. [M]');
```

Kinetic model

```
function r=enfun(t,y,p,weight,c)

r=zeros(5,1);
p=p.*weight;

%linear dependency of activity coefficient on BA concentration
g1 = c(2) * y(1)+ c(3);
g2 = c(4) * y(1)+ c(5);
g3 = c(6) * y(1)+ c(7);
```

```

g4 = c(8) * y(1) + c(9);
g5 = c(10) * y(1) + c(11);

% Kinetic model derived from Michaelis Menten model
% linear dependency of  $\nu_{max}^*$  on substrate ratio:
%  $\nu_{max}^* = 12.851 * (1.2398 * c(1) + 0.2964)$ 
%  $K_{m_1} = 0.045$ 
%  $K_{i_1} = 0.898$ 
%  $K_{i_{rac-4}} = 0.958$ 

vr = 12.851 * (1.2398 * c(1) + 0.2964) * y(2) * g2 * y(1) * g1 / ((0.045 + (1 + y(1) * g1 / 0.898) *
    y(1) * g1) * (1 + (y(4) * g4 + y(5) * g5) / 0.958));
vs = p(1) * (1.2398 * c(1) + 0.2964) * y(3) * g3 * y(1) * g1 / ((0.045 + (1 + y(1) * g1 / 0.898) *
    y(1) * g1) * (1 + (y(4) * g4 + y(5) * g5) / 0.958));

% non-catalyzed blind reaction with  $k_2=0.0012$ 
bl1 = 0.0012 * y(1) * y(2);
bl2 = 0.0012 * y(1) * y(3);

% enzyme concentration and deactivation
E0 = 0.152;
kdeact = exp(6.75 - 38.73 * c(1) + 28.00 * c(1)^2);
E = E0 * exp(-kdeact * t);

% rate equations
r(1) = (-vs - vr) * E - bl1 - bl2;
r(2) = -vr * E - bl1;
r(3) = -vs * E - bl2;
r(4) = vr * E + bl1;
r(5) = vs * E + bl2;

end

```


B Supplemental information

Definitions

Some important definitions that have been frequently used to characterize reactions in this study are given below:

$$\text{Conversion:} \quad X_s = \frac{n_{s_0} - n_s}{n_{s_0}} \quad (\text{B.1})$$

$$\text{Selectivity:} \quad \sigma_p = \frac{n_p - n_{p_0}}{n_{s_0} - n_s} \cdot \frac{|\nu_s|}{|\nu_p|} \quad (\text{B.2})$$

$$\text{Yield:} \quad \eta_p = \frac{n_{p_0}}{n_{s_0}} \cdot \frac{|\nu_s|}{|\nu_p|} \quad (\text{B.3})$$

$$\text{Enantiomeric excess:} \quad ee = \frac{n_R - n_S}{n_R + n_S} \quad (\text{B.4})$$

$$\text{Space-time yield:} \quad STY = \frac{m_p}{\tau \cdot V_R} \quad (\text{B.5})$$

The total turnover number is defined as the total amount of product produced in mol per amount of enzyme in mol (Equation B.6). The specific ttn was defined accordingly in this work as the total amount of product produced in mol per amount of enzyme in gram.

$$\text{Total turnover number:} \quad ttn = \frac{n_{product}}{n_{enzyme}} \quad (\text{B.6})$$

According to Rogers and Bommarius [108], the ttn can be estimated from $k_{cat,obs}$ and k_{deact} according to Equation B.7.

$$\text{Total turnover number:} \quad ttn = \frac{k_{cat,obs}}{k_{deact}} \quad (\text{B.7})$$

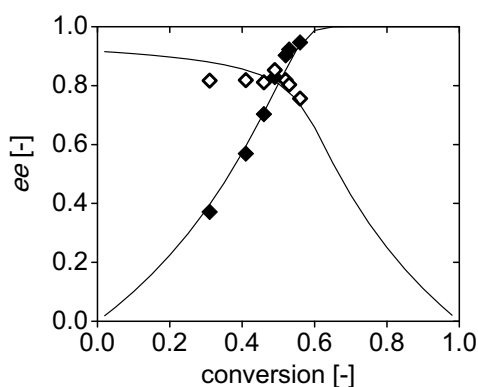
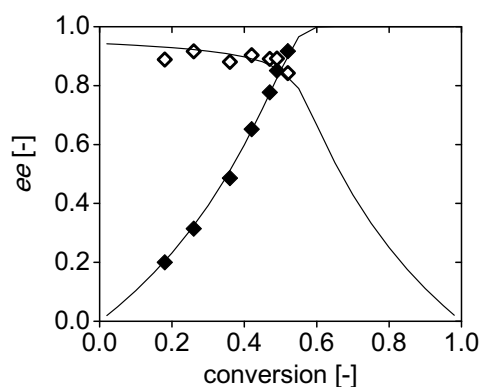
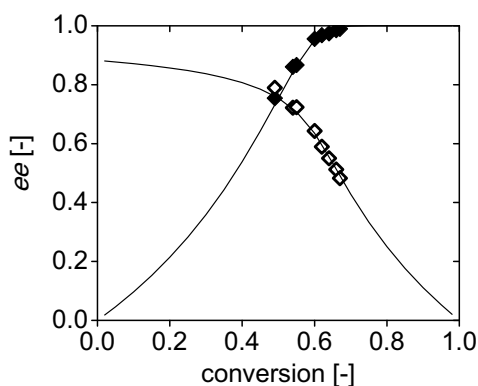
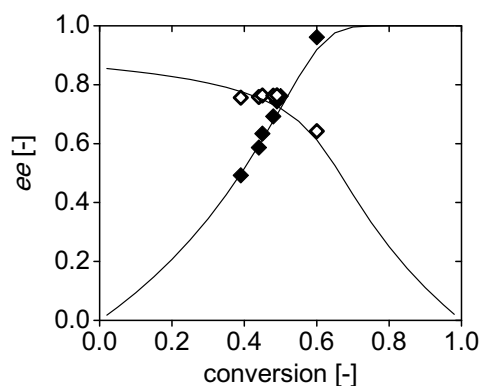
The constant $k_{cat,obs}$ can be calculated from the specific activity according to Equation B.8.

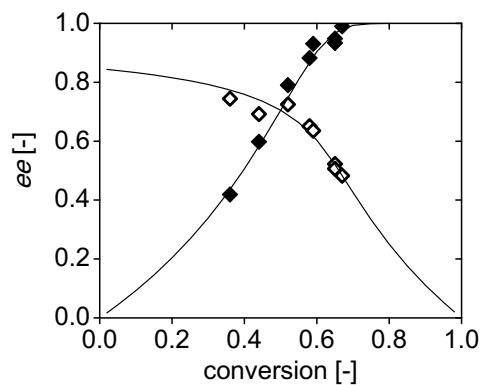
Apparent turnover number:

$$k_{cat,obs} = \frac{\text{spec. activity } [U \cdot mg^{-1}] \cdot MW_{Enz.} [g \cdot mol^{-1}]}{60000} \quad (\text{B.8})$$

With a production rate of $10.4 \text{ U g}_{\text{Novozym 435}}^{-1}$ under process conditions, a molecular mass of CALB of 33000 g mol^{-1} and an estimated protein load of 5 % (w/w) CALB on the carrier material, an apparent $k_{cat,obs}=414 \text{ h}^{-1}$ is calculated. A deactivation constant $k_{deact}=0.0026 \text{ h}^{-1}$ had been determined in batch experiments and used for an estimation of the ttn in a continuous process using Equation B.8 (see Section 6.3).

Enantioselectivity of Novozym 435 in organic solvents

(a) Acetonitrile ($\log P=0.34$, $E=23$).(b) Tetrahydrofuran ($\log P=0.46$, $E=34$).(c) Diisopropylether ($\log P=1.52$, $E=16$).(d) Toluene ($\log P=2.73$, $E=13$).



(e) *n*-Hexane (logP=3.9, E=12).

Figure B.1: Enantiomeric excess as a function of conversion in different organic solvents. 0.2 M of substrates **1** and *rac*-**3**, 45 mg ml⁻¹ Novozym 435, 60 °C.

Temperature effect on selectivity

Table B.1: Calculation of ideal enantioselectivity E based on the overall rate constant k_r (spontaneous side reaction and enzyme-catalyzed), k_{sp} for the spontaneous side reaction and E using the software Selectivity-KRESH.

Temperature [°C]	k_r ([h ⁻¹])	k_{sp} ([h ⁻¹])	E' [-]	E [-]
40	0.232	0.00019	40	42
50	0.375	0.0004	34	35
60	0.659	0.00072	32	33
70	0.826	0.00117	20	21
80	0.998	0.00211	17	19

FTIR reference spectra

FTIR reference spectra of benzylamine **1** and *trans*-ethyl crotonate **2** are shown in Figure B.2, spectra of the ester **3** and the amide **4** shown in Figure B.3.

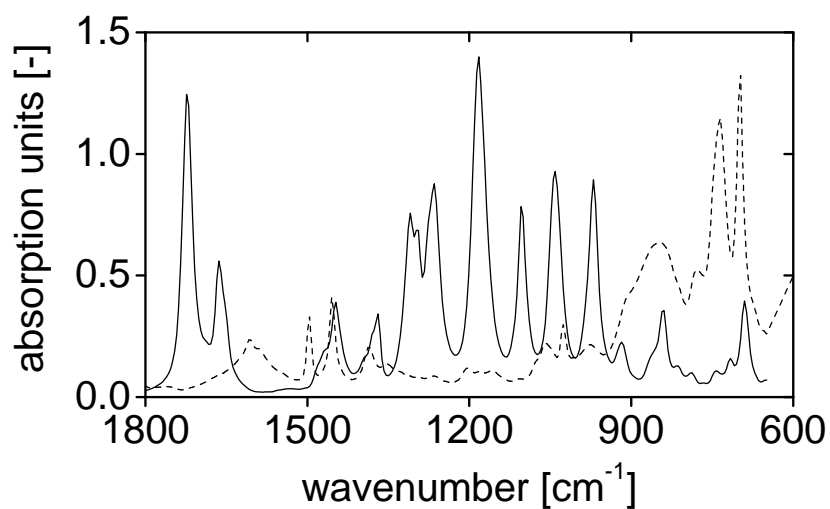


Figure B.2: Reference FTIR spectra of pure compounds **1** (- -) and **2** (-).

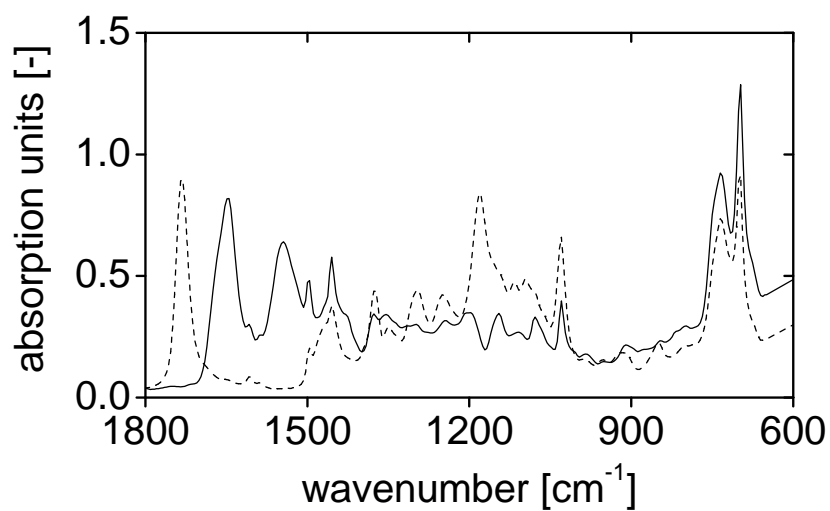


Figure B.3: Reference FTIR spectra of pure compounds **3** (- -) and **4** (-).

FTIR model development: statistical data

Relevant statistical data for the development of the chemometric model as applied for the inline prediction of concentrations in the aza-Michael addition of **1** and **2** (Section 5.2.1 on page 58) and the Novozym 435-catalyzed aminolysis of **3** with **1** (Section 5.2.2 on page 60) using a Silver Halide (AgX) FiberConduitTM with a DiCompTM diamond probe tip is provided in Table B.2. The statistically optimized selection of the minimum number of factors required via principal component analysis is selected automatically in Mettler Toledo's iC Quant Modeling Package[®] (see Figure B.4).

Table B.2: Summary of relevant data of the chemometric models obtained from inline FTIR analysis of aza-Michael reaction and subsequent biocatalytic aminolysis using ATR probe.

Description	aza-Michael addition	Biocatalytic aminolysis
spectral range	770 - 1866 cm ⁻¹	770 - 1866 cm ⁻¹
spectrum manipulation	1st order derivative	no derivative
number of factors	2	1
RMSEC	1: 0.001 g mol ⁻¹ 2: 0.004 g mol ⁻¹ 3: 0.001 g mol ⁻¹	1: 0.004 g mol ⁻¹ 3: 0.001 g mol ⁻¹ 4: 0.002 g mol ⁻¹
RMSEP	1: 0.001 g mol ⁻¹ 2: 0.002 g mol ⁻¹ 3: 0.004 g mol ⁻¹	1: 0.005 g mol ⁻¹ 3: 0.003 g mol ⁻¹ 4: 0.002 g mol ⁻¹

Relevant statistical data for the development of the chemometric model as applied for the inline prediction of concentrations in the aza-Michael addition of **1** and **2** (Section 5.2.1 on page 58) and the Novozym 435-catalyzed aminolysis of **3** with **1** (Section 5.2.2 on page 60) using a DS Micro Flowcell is provided in Table B.3. The selection of the minimum number of factors required via principal component analysis was again selected automatically in Mettler Toledo's iC Quant Modeling Package[®] (see Figure B.5).

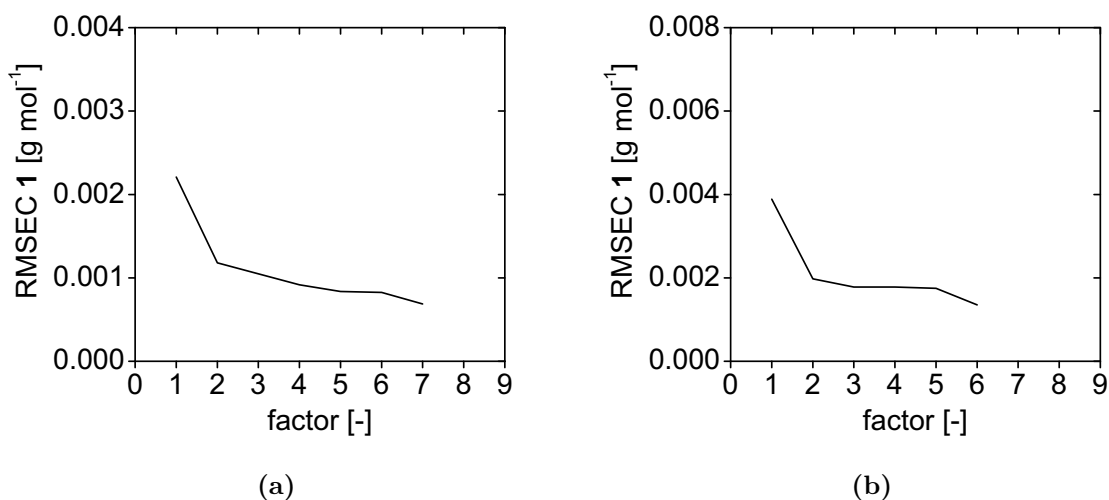


Figure B.4: Principle component analysis for the determination of factors required in chemometric model for the inline analysis of (a) aza-Michael addition and (b) biocatalytic aminolysis using ATR probe.

Table B.3: Summary of relevant data of the chemometric models obtained from inline FTIR analysis of aza-Michael addition and subsequent biocatalytic aminolysis using ATR micro flowcell.

Description	aza-Michael addition	Biocatalytic aminolysis
spectral range	800 - 1800 cm^{-1}	800 - 1800 cm^{-1}
spectrum manipulation	2nd order derivative	1st order derivative
number of factors	3	4
RMSEC	1: 0.206 g mol^{-1} 2: 0.122 g mol^{-1} 3: 0.135 g mol^{-1}	1: 0.158 g mol^{-1} 3: 0.032 g mol^{-1} 4: 0.030 g mol^{-1}
RMSEP	1: 0.189 g mol^{-1} 2: 0.103 g mol^{-1} 3: 0.187 g mol^{-1}	1: 0.154 g mol^{-1} 3: 0.041 g mol^{-1} 4: 0.057 g mol^{-1}

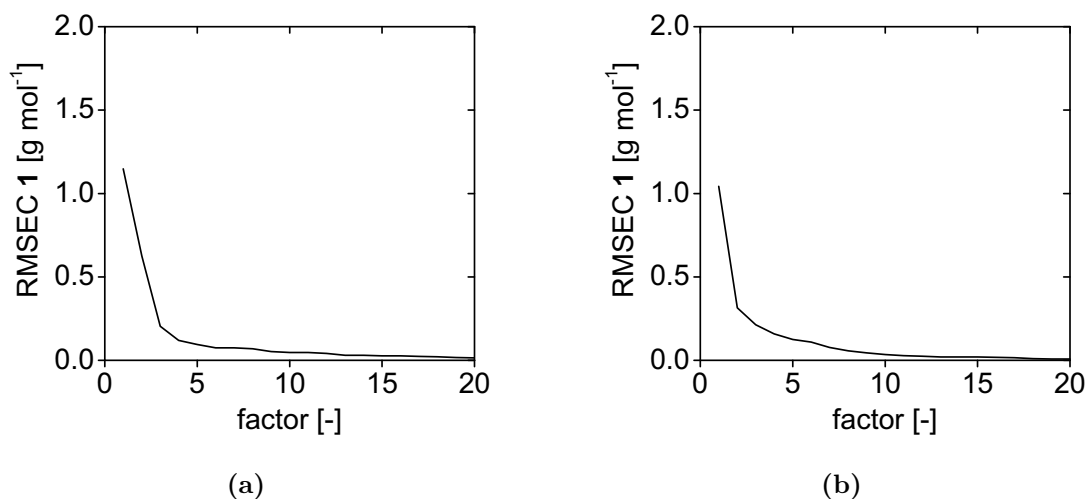


Figure B.5: Principle component analysis for the determination of factors required in chemometric model for the inline analysis of (a) aza-Michael addition and (b) biocatalytic aminolysis using ATR micro flowcell.

Calculation of process costs

The calculation of the process costs were based solely on costs for substrates, enzymes and reagents required for downstream processing. Costs for energy, capital costs, water and wastewater treatment are not considered. A possible recycling of solvents and other reagents was not considered, but can be assumed to further reduce costs. Current prices were taken from Sigma Aldrich (Taufkirchen, Germany) and Linde AG (Hamburg, Germany). Quantities necessary for the production of 1 kg of the final product (*S*)- β -aminobutanoic acid hydrochloride (MW=139.6 g mol⁻¹) are summarized in table B.4. Amounts of reagents necessary for downstream processing were taken from Weiß et al. [139].

Table B.4: Cost estimation for the production of (*S*)- β -aminobutanoic acid hydrochloride based on consumption of reactants and reagents for downstream processing.

	Current reagent price [€ kg ⁻¹]	Input quantity [kg kg _{product} ⁻¹]	Costs [€ kg _{product} ⁻¹]
chemoenzymatic reaction sequence			
<i>trans</i> -ethyl crotonate	70	2.89	202.3
benzylamine	104	4.61	479.3
Novozym 435	1400	0.03	42.0
Sum			723.6
downstream processing			
Hydrogen	70.9	0.07	4.96
NaOH (0.1 M)	0.15	0.25	0.04
NaOH (1.0 M)	1.5	2.06	3.1
NaOH (2.0 M)	3.0	3.92	11.9
MTBE	14	1.87	26.0
NaHCO ₃	4.1	0.36	1.5
HCl (1.0 M)	1.3	12.26	15.9
Sum			63.4
Sum total			787.0

List of Tables

1.1	Advantages and disadvantages of the three approaches to continuous coupled-reaction (chemo)enzymatic processes according to Yuryev et al. [147].	10
3.1	Kinetic parameters for aza-Michael addition.	19
4.1	Apparent enantioselectivity E' at different initial substrate mole fractions.	30
4.2	Estimated kinetic parameters for Novozym 435-catalyzed aminolysis in THF at 60 °C.	42
5.1	Characteristic IR absorption bands of compounds 1-5	53
6.1	Calculated and observed data characterizing the packed bed reactor used in a coupled, continuous flow reactor setup.	75
6.2	Comparison of the PFR performance for the aza-Michael addition as carried out by Weiß, 2011 [138] and under optimized conditions (this study).	77
6.3	Comparison of the PBR performance for the Novozym 435-catalyzed aminolysis as carried out by Weiß, 2011 [138] and under optimized conditions (this study).	77
B.1	Calculation of ideal enantioselectivity E using the software Selectivity-KRESH.	111
B.2	Summary of relevant data of the chemometric models obtained from in-line FTIR analysis of aza-Michael reaction and subsequent biocatalytic aminolysis using ATR probe.	113
B.3	Summary of relevant data of the chemometric models obtained from in-line FTIR analysis of aza-Michael addition and subsequent biocatalytic aminolysis using ATR micro flowcell.	114
B.4	Cost estimation for the production of (<i>S</i>)- β -aminobutanoic acid hydrochloride based on consumption of reactants and reagents for downstream processing.	116

List of Tables

List of Figures

1.1	Kinetic resolution of racemates vs. asymmetric synthesis. Grey arrows indicate a possible dynamic kinetic resolution (DKR).	2
1.2	Enantiomeric excess of the substrate (a) or product (b) as a function of conversion in dependence of enzyme enantioselectivity E	3
1.3	Reaction scheme of the racemase/D-hydantoinase/D-carbamoylase system for the enantioselective production of α -amino acids [84].	4
1.4	(Bio)process development: aspects for optimization.	5
1.5	Hydroxynitrile lyase-catalyzed conversion of acetophenone to corresponding cyanohydrin [134].	6
1.6	Nuclease p1-catalyzed aldol addition in solvent-free system [71].	6
1.7	<i>Candida antarctica</i> lipase A (CALA)-catalyzed kinetic resolution of methyl 2-chloromandelate via transesterification with vinylpropionate [131].	7
1.8	Phenylalanine aminomutase (PAM)-catalyzed synthesis of (<i>S</i>)- α -phenylalanine and (<i>R</i>)- β -phenylalanine [144].	8
1.9	Asymmetric synthesis of (<i>S</i>)- β -phenylalanine via sequential action of <i>Candida rugosa</i> lipase and <i>Mesorhizobium sp.</i> β -transaminase [62].	8
1.10	Asymmetric route towards β^2 -amino acids applying old yellow enzyme (OYE) [125].	9
1.11	Enantioselective conversion of benzyl-protected β -amino alkanenitriles to the corresponding β -amino amides and acids, respectively, applying <i>Rhodococcus erythropolis</i> AJ270 as a whole cell catalyst [76].	9
3.1	General scheme of Michael addition.	15
3.2	General scheme of <i>Candida antarctica</i> lipase B catalyzed Michael addition of thiol, amine- or carbon nucleophile to α , β -unsaturated carbonyl.	16
3.3	Chemoenzymatic reaction sequence for the synthesis of β -amino acid ester (<i>S</i>)- 3	16
3.4	Potential routes towards the amide side product <i>rac</i> - 4	17
3.5	Progress curve of the solvent-free aza-Michael addition of benzylamine and <i>trans</i> -ethyl crotonate at 60 °C.	20
3.6	Simulation of progress curve of solvent-free aza-Michael addition.	21
3.7	Fundamental reaction engineering parameters conversion, selectivity and yield in thermal aza-Michael addition as a function of time.	22
3.8	Yield and selectivity as a function of conversion in thermal aza-Michael addition.	23
4.1	Novozym 435-catalyzed aminolysis for the kinetic resolution of <i>rac</i> - 3	25

List of Figures

4.2	Mechanism of ester cleavage via acyl-enzyme intermediate.	26
4.3	Selectivity of the Novozym 435-catalyzed solvent-free kinetic resolution of <i>rac</i> - 3 via aminolysis at 60 °C.	27
4.4	Temperature dependence of enantioselectivity of Novozym 435 in solvent-free kinetic resolution of <i>rac</i> - 3 via aminolysis. $\chi_{0, rac-3} = 0.5, \chi_{0,1} = 0.5, 0.152 \text{ g}_{N435} \text{ g}^{-1}$	28
4.5	Enantioselectivity as a function of temperature in the Novozym 435-catalyzed solvent-free kinetic resolution of <i>rac</i> - 3 via aminolysis.	29
4.6	Dependence of enantioselectivity on solvent polarity expressed as logP.	30
4.7	Influence of substrate ratio and uncatalyzed side reaction on enantioselectivity.	31
4.8	Temperature dependence of stability of Novozym 435 in solvent-free system.	32
4.9	Stability of Novozym 435 as function of initial substrate mole fraction in solvent-free system at 60 °C.	33
4.10	Investigation of diffusion limitation by comparison of initial reaction rates in Novozym 435-catalyzed aminolysis of <i>rac</i> - 3 using intact and pestled enzyme carrier.	34
4.11	Polarity of solvent-free medium depending on substrate fraction on π^* -scale.	37
4.12	Reaction rate in organic solvents as a function of solvent polarity expressed by solvatochromic polarity scales. 0.2 M of 1 and <i>rac</i> - 3 , 45 $\text{mg}_{N435} \text{ ml}^{-1}$, 60 °C.	38
4.13	Formation of precipitate in Novozym 435-catalyzed aminolysis at defined water activities a_w	38
4.14	Infinite dilution water activity coefficient γ_w^∞ as a function of mole fraction of <i>rac</i> - 3 in solvent-free system with benzylamine.	39
4.15	Molecule geometry and charge distribution of most abundant (<i>S</i>)- 3 conformer in racemic mixture calculated and optimized using HyperChem, Turbomole and COSMO-RS-software.	40
4.16	Initial rate measurements of Novozym 435-catalyzed aminolysis of <i>rac</i> - 3 with benzylamine 1 in THF at 60 °C.	43
4.17	Initial rate measurements of Novozym 435-catalyzed aminolysis of <i>rac</i> - 3 with benzylamine 1 in solvent-free system at 60 °C. a) Linear adaption of ν'_{max} in order to account for solvent effects according to Sandoval et al., 2001. b) Dependence of initial rate on mole fraction of <i>rac</i> - 3	44
4.18	Temperature dependence of initial reaction rate in Novozym 435-catalyzed aminolysis of <i>rac</i> - 3	45
4.19	Simulation of Novozym 435-catalyzed aminolysis of <i>rac</i> - 3 with benzylamine 1 according to model Equations 4.8 - 4.16. All reactions were carried out in a solvent-free system at 60 °C with 0.152 g g^{-1} Novozym 435.	47
4.20	Comparison of batch and fed batch operation in Novozym 435-catalyzed kinetic resolution of <i>rac</i> - 3 with 1 by simulation and experimentally.	48

5.1	Schematic and photographic depiction of ATR crystal for FTIR spectroscopy.	52
5.2	Schematic depiction of general procedure in chemometric modelling.	53
5.3	Experimental setup for inline monitoring of aza-Michael addition via ATR-FTIR spectroscopy.	55
5.4	3-Dimensional depiction of FTIR spectra vs. time in thermal aza-Michael addition of 1 and 2	56
5.5	Offline HPLC-data and inline FTIR spectroscopic data as interpreted using chemometric model in aza-Michael addition.	57
5.6	3-Dimensional depiction of FTIR spectra vs. time in Novozym 435-catalyzed aminolysis of <i>rac</i> - 3 and 1	57
5.7	Offline HPLC-data and inline FTIR spectroscopic data as interpreted using chemometric model in Novozym 435-catalyzed aminolysis.	58
5.8	Batch reactor setup with bypass analytics for the inline reaction monitoring of the solvent-free aza-Michael addition of 1 and 2 applying an FTIR flowcell. (a) photographic. (b) schematic.	59
5.9	Internal and external validation of regression model for the prediction of concentrations in aza-Michael addition of 1 and 2 monitored inline using FTIR flowcell.	60
5.10	Batch reactor setup with bypass analytics for the inline reaction monitoring of the solvent-free Novozym 435-catalyzed aminolysis of <i>rac</i> - 3 and 1 applying an FTIR flowcell. (a) photographic. (b) schematic.	61
5.11	Internal and external validation of regression model for the prediction of concentrations in biocatalytic aminolysis of <i>rac</i> - 3 and 1 monitored inline using FTIR flowcell.	62
6.1	Simulation of enantiomeric excess as a function of conversion in PBR and CSTR reactor in the kinetic resolution of <i>rac</i> - 3 and 1	66
6.2	Schematic depiction of coupled reactor setup for the chemoenzymatic production of (<i>S</i>)-ethyl 3-(benzylamino)butanoate.	67
6.3	Residence time distribution ($F(\theta)$ -curve) in tube reactor.	68
6.4	Aza-Michael addition of 1 and 2 in a plug flow reactor.	70
6.5	Temperature dependence of selectivity in thermal aza-Michael addition of 1 and 2 in plug flow reactor.	71
6.6	Diffusion limitation in packed bed reactor for Novozym 435-catalyzed aminolysis.	72
6.7	Summary of optimized parameters as obtained from batch experiments.	73
6.8	Simulation of conversion and <i>ee</i> as a function of residence time in a packed bed reactor.	74
6.9	Photographic depiction of reactor setup for the continuous aza-Michael addition and subsequent Novozym 435-catalyzed aminolysis.	74
6.10	Photographic depiction of helically wound tube reactor for the aza-Michael addition as applied in the coupled reactor setup.	75

List of Figures

6.11	Conversion and <i>ee</i> as a function of reaction time in coupled reactor for the continuous aza-Michael addition of 1 and 2 and subsequent Novozym 435 catalyzed aminolysis.	76
7.1	Schematic depiction of high pressure batch reactor.	79
7.2	Photographic depiction of thermostated high pressure batch reactor including screw-press hand pump, pressure gauge, sampling valve and magnetic stirrer.	80
7.3	Enantioselectivity of Novozym 435-catalyzed aminolysis of <i>rac</i> - 3 with 1 in THF at atm pressure in a glass or steel reactor and at 200 MPa.	81
7.4	Enantioselectivity of Novozym 435-catalyzed aminolysis of <i>rac</i> - 3 with 1 at atm pressure and 200 MPa in DIPE.	82
7.5	Comparison of reaction rate of Novozym 435-catalyzed aminolysis of <i>rac</i> - 3 with 1 at atm pressure and at 200 MPa.	84
7.6	Stability of lipase Novozym 435 at atm pressure and 200 MPa in THF.	85
8.1	Estimation of cost distribution in optimized chemoenzymatic synthesis of (<i>S</i>)-aminobutanoic acid hydrochloride.	89
8.2	Combinatorial approach including asymmetric synthesis and kinetic resolution for the achievement of high enantiomeric excesses in non-ideal asymmetric syntheses.	90
A.1	Exemplary HPLC spectrum for the determination of conversion. Retention times: 1 : 3.9 min, 2 : 8.5 min, <i>rac</i> - 3 : 15.5 min, <i>rac</i> - 4 : 18 min, 5 : 6.1 min.	99
A.2	HPLC analysis of enantiomeric excess of (a) (<i>R/S</i>)- 3 and (b) (<i>R/S</i>)- 4 on chiral stationary phases.	100
B.1	Enantiomeric excess as a function of conversion in organic solvents.	111
B.2	Reference FTIR spectra of pure compounds 1 (- -) and 2 (-).	112
B.3	Reference FTIR spectra of pure compounds 3 (- -) and 4 (-).	112
B.4	Principle component analysis for the determination of factors required in chemometric model for the inline analysis of (a) aza-Michael addition and (b) biocatalytic aminolysis using ATR probe.	114
B.5	Principle component analysis for the determination of factors required in chemometric model for the inline analysis of (a) aza-Michael addition and (b) biocatalytic aminolysis using ATR micro flowcell.	115

Bibliography

- [1] A. Aertsen, F. Meersman, M. E. Hendrickx, R. F. Vogel, and C. W. Michiels. Biotechnology under high pressure: applications and implications. *Trends in Biotechnology*, 27(7):434–441, 2009.
- [2] E. M. Anderson, K. M. Larsson, and O. Kirk. One biocatalyst-many applications: The use of *Candida antarctica* B-lipase in organic synthesis. *Biocatalysis and Biotransformation*, 16(3):181–204, 1998.
- [3] S. Bartsch, R. Kourist, and U. Bornscheuer. Complete inversion of enantioselectivity towards acetylated tertiary alcohols by a double mutant of a *Bacillus subtilis* esterase. *Angewandte Chemie International Edition*, 47(8):1508–1511, 2008.
- [4] R. P. Bell, J. E. Critchlow, and M. I. Page. Ground state and transition state effects in the acylation of α -chymotrypsin in organic solvent-water mixtures. *Journal of the Chemical Society, Perkin Transactions 2*, 1:66–70, 1974.
- [5] M. Berheide, S. Peper, S. Kara, W. S. Long, S. Schenkel, M. Pohl, B. Niemeyer, and A. Liese. Influence of the hydrostatic pressure and pH on the asymmetric 2-hydroxyketone formation catalyzed by *Pseudomonas putida* benzoylformate decarboxylase and variants thereof. *Biotechnology and Bioengineering*, 106(1):18–26, 2010.
- [6] D. Bezbradica, D. Mijin, S. Siler-Marinkovic, and Z. Knezevic. The *Candida rugosa* lipase catalyzed synthesis of amyl isobutyrate in organic solvent and solvent-free system: A kinetic study. *Journal of Molecular Catalysis B: Enzymatic*, 38(1):11–16, 2006.
- [7] D. G. Blackmond. Reaction progress kinetic analysis: A powerful methodology for mechanistic studies of complex catalytic reactions. *Angewandte Chemie International Edition*, 44(28):4302–4320, 2005.
- [8] S. Bok and Lee. Enzyme reaction kinetics in organic solvents: A theoretical kinetic model and comparison with experimental observations. *Journal of Fermentation and Bioengineering*, 79(5):479 – 484, 1995.
- [9] A. S. Bommarius, J. K. Blum, and M. J. Abrahamson. Status of protein engineering for biocatalysts: how to design an industrially useful biocatalyst. *Current Opinion in Chemical Biology*, 15(2):194–200, 2011.

Bibliography

- [10] B. B. Boonyaratanakornkit, C. B. Park, and D. S. Clark. Pressure effects on intra- and intermolecular interactions within proteins. *Biochimica et Biophysica Acta (BBA) - Protein Structure and Molecular Enzymology*, 1595(1-2):235–249, 2002.
- [11] S. Briechle, M. Howaldt, T. Röthig, and A. Liese. *Bioprozesstechnik*, chapter 12, Enzymatische Prozesse, pages 361–408. Spektrum, Heidelberg, 2nd edition, 2006.
- [12] B. Brucher, C. Syldatk, and J. Rudat. Mikrobielle Umsetzung von β -Phenylalanin mittels neuer Transaminasen. *Chemie Ingenieur Technik*, 82(1-2):155–160, 2010.
- [13] J. Brummund, F. Meyer, A. Liese, R. Eggers, and L. Hilterhaus. Dissolving carbon dioxide in high viscous substrates to accelerate biocatalytic reactions. *Biotechnology and Bioengineering*, 108(11):2765–2769, 2011.
- [14] E. Burda, W. Hummel, and H. Grger. Modular chemoenzymatic one-pot syntheses in aqueous media: Combination of a palladium-catalyzed cross-coupling with an asymmetric biotransformation. *Angewandte Chemie International Edition*, 47(49):9551–9554, 2008.
- [15] Y. Cai, Q. Wu, Y.-M. Xiao, D.-S. Lv, and X.-F. Lin. Hydrolase-catalyzed Michael addition of imidazoles to acrylic monomers in organic medium. *Journal of Biotechnology*, 121(3):330 – 337, 2006.
- [16] Y. Cai, S.-P. Yao, Q. Wu, and X.-F. Lin. Michael addition of imidazole with acrylates catalyzed by alkaline protease from *Bacillus subtilis* in organic media. *Biotechnology Letters*, 26:525–528, 2004.
- [17] P. Carlqvist, M. Svedendahl, C. Branneby, K. Hult, T. Brinck, and P. Berglund. Exploring the active-site of a rationally redesigned lipase for catalysis of Michael-type additions. *ChemBioChem*, 6(2):331–336, 2005.
- [18] G. Carrea and S. Riva. Enzyme in organischen Lösungsmitteln: Eigenschaften und Einsatz in der Synthese. *Angewandte Chemie*, 112(13):2312–2341, 2000.
- [19] C. F. Carter, I. R. Baxendale, M. O’Brien, J. B. J. Pavey, and S. V. Ley. Synthesis of acetal protected building blocks using flow chemistry with flow I.R. analysis: preparation of butane-2,3-diacetal tartrates. *Organic & Biomolecular Chemistry*, 7:4594–4597, 2009.
- [20] C. F. Carter, H. Lange, S. V. Ley, I. R. Baxendale, B. Wittkamp, J. G. Goode, and N. L. Gaunt. Reactir flow cell: A new analytical tool for continuous flow chemical processing. *Organic Process Research & Development*, 14(2):393–404, 2010.
- [21] C. S. Chen, Y. Fujimoto, G. Girdaukas, and C. J. Sih. Quantitative analyses of biochemical kinetic resolutions of enantiomers. *Journal of the American Chemical Society*, 104(25):7294–7299, 1982.

- [22] H. Chmiel, editor. *Bioprozesstechnik: Einführung in die Bioverfahrenstechnik*. Elsevier, Spektrum Akademischer Verlag, München, 2nd edition, 2006.
- [23] V. Consonni, D. Ballabio, and R. Todeschini. Evaluation of model predictive ability by external validation techniques. *Journal of Chemometrics*, 24(3-4):194–201, 2010.
- [24] K. Danzer, H. Hobert, C. Fischbacher, and K.-U. Jagemann. *Chemometrik: Grundlagen und Anwendungen*. Springer, Berlin, 2001.
- [25] S. G. Davies, A. W. Mulvaney, A. J. Russell, and A. D. Smith. Parallel synthesis of homochiral β -amino acids. *Tetrahedron: Asymmetry*, 18(13):1554 – 1566, 2007.
- [26] M. S. de Castro and J. S. Gago. Lipase-catalyzed synthesis of chiral amides. A systematic study of the variables that control the synthesis. *Tetrahedron*, 54(12):2877–2892, 1998.
- [27] K. Dimroth and C. Reichardt. Über Pyridinium-N-phenol-betaine und ihre Verwendung zur Charakterisierung der Polarität von Lösungsmitteln, Erweiterung der Lösungsmittelpolaritätsskala durch Verwendung Alkyl-substituierter Pyridinium-N-phenol-betaine. *Justus Liebigs Annalen der Chemie*, 727(1):93–105, 1969.
- [28] F. Eckert and A. Klamt. COSMOtherm, Version c2.1, Release 01.10; COSMOlogic GmbH & Co. KG, Leverkusen, Germany, 2009.
- [29] M. Eissen, M. Weiß, T. Brinkmann, and S. Steinigeweg. Comparison of two alternative routes to an enantiomerically pure β -amino acid. *Chemical Engineering and Technology*, 33(4):629–637, 2010.
- [30] P. A. Fitzpatrick and A. M. Klivanov. How can the solvent affect enzyme enantioselectivity? *Journal of the American Chemical Society*, 113(8):3166–3171, 1991.
- [31] P. A. Fitzpatrick, A. C. Steinmetz, D. Ringe, and A. M. Klivanov. Enzyme crystal structure in a neat organic solvent. *Proceedings of the National Academy of Sciences of the United States of America*, 90(18):8653–8657, 1993.
- [32] R. G. and Duggleby. Quantitative analysis of the time courses of enzyme-catalyzed reactions. *Methods*, 24(2):168 – 174, 2001.
- [33] A. Ghanem and H. Y. Aboul-Enein. Application of lipases in kinetic resolution of racemates. *Chirality*, 17(1):1–15, 2005.
- [34] R. L. Giordano, R. C. Giordano, and C. L. Cooney. Performance of a continuous taylor-couette-poiseuille vortex flow enzymic reactor with suspended particles. *Process Biochemistry*, 35(10):1093 – 1101, 2000.

Bibliography

- [35] Y. Gnas and F. Glorius. Chiral auxiliaries - principles and recent applications. *ChemInform*, 37(37):1899–1930, 2006.
- [36] H. L. Goderis, G. Ampe, M. P. Feyten, B. L. Fouw, W. M. Guffens, S. M. Van Cauwenbergh, and P. P. Tობback. Lipase-catalyzed ester exchange reactions in organic media with controlled humidity. *Biotechnology and Bioengineering*, 30(2):258–266, 1987.
- [37] M. V. Golynskiy and B. Seelig. De novo enzymes: from computational design to mRNA display. *Trends in Biotechnology*, 28(7):340 – 345, 2010.
- [38] Z. W. Guo and C. J. Sih. Enantioselective inhibition: strategy for improving the enantioselectivity of biocatalytic systems. *Journal of the American Chemical Society*, 111(17):6836–6841, 1989.
- [39] M. Hermann, M. U. Kietzmann, M. Ivančić, C. Zenzmaier, R. G. Luiten, W. Skranc, M. Wubbolts, M. Winkler, R. Birner-Gruenberger, H. Pichler, and H. Schwab. Alternative pig liver esterase (APLE) - cloning, identification and functional expression in *Pichia pastoris* of a versatile new biocatalyst. *Journal of Biotechnology*, 133(3):301 – 310, 2008.
- [40] M. Hesse, H. Meier, and B. Zeeh. *Spektroskopische Methoden in der organischen Chemie*. Thieme, Stuttgart, 7th edition, 2005.
- [41] L. Heuer. *Benzylamine*. *Ullmann's Encyclopedia of Industrial Chemistry*. Wiley-VCH, Weinheim, 2006.
- [42] L. Hilterhaus, M. Howaldt, A. Liese, and H. Chmiel. *Bioprozesstechnik: Einführung in die Bioverfahrenstechnik*, chapter Enzymkinetik, pages 67–97. Elsevier, Spektrum Akademischer Verlag, München, 2006.
- [43] L. Hilterhaus, A. Liese, and U. Kragl. *Biotransformation, Process Optimization, Kinetics and Engineering Aspects*. John Wiley & Sons, Inc., 2009.
- [44] Y. Hirose, K. Kariya, I. Sasaki, Y. Kurono, H. Ebiike, and K. Achiwa. Drastic solvent effect on lipase-catalyzed enantioselective hydrolysis of prochiral 1,4-dihydropyridines. *Tetrahedron Letters*, 33(47):7157–7160, 1992.
- [45] F. Hollmann, P. Grzebyk, V. Heinrichs, K. Doderer, and O. Thum. On the inactivity of *Candida antarctica* lipase B towards strong acids. *Journal of Molecular Catalysis B: Enzymatic*, 57(1-4):257–261, 2009.
- [46] P. B. Howell, Jr, D. R. Mott, J. P. Golden, and F. S. Ligler. Design and evaluation of a dean vortex-based micromixer. *Lab Chip*, 4:663–669, 2004.
- [47] E. P. Hudson, R. K. Eppler, J. M. Beaudoin, J. S. Dordick, J. A. Reimer, and D. S. Clark. Active-site motions and polarity enhance catalytic turnover of hydrated subtilisin dissolved in organic solvents. *Journal of the American Chemical Society*, 131(12):4294–4300, 2009.

- [48] S. Hwang, C. Choi, and E. Lee. One-pot biotransformation of racemic styrene oxide into (*R*)-1,2-phenylethandiol by two recombinant microbial epoxide hydrolases. *Biotechnology and Bioprocess Engineering*, 13:453–457, 2008.
- [49] H. Iding, T. Dünnwald, L. Greiner, A. Liese, M. Müller, P. Siegert, J. Grötzinger, A. S. Demir, and M. Pohl. Benzoylformate decarboxylase from *Pseudomonas putida* as stable catalyst for the synthesis of chiral 2-hydroxy ketones. *Chemistry A European Journal*, 6(8):1483–1495, 2000.
- [50] A. E. M. Janseen, A. Van der Padt, H. M. Van Sonsbeek, and K. Van't Riet. The effect of organic solvents on the equilibrium position of enzymatic acylglycerol synthesis. *Biotechnology and Bioengineering*, 41(1):95–103, 1993.
- [51] A. E. M. Janssen, A. M. Vaidya, and P. J. Halling. Substrate specificity and kinetics of *Candida rugosa* lipase in organic media. *Annals of the New York Academy of Sciences*, 799(1):257–261, 1996.
- [52] J. N. Jin, S. H. Lee, and S. B. Lee. Enzymatic production of enantiopure ketoprofen in a solvent-free two-phase system. *Journal of Molecular Catalysis B: Enzymatic*, 26(3-6):209 – 216, 2003.
- [53] E. Juaristi, D. Quintana, and J. Escalante. Enantioselective synthesis of β -amino acids. *Aldrichimica Acta*, 27(1):3–11, 1994.
- [54] E. Juaristi and V. A. Soloshonok, editors. *Enantioselective Synthesis of β -Amino Acids*. Wiley-VCH, New York, 2nd edition, 2005.
- [55] U. H. Kahlow, R. D. Schmid, and J. Pleiss. A model of the pressure dependence of the enantioselectivity of *Candida rugosa* lipase towards (\pm)-menthol. *Protein Science*, 10(10):1942–1952, 2001.
- [56] M. J. Kamlet, J. L. Abboud, and R. W. Taft. The solvatochromic comparison method. 6. The .pi.* scale of solvent polarities. *Journal of the American Chemical Society*, 99(18):6027–6038, 1977.
- [57] S. Kara, W. S. Long, M. Berheide, S. Peper, B. Niemeyer, and A. Liese. Influence of reaction conditions on the enantioselectivity of biocatalyzed C-C bond formations under high pressure conditions. *Journal of Biotechnology*, 152(3):87–92, 2011.
- [58] V. Kasche, G. Michaelis, and B. Galunsky. Binding of organic solvent molecules influences the P1'-P2' stereo- and sequence-specificity of α -chymotrypsin in kinetically controlled peptide synthesis. *Biotechnology Letters*, 13(2):75–80, 1991.
- [59] K. Kataoka, N. Ohmura, M. Kouzu, Y. Simamura, and M. Okubo. Emulsion polymerization of styrene in a continuous taylor vortex flow reactor. *Chemical Engineering Science*, 50(9):1409 – 1416, 1995.

Bibliography

- [60] R. Kessler. *Prozessanalytik: Strategien und Fallbeispiele aus der industriellen Praxis*, chapter Strategien für wissensbasierte Produkte und Verfahren. VCH-Wiley, Weinheim, 2006.
- [61] J. Kim and J. S. Dordick. Pressure affects enzyme function in organic media. *Biotechnology and Bioengineering*, 42(6):772–776, 1993.
- [62] J. Kim, D. Kyung, H. Yun, B.-K. Cho, J.-H. Seo, M. Cha, and B.-G. Kim. Cloning and characterization of a novel β -transaminase from *Mesorhizobium sp.* strain LUK: a new biocatalyst for the synthesis of enantiomerically pure β -amino acids. *Applied and Environmental Microbiology*, 73(6):1772–1782, March 15, 2007.
- [63] T. Kitazume, T. Ikeya, and K. Murata. Synthesis of optically active trifluorinated compounds: asymmetric Michael addition with hydrolytic enzymes. *Journal of the Chemical Society, Chemical Communications*, 17:1331–1333, 1986.
- [64] A. M. Klibanov. Improving enzymes by using them in organic solvents. *Nature*, 409(6817):241–246, 2001.
- [65] S. Kunugi, M. Kitayaki, Y. Yanagi, N. Tanaka, R. Lange, and C. Balny. The effect of high pressure on thermolysin. *European Journal of Biochemistry*, 248(2):567–574, 1997.
- [66] A. L. L. Hilterhaus. *Bioprocess Development*, chapter Manual of Industrial Microbiology and Biotechnology. ASM Press, Washington, 2010.
- [67] C. Laane, S. Boeren, K. Vos, and C. Veeger. Rules for optimization of biocatalysis in organic solvents. *Biotechnology and Bioengineering*, 30(1):81–87, 1987.
- [68] C. Laurence, P. Nicolet, M. T. Dalati, J.-L. M. Abboud, and R. Notario. The empirical treatment of solvent-solute interactions: 15 years of π^* . *The Journal of Physical Chemistry*, 98(23):5807–5816, 1994.
- [69] C. Laurence, P. Nicolet, and M. Helbert. Polarity and basicity of solvents. part 2. solvatochromic hydrogen-bonding shifts as basicity parameters. *Journal of the Chemical Society, Perkin Transactions 2*, 7:1081–1090, 1986.
- [70] O. Levenspiel, editor. *Chemical Reaction Engineering*. John Wiley & Sons, New York, 3rd edition, 1999.
- [71] H.-H. Li, Y.-H. He, Y. Yuan, and Z. Guan. Nuclease pl: a new biocatalyst for direct asymmetric aldol reaction under solvent-free conditions. *Green Chemistry*, 13:185–189, 2011.
- [72] A. Liese, K. Seelbach, and C. Wandrey. *Industrial Biotransformations*. Wiley-VCH, Weinheim, 2006.

- [73] A. Liljeblad and L. T. Kanerva. Biocatalysis as a profound tool in the preparation of highly enantiopure β -amino acids. *Tetrahedron*, 62(25):5831–5854, 2006.
- [74] H. Löwe, V. Hessel, P. Löb, and S. Hubbard. Addition of secondary amines to α,β -unsaturated carbonyl compounds and nitriles by using microstructured reactors. *Organic Process Research & Development*, 10(6):1144–1152, 2006.
- [75] S. Lutz. Beyond directed evolution: semi-rational protein engineering and design. *Current Opinion in Biotechnology*, 21(6):734 – 743, 2010.
- [76] D.-Y. Ma, D.-X. Wang, J. Pan, Z.-T. Huang, and M.-X. Wang. Nitrile biotransformations for the synthesis of highly enantioenriched β -hydroxy and β -amino acid and amide derivatives: A general and simple but powerful and efficient benzyl protection strategy to increase enantioselectivity of the amidase. *The Journal of Organic Chemistry*, 73(11):4087–4091, 2008.
- [77] S. S. Machado, U. Wandel, J. A. Jongejan, A. J. J. Straathof, and J. A. Duine. Characterization of the enantioselective properties of the quinoxinoprotein alcohol dehydrogenase of *Acetobacter pasteurianus* LMG 1635. 1. Different enantiomeric ratios of whole cells and purified enzyme in the kinetic resolution of racemic glycidol. *Bioscience, Biotechnology, and Biochemistry*, 63(1):10–20, 1999.
- [78] M. S. Mahmud, T. Safinski, M. I. Nelson, H. S. Sidhu, and A. A. Adesina. Kinetic analysis of oleic acid esterification using lipase as catalyst in a microaqueous environment. *Industrial & Engineering Chemistry Research*, 49(3):1071–1078, 2010.
- [79] P. Masson, C. Tonello, and C. Balny. High-pressure biotechnology in medicine and pharmaceutical science. *Journal of Biomedicine and Biotechnology*, 1(2):85–88, 2001.
- [80] T. Matsuda, T. Harada, K. Nakamura, and T. Ikariya. Asymmetric synthesis using hydrolytic enzymes in supercritical carbon dioxide. *Tetrahedron: Asymmetry*, 16(5):909–915, 2005.
- [81] T. Matsuda, R. Kanamaru, K. Watanabe, T. Harada, and K. Nakamura. Control on enantioselectivity with pressure for lipase-catalyzed esterification in supercritical carbon dioxide. *Tetrahedron Letters*, 42(47):8319–8321, 2001.
- [82] T. Matsuda, R. Kanamaru, K. Watanabe, T. Kamitanaka, T. Harada, and K. Nakamura. Control of enantioselectivity of lipase-catalyzed esterification in supercritical carbon dioxide by tuning the pressure and temperature. *Tetrahedron: Asymmetry*, 14(14):2087–2091, 2003.
- [83] O. May, P. T. Nguyen, and F. H. Arnold. Inverting enantioselectivity by directed evolution of hydantoinase for improved production of L-methionine. *Nat Biotech*, 18(2):317–320, 2000.

Bibliography

- [84] O. May, S. Verseck, A. Bommarius, and K. Drauz. Development of dynamic kinetic resolution processes for biocatalytic production of natural and nonnatural L-amino acids. *Organic Process Research & Development*, 6(4):452–457, 2002.
- [85] A. M. Mehranpour and S. Hashemnia. Solvatochromism in binary solvent mixtures by means of a penta-tert-butyl pyridinium N-phenolate betaine dye. *Journal of the Chinese Chemical Society*, 53:759–765, 2006.
- [86] P. C. Michels, D. Hei, and D. S. Clark. Pressure effects on enzyme activity and stability at high temperatures. In D. S. E. Frederic M. Richards and P. S. Kim, editors, *Enzymes and Proteins from Hyperthermophilic Microorganisms*, volume 48 of *Advances in Protein Chemistry*, pages 341–376. Academic Press, 1996.
- [87] C. B. Minnich. *Reaction calorimetric and spectroscopic studies of an Ionic Liquid synthesis*. PhD thesis, RWTH Aachen, Aachen, 2009.
- [88] C. B. Minnich, L. Greiner, C. Reimers, M. Uerdingen, and M. A. Liauw. Bridging the gap: A nested-pipe reactor for slow reactions in continuous flow chemical synthesis. *Chemical Engineering Journal*, 168(2):759 – 764, 2011.
- [89] E. Morild. The theory of pressure effects on enzymes. In C. Anfinsen, J. T. Edsall, and F. M. Richards, editors, *Advances in Protein Chemistry*, volume 34, pages 93–166. Academic Press, 1981.
- [90] V. V. Mozhaev, K. Heremans, J. Frank, P. Masson, and C. Balny. High pressure effects on protein structure and function. *Proteins: Structure, Function, and Bioinformatics*, 24(1):81–91, 1996.
- [91] B. N. Naidu, M. E. Sorenson, T. P. Connolly, and Y. Ueda. Michael addition of amines and thiols to dehydroalanine amides: a remarkable rate acceleration in water. *The Journal of Organic Chemistry*, 68(26):10098–10102, 2003.
- [92] B. M. Nestl, B. A. Nebel, and B. Hauer. Recent progress in industrial biocatalysis. *Current Opinion in Chemical Biology*, 15(2):187 – 193, 2011.
- [93] P. Nicolet and C. Laurence. Polarity and basicity of solvents. Part 1. A thermosolvatochromic comparison method. *Journal of the Chemical Society, Perkin Transactions 2*, 7:1071–1079, 1986.
- [94] H. Noritomi, O. Almarsson, G. L. Barletta, and A. M. Klivanov. The influence of the mode of enzyme preparation on enzymatic enantioselectivity in organic solvents and its temperature dependence. *Biotechnology and Bioengineering*, 51(1):95–99, 1996.
- [95] A. Ochoa-Leyva, F. Barona-Gómez, G. Saab-Rincón, K. Verdel-Aranda, F. Sánchez, and X. Soberón. Exploring the structure-function loop adaptability of a (β/α)₈-barrel enzyme through loop swapping and hinge variability. *Journal of Molecular Biology*, 411(1):143 – 157, 2011.

- [96] J. Ottosson. *Enthalpy and Entropy in Enzyme Catalysis - A Study of Lipase Enantioselectivity*. PhD thesis, Department of Biotechnology, KTH, Stockholm, Sweden, 2001.
- [97] J. Ottosson, L. Fransson, and K. Hult. Substrate entropy in enzyme enantioselectivity: An experimental and molecular modeling study of a lipase. *Protein Science*, 11(6):1462–1471, 2002.
- [98] A. Overmeyer, S. Schrader-Lippelt, V. Kasche, and G. Brunner. Lipase-catalysed kinetic resolution of racemates at temperatures from 40 °C to 160 °C in supercritical CO₂. *Biotechnology Letters*, 21:65–69, 1999.
- [99] K. Pervushin, K. Vamvaca, B. Vogeli, and D. Hilvert. Structure and dynamics of a molten globular enzyme. *Nature Structural & Molecular Biology*, 14(7):1202–1206, 2007.
- [100] C. Qian, J.-M. Xu, Q. Wu, D.-S. Lv, and X.-F. Lin. Promiscuous acylase-catalyzed aza-Michael additions of aromatic N-heterocycles in organic solvent. *Tetrahedron Letters*, 48(35):6100–6104, 2007.
- [101] Z. Qian, I. R. Baxendale, and S. V. Ley. A continuous flow process using a sequence of microreactors with in-line IR analysis for the preparation of N,N-diethyl-4-(3-fluorophenylpiperidin-4-ylidenemethyl)benzamide as a potent and highly selective δ -opioid receptor agonist. *Chemistry - A European Journal*, 16(41):12342–12348, 2010.
- [102] J. Rakels, A. Straathof, and J. Heijnen. A simple method to determine the enantiomeric ratio in enantioselective biocatalysis. *Enzyme and Microbial Technology*, 15(12):1051–1056, 1993.
- [103] B. C. Ranu, S. S. Dey, and A. Hajra. Solvent-free, catalyst-free Michael-type addition of amines to electron-deficient alkenes. *ARKIVOC*, 7:76–81, 2002.
- [104] N. K. Rastogi, K. S. M. S. Raghavarao, V. M. Balasubramaniam, K. Niranjana, and D. Knorr. Opportunities and challenges in high pressure processing of foods. *Critical Reviews in Food Science and Nutrition*, 47(1):69–112, 2007.
- [105] B. Reddy, M. Patil, and B. Reddy. An efficient protocol for aza-Michael addition reactions under solvent-free condition employing sulfated zirconia catalyst. *Catalysis Letters*, 126:413–418, 2008.
- [106] C. Reichardt. Solvatochromic dyes as solvent polarity indicators. *Chemical Reviews*, 94(8):2319–2358, 1994.
- [107] F. Richter, A. Leaver-Fay, S. D. Khare, S. Bjelic, and D. Baker. *De Novo* enzyme design using Rosetta3. *PLoS ONE*, 6:e19230, 05 2011.

Bibliography

- [108] T. A. Rogers and A. S. Bommarius. Utilizing simple biochemical measurements to predict lifetime output of biocatalysts in continuous isothermal processes. *Chemical Engineering Science*, 65(6):2118 – 2124, 2010.
- [109] P. A. Romero and F. H. Arnold. Exploring protein fitness landscapes by directed evolution. *Nature Reviews Molecular Cell Biology*, 10(12):866–867, 2009.
- [110] T. Sakurai, A. L. Margolin, A. J. Russell, and A. M. Klivanov. Control of enzyme enantioselectivity by the reaction medium. *Journal of the American Chemical Society*, 110(21):7236–7237, 1988.
- [111] G. Sandoval, J. S. Condoret, P. Monsan, and A. Marty. Esterification by immobilized lipase in solvent-free media: Kinetic and thermodynamic arguments. *Biotechnology and Bioengineering*, 78(3):313–320, 2002.
- [112] G. C. Sandoval, A. Marty, and J.-S. Condoret. Thermodynamic activity-based enzyme kinetics: Efficient tool for nonaqueous enzymology. *AIChE Journal*, 47(3):718–726, 2001.
- [113] C. K. Savile, J. M. Janey, E. C. Mundorff, J. C. Moore, S. Tam, W. R. Jarvis, J. C. Colbeck, A. Krebber, F. J. Fleitz, J. Brands, P. N. Devine, G. W. Huisman, and G. J. Hughes. Biocatalytic asymmetric synthesis of chiral amines from ketones applied to Sitagliptin manufacture. *Science*, 329(5989):305–309, 2010.
- [114] R. Sheldon. Organic synthesis - past, present and future. *Chemistry & Industry*, 1992.
- [115] R. A. Sheldon. Chirotechnology: Designing economic chiral syntheses. *Journal of Chemical Technology & Biotechnology*, 67(1):1–14, 1996.
- [116] J. L. Silva and G. Weber. Pressure stability of proteins. *Annual Review of Physical Chemistry*, 44(1):89–113, 1993.
- [117] D. A. Skoog and J. J. Leary. *Instrumentelle Analytik: Grundlagen - Geräte - Anwendungen*. Springer, Berlin, 1996.
- [118] R. R. Smith and W. J. Canady. Solvation effects upon the thermodynamic substrate activity; correlation with the kinetics of enzyme catalyzed reactions. II. more complex interactions of α -chymotrypsin with dioxane and acetone which are also competitive inhibitors. *Biophysical Chemistry*, 43(2):189 – 195, 1992.
- [119] A. Straathof and P. Adlercreutz. *Applied Biocatalysis*. Harwood Academic Publishers, Amsterdam, 2nd edition, 2005.
- [120] A. Straathof and J. Jongejan. The enantiomeric ratio: origin, determination and prediction. *Enzyme and Microbial Technology*, 21(8):559–571, 1997.

- [121] A. J. Straathof, S. Panke, and A. Schmid. The production of fine chemicals by biotransformations. *Current Opinion in Biotechnology*, 13(6):548 – 556, 2002.
- [122] G. A. Strohmeier, T. Sovic, G. Steinkellner, F. S. Hartner, A. Andryushkova, T. Purkarthofer, A. Glieder, K. Gruber, and H. Griengl. Investigation of lipase-catalyzed Michael-type carbon-carbon bond formations. *Tetrahedron*, 65(29-30):5663 – 5668, 2009.
- [123] S. Strompen, M. Weiß, T. Ingram, I. Smirnova, H. Gröger, L. Hilterhaus, and A. Liese. Kinetic investigation of a solvent-free, chemoenzymatic reaction sequence towards enantioselective synthesis of a β -amino acid ester. *Biotechnology and Bioengineering*, 2012. Accepted for publication.
- [124] M. Svedendahl, K. Hult, and P. Berglund. Fast carbon-carbon bond formation by a promiscuous lipase. *Journal of the American Chemical Society*, 127(51):17988–17989, 2005.
- [125] M. A. Swiderska and J. D. Stewart. Asymmetric bioreductions of β -nitro acrylates as a route to chiral β^2 -amino acids. *Organic Letters*, 8(26):6131–6133, 2006.
- [126] W. Szymanski, B. Wu, B. Weiner, S. de Wildeman, B. L. Feringa, and D. B. Janssen. Phenylalanine aminomutase-catalyzed addition of ammonia to substituted cinnamic acids: a route to enantiopure α - and β -amino acids. *The Journal of Organic Chemistry*, 74(23):9152–9157, 2009. PMID: 19894731.
- [127] F. Terradas, M. Teston-Henry, P. A. Fitzpatrick, and A. M. Klivanov. Marked dependence of enzyme prochiral selectivity on the solvent. *Journal of the American Chemical Society*, 115(2):390–396, 1993.
- [128] O. Torre, I. Alfonso, and V. Gotor. Lipase catalysed Michael addition of secondary amines to acrylonitrile. *Chemical Communications*, 15:1724–1725, 2004.
- [129] A. Tousignant and J. N. Pelletier. Protein motions promote catalysis. *Chemistry & Biology*, 11(8):1037–1042, 2004.
- [130] N. J. Turner. Ammonia lyases and aminomutases as biocatalysts for the synthesis of α -amino and β -amino acids. *Current Opinion in Chemical Biology*, 15(2):234 – 240, 2011.
- [131] K.-N. Uhm, S.-J. Lee, H. kwoun Kim, H.-Y. Kang, and Y. Lee. Enantioselective resolution of methyl 2-chloromandelate by *Candida antarctica* lipase a in a solvent-free transesterification reaction. *Journal of Molecular Catalysis B: Enzymatic*, 45(1-2):34 – 38, 2007.
- [132] J. B. A. van Tol, R. M. M. Stevens, W. J. Veldhuizen, J. A. Jongejan, and J. A. Duine. Do organic solvents affect the catalytic properties of lipase? Intrinsic kinetic parameters of lipases in ester hydrolysis and formation in various organic solvents. *Biotechnology and Bioengineering*, 47(1):71–81, 1995.

Bibliography

- [133] D. Vasic-Racki, U. Kragl, and A. Liese. Benefits of enzyme kinetics modelling. *Chemical Biochemical Engineering Quarterly*, 17(1):7–18, 2003.
- [134] J. von Langermann, A. Mell, E. Paetzold, T. Daubmann, and U. Kragl. Hydroxynitrile lyase in organic solvent-free systems to overcome thermodynamic limitations. *Advanced Synthesis & Catalysis*, 349(8-9):1418–1424, 2007.
- [135] P. J. Walsh, H. Li, and C. A. de Parrodi. A green chemistry approach to asymmetric catalysis: Solvent-free and highly concentrated reactions. *Chemical Reviews*, 107(6):2503–2545, 2007.
- [136] S.-Z. Wang, J.-P. Wu, G. Xu, and L.-R. Yang. Kinetic modelling of lipase-catalyzed remote resolution of citalopram intermediate in solvent-free system. *Biochemical Engineering Journal*, 45(2):113–119, 2009.
- [137] E. Wehtje, D. Costes, and P. Adlercreutz. Enantioselectivity of lipases: effects of water activity. *Journal of Molecular Catalysis B: Enzymatic*, 3(5):221–230, 1997.
- [138] M. Weiß. *Sustainable bio- and organocatalytic syntheses of enantiomerically pure β -amino acids and derivatives*. PhD thesis, Universität Erlangen-Nürnberg, Universitätsstraße. 4, 91054 Erlangen, 2011.
- [139] M. Weiß, T. Brinkmann, and H. Gröger. Towards a greener synthesis of (*S*)-3-aminobutanoic acid: process development and environmental assessment. *Green Chemistry*, 12:1580–1588, 2010.
- [140] M. Weiß and H. Gröger. Practical, highly enantioselective chemoenzymatic one-pot synthesis of short-chain aliphatic β -amino acid esters. *Synlett*, 8:1251–1254, 2009.
- [141] L. S.-C. Weyer, L.G. *Handbook of Vibrational Spectroscopy*, chapter Spectra-Structure Correlations in the Near-Infrared, pages 1817–1837. Wiley, Chichester, UK, 2002.
- [142] C. Wiles and P. Watts. Continuous flow reactors, a tool for the modern synthetic chemist. *European Journal of Organic Chemistry*, 2008(10):1655–1671, 2008.
- [143] R. Wohlgemuth. Biocatalysis - key to sustainable industrial chemistry. *Current Opinion in Biotechnology*, 21(6):713 – 724, 2010.
- [144] B. Wu, W. Szymanski, P. Wietzes, S. de Wildeman, G. J. Poelarends, B. L. Feringa, and D. B. Janssen. Enzymatic synthesis of enantiopure α - and β -amino acids by phenylalanine aminomutase-catalysed amination of cinnamic acid derivatives. *ChemBioChem*, 10(2):338–344, 2009.
- [145] J. Xiong, J. Wu, G. Xu, and L. Yang. Kinetic study of lipase catalyzed asymmetric transesterification of mandelonitrile in solvent-free system. *Chemical Engineering Journal*, 138(1-3):258–263, 2008.

- [146] L.-W. Xu and C.-G. Xia. A catalytic enantioselective aza-Michael reaction: Novel protocols for asymmetric synthesis of β -amino carbonyl compounds. *European Journal of Organic Chemistry*, 2005(4):633–639, 2005.
- [147] R. Yuryev, S. Strompen, and A. Liese. Coupled (chemo)enzymatic reactions in continuous flow. *Beilstein Journal of Organic Chemistry*, 7:1449–1467, 2011.
- [148] A. Zaks. Industrial biocatalysis. *Current Opinion in Chemical Biology*, 5(2):130 – 136, 2001.
- [149] A. Zaks and A. M. Klivanov. The effect of water on enzyme action in organic media. *The Journal of Biological Chemistry*, 263(17):8017–8021, 1988.

Lebenslauf

Name	Strompen
Vorname	Simon
Geburtsdatum	9. Juni, 1982
Geburtsort	Münster, Deutschland
07/1998 – 05/1999	Austauschschüler an der Sea Island Academy, Charleston, SC, USA
06/2001	Abitur am Amplonius Gymnasium, Rheinberg, Deutschland
07/2001 – 04/2002	Zivildienst am "Pflegezentrum am Wiesenhof", Rheinberg, Deutschland
10/2002 – 07/2007	Studium der Biotechnologie an der Westfälischen Wilhelms-Universität, Münster, Deutschland
02/2005 – 08/2005	Praktikum bei der Degussa AG, Service Center Biokatalyse, Hanau-Wolfgang, Deutschland
07/2007	Diplom Biotechnologie
10/2007 – 02/2008	Praktikum bei DSM ASC&D, Geleen, Niederlande
03/2008 – 09/2011	Wissenschaftlicher Mitarbeiter, Prof. Dr. A. Liese, Institut für Technische Biokatalyse, Hamburg, Deutschland
05/2010 – 07/2010	Forschungsaufenthalt, Prof. Dr. J. D. Stewart, Department of Chemistry, University of Florida, Gainesville, FL, USA
10/2011 – 02/2012	Berufstätigkeit bei Oleon GmbH, Emmerich am Rhein